
GAZİ ÜNİVERSİTESİ
Gazi
1926

SIMULATION AND OPTIMIZATION OF THE USE OF A PARABOLIC DISH SOLAR COLLECTOR UNDER GAZA PROVINCE CONDITIONS

A THESIS SUBMITTED TO
THE GRADUATE SCHOOL OF NATURAL AND APPLIED SCIENCES
OF
GAZİ UNIVERSITY

BY

Sameh M. S. YOUNIS

IN PARTIAL FULFILLMENT OF THE REQUIREMENTS
FOR
THE DEGREE OF MASTER OF SCIENCE
IN
ENERGY SYSTEMS ENGINEERING

AUGUST 2023

ETHICAL STATEMENT

I hereby declare that in this thesis study I prepared in accordance with thesis writing rules of Gazi University Graduate School of Natural and Applied Sciences;

- All data, information and documents presented in this thesis have been obtained within the scope of academic rules and ethical conduct,
- All information, documents, assessments and results have been presented in accordance with scientific ethical conduct and moral rules,
- All material used in this thesis that are not original to this work have been fully cited and referenced,
- No change has been made in the data used,
- The work presented in this thesis is original,

or else, I admit all loss of rights to be incurred against me.

Signature
Sameh M. S. YOUNIS
18/08/2023

SIMULATION AND OPTIMIZATION OF THE USE OF A PARABOLIC DISH SOLAR COLLECTOR UNDER GAZA PROVINCE CONDITIONS

(M. Sc. Thesis)

Sameh M. S. YOUNIS

GAZİ UNIVERSITY

GRADUATE SCHOOL OF NATURAL AND APPLIED SCIENCES

August 2023

ABSTRACT

This study endeavors to address the acute electricity shortage in the Gaza Strip by introducing an innovative solar energy system. The central objective involves the integration of a parabolic dish solar collector with a high-concentration solar cell sourced from Azurspace company, thereby enabling efficient solar energy utilization for both electricity generation and thermal applications. A comprehensive assessment, employing established mathematical formulations and advanced modeling within the SAM software, is conducted to evaluate the electric power and thermal output of the integrated system. Positioned strategically at the focal point of the collector, the high-concentration solar cell effectively transforms captured solar energy into both electricity and usable heat. The study encompasses two distinct scenarios, each emphasizing system performance across varying collector dimensions. Validation via SAM software confirms the system's efficacy, with notably superior performance observed during summer conditions. Notably, the second scenario demonstrates a more pronounced advantage over the first, in terms of both electricity and thermal energy production. During the summer season, the first scenario achieves an electricity output of 1.6 KW and a thermal energy yield of approximately 3.3 KW. Conversely, the second scenario attains an electricity output of approximately 2.6 KW and a corresponding thermal energy yield of approximately 5.8 KW. By providing a groundbreaking solar solution, this research not only addresses energy scarcity, particularly in confined spaces, but also propels advancements within the realm of Concentrated Photovoltaic Thermal (CPVT) systems, thus underscoring its potential to alleviate energy challenges within resource-constrained environments.

Science Code	:	928.02
Key Words	:	Gaza Strip electricity shortage, Concentrated Photovoltaic Thermal (CPVT) systems, Solar energy, Thermal applications, Electricity
Page Number	:	95
Supervisor	:	Assist. Prof. Dr. Güven TUNÇ

GAZZE ILI KOŞULLARINDA BIR PARABOLIK ÇANAK GÜNEŞ KOLLEKTÖRÜNÜN KULLANIMININ SIMÜLASYONU VE OPTIMIZASYONU

(Yüksek Lisans Tezi)

Sameh M. S. YOUNIS

GAZİ ÜNİVERSİTESİ

FEN BİLİMLERİ ENSTİTÜSÜ

Ağustos 2023

ÖZET

Bu çalışma, Gazze Şeridi'ndeki akut elektrik sıkıntısına yenilikçi bir güneş enerjisi sistemi tanıtarak çözüm getirmeyi amaçlamaktadır. Temel amaç, parabolik çanak güneş kolektörünü Azurspace tarafından temin edilen yüksek konsantrasyonlu güneş hücresi ile entegre etmek suretiyle verimli güneş enerjisi kullanımını, hem elektrik üretimi hem de termal uygulamalar için sağlamaktır. Kuramsal denklemler ve SAM software içinde gelişmiş modelleme kullanılarak gerçekleştirilen kapsamlı bir değerlendirme, entegre sistemin elektrik gücü ve termal çıkışını değerlendirmek amacıyla gerçekleştirilir. Yüksek konsantrasyonlu güneş hücresi, kolektörün odak noktasına stratejik olarak yerleştirilerek yakalanan güneş enerjisini hem elektriğe hem de kullanılabilir ısıya dönüştürme kapasitesine sahiptir. Çalışma, farklı kolektör boyutlarına göre sistem performansını vurgulayan iki farklı senaryoyu kapsamaktadır. SAM yazılımı aracılığıyla gerçekleştirilen doğrulama, sistemin etkililiğini onaylayarak özellikle yaz koşullarında belirgin bir üstünlük sergilemektedir. Özellikle ikinci senaryo, hem elektrik üretimi hem de termal enerji üretimi açısından birinciden daha belirgin bir avantaj sunmaktadır. Yaz mevsiminde birinci senaryo, 1,6 KW elektrik üretimi ve yaklaşık 3,3 KW termal enerji verimi elde ederken, ikinci senaryo yaklaşık 2,6 KW elektrik üretimi ve yaklaşık 5,8 KW karşılık gelen termal enerji verimi elde etmektedir. Bu araştırma, enerji sıkıntısını özellikle sınırlı alanlarda ele almanın yanı sıra Konsantre Fotovoltaik Termal (CPVT) sistemler alanındaki gelişmeleri destekleyerek yenilikçi bir güneş enerjisi çözümü sunarak, kaynak kısıtlı ortamlarda enerji sorunlarını hafifletme potansiyelini vurgulamaktadır.

Bilim Kodu	:	928.02
Anahtar Kelimeler	:	Gazze Şeridi elektrik kıtlığı, Konsantre Fotovoltaik Termal (KFTT) sistemler, Güneş enerjisi, Isı uygulamaları, Elektrik üretimi
Sayfa Adedi	:	95
Danışman	:	Dr. Öğr. Üyesi Güven TUNÇ

ACKNOWLEDGEMENTS

I extend my profound gratitude to my advisor Asst. Prof. Dr. Güven TUNÇ, whose expert guidance and invaluable insights have been pivotal in shaping the direction and quality of this research. Their unwavering commitment to excellence, coupled with constructive feedback at every stage, has refined my ideas and honed my research skills. I am deeply appreciative of the expertise and rigorous academic standards upheld by the faculty members of the Energy Systems Department at Gazi University, fostering an environment conducive to learning and growth. My family's unwavering encouragement, love, and patience have been a constant source of inspiration, while the support and information provided by Azurspace company, the Gaza Strip's power plant, and the Palestinian Statistics Centre have been integral to this work. I am also grateful to all contributors, whose encouragement, feedback, and support have played an indispensable role in bringing this thesis to fruition. In conclusion, this thesis stands as a testament to collective collaboration, acknowledging those who have contributed to this significant milestone in my academic journey.

LIST OF CONTENTS

Page

Page

Page

LIST OF FIGURES

Figure **Page**

Figure **Page**

Figure **Page**

LIST OF TABLES

Table **Page**

NOMENCLATURE

In this study, the symbols and abbreviations used are presented below, along with their explanations.

Symbol	Meaning
$\mathbf{A_a}$	Unshaded collector aperture area, m^2
$\mathbf{A_{con}}$	Aperture area of dish concentrator, m^2
$\mathbf{A_f}$	Geometric factor (shaded area/total aperture area)
$\mathbf{A_r}$	Receiver area, m^2
C	Concentration ratio
cp	Specific heat capacities, J/kg.k
d	Diameter of the focal point, m
$\mathbf{D_{con}}$	Diameter of the concentrator, m
$\boldsymbol{f}$	Focal length, m
$\mathbf{H_{alt}}$	Altitude above sea level, m
$\mathbf{h_{fi}}$	Convective heat transfer coefficient inside the receiver tube, $w/m^2.k$
hw	Convection coefficient, $w/m^2.k$
$\mathbf{I_B}$	Beam radiation, w/m^2
$\mathbf{I_o}$	Solar constant, w/m^2
$\mathbf{I_{on}}$	Extraterrestrial radiation, w/m^2
$\mathbf{I_{TN}}$	Total solar radiation at the earth's surface, w/m^2
$\dot{\boldsymbol{m}}$	Mass flow rate of fluid, kg/s
N	Day of the year
$\mathbf{T_a}$	Ambient temperature, kelvin
$\mathbf{T_i}$	Entering fluid temperature, kelvin
$\mathbf{T_o}$	Exit fluid temperature, kelvin
$\mathbf{T_r}$	Receiver temperature, kelvin
$\mathbf{V_{air}}$	Wind speed, m/s
Y	Depth of dish collector, m
$\boldsymbol{\eta}$	Collector efficiency
$\boldsymbol{\eta_o}$	Optical efficiency
$\boldsymbol{\eta_{CPV}}$	Concentration photovoltaic module efficiency

Symbol	Meaning
Ǿ	Acceptance angle
Ʀ	Reflectance of the mirror, %
z	Azimuth angle
α	Altitude angle
δ	Declination angle
θ	Incidence angle
м	Fluid viscosity, kg/m.s
ρ	Fluid density, kg/m^3
φ	Zenith angle
ψ	Rim angle
ω	Hour angle
Б	Absorptance of the receiver, %

Acronyms	Meaning
AC	Alternating Current
AST	Apparent Solar Time
CSP	Concentrated Solar Power
DC	Direct Current
DCP	Double Copper Board
DNI	Direct Normal Irradiation
DS	Daylight Saving Time
ET	Equation Of Time
FEA	Finite Element Analysis
GBV	Gender-Based Violence
GPP	Gaza Power Plant
GS	Gaza Strip
JSC	Joint Service Council
kWh	Kilo Watt Hour
L	Local Latitude
LL	Local Longitude
LST	Local Standard Time

Acronyms	Meaning
MWh	Mega Watt Hour
OCD	Obsessive Compulsive Disorder
PTSD	Post-Traumatic Stress Disorder
PV	Photovoltaic
RPM	Revolution Per Minute
SDG	sustainable development goals
SHC	Solar Heating & Cooling
SL	Standard Longitude
UN	United Nations
UNRWA	United Nations Relief and Works Agency for Palestine Refugees in the Near East
UPS	Uninterruptible Power Supply
WHO	World Health Organization

1. INTRODUCTION

Electricity is a vital resource that powers essential services such as healthcare, transportation, and communication, making it indispensable in modern societies. However, in the Gaza Strip (GS), the supply and distribution of electricity have been a constant challenge, with frequent power cuts and shortages. These outages have adverse effects on the region's economic, social, and health sectors, ultimately hindering its overall development and this will be reviewed in detail in Section 2. Furthermore, Palestine faces a unique situation in the Middle East due to several factors such as an unstable political climate, financial crisis, high population density, and lack of natural resources. The Palestinian Central Bureau of Statistics (PCBS) reported that as of the end of 2022, there were approximately 14,3 million Palestinians worldwide, with 5,35 million residing in the State of Palestine. Palestine has one of the highest population densities in the world, where the population density in GS is 5740 people / km^2 [1].

The physical disconnection between GS and West Bank, including East Jerusalem, presents both technical and political challenges for energy transportation, storage, and importation [2]. Israel's control over energy imports to Palestine, predominantly through Israeli companies, hinders open trade in electricity and petroleum products and restricts development initiatives [3]. Abu Hamed et al. have emphasized the high energy cost in Palestine compared to neighbouring regions [2]. Additionally, the absence of a clear national energy policy, fragmented institutional framework, and incomplete framework in Palestine pose further obstacles. Political instability, economic conditions, and limited indigenous resources have increased energy demand, while concerns over political risks have deterred significant investments in energy and industrial sectors [2]. In the long run, renewable energy holds considerable potential for fostering sustainable energy development in Palestine [4].

The researcher made a detailed study on how to use renewable energy as a means to solve the electricity crisis in Palestine (see Section 2). Where it turns out that Palestine has significant solar, wind, and biomass energy potential, with abundant sunshine hours exceeding 3000 annually [5]. In Gaza Strip, the average solar resource ranges from 5.4-6 $kWh/m^2/day$ [6]. Solar photovoltaic and thermal systems utilize global solar radiation, while solar concentrating systems harness beam solar radiation [7]. Compared to Ankara, Turkey

(4.36 kWh/m^2/day), and Madrid, Spain (4.88 kWh/m^2/day), Palestine exhibits exceptional solar energy potential [8, 9].

The Gaza Strip has experienced rapid population growth, resulting in a significant increase in energy demand that is primarily met through imports. Therefore, finding alternative, clean energy sources is critical for the region's future. However, several challenges impede power generation in GS, including political instability, economic crisis, infrastructure deficits, and insufficient implementation of strategies to manage supply and demand. In addition, the region faces significant economic challenges in importing electricity an fuel. For almost 15 years, GS has suffered from an energy crisis, with severe electricity shortages for the past decade. These energy shortages have severely impacted essential services such as health, water and sanitation services, and undermined the fragile economy, particularly the industrial and agricultural sectors. The continuous conflict with Israel, including four wars on Gaza in 2008, 2012, 2014, and 2021, exacerbates the electricity crisis and causes high levels of stress that adversely affect people's physical, mental health, and well-being.

Gaza Strip requires around 550 MW of electricity with an increase in demand during peak winter and summer months, reaching up to 622 MW. Nonetheless, the primary electricity sources in GS, namely the Gaza Power Plant, Egyptian Power Lines, and Israeli Electricity Lines, can only provide 50% of the required electricity [10]. With the limited supply, residents initially resorted to using candles and small generators which led to unfortunate incidents of human and material losses from fires caused by candles or generator explosions [11]. Today, the majority of residents use other sources like street generators, batteries, and PV cells, however, these sources are limited and lack flexibility [11]. Hence, it is crucial for the government to shift towards sustainable energy sources for a better environment, economy, and well-being of the people.

There are existing reviews in the specialized literature that discuss the energy situation in the Gaza Strip and Palestine. Since January 2010, the United Nations document emphasizes the severe deterioration of electricity supply in Gaza Strip. Insufficient funds for purchasing industrial fuel to operate the Gaza Power Plant have led to daily electricity cuts of 8-12 hours, exacerbating living conditions and disrupting various essential services including healthcare, hospitals, clinics, education, and water and sanitation [12].

In 1995, Abualkhair [13] highlighted the energy crisis in Palestine, revealing that 65 localities lacked access to the public electricity network. The author highlights the West Bank region's estimated annual electricity consumption of 890 GWh, averaging 496 kWh/capita. In contrast, the Gaza Strip exhibits the modest consumption rate in the region, with 47.91 GW h per year. Five years later, Abu Hamed et al. [2] reached similar conclusions for the year 2009. Despite an increase in electricity consumption to 1606 GWh and 3808 GWh in Gaza Strip and West Bank respectively, the rates remained the lowest in the region. Additionally, the costs were significantly higher compared to other areas, placing a greater burden on household expenditure [2].

Based on the information and data collected by the researcher, the Gaza Strip suffers from a real problem, which is the problem of power outages, and it needs to find appropriate solutions. According to what has been mentioned in section 0, wind energy is not feasible in the Gaza Strip, and wave energy needs challenges and capabilities that outweigh the current ones in the Strip, and the use of solid waste to energy needs a high cost, so the researcher believes that using solar energy is the best choice to solve the problem of power outages in the Gaza Strip, and this is what this study will focus on.

Many researchers have studied how to use and benefit from solar energy in the Gaza Strip. Among the most important studies conducted on this topic as given below.

Nassara and Alsadi, by making a comprehensive comparison between (PV) and (CS) technologies, they summarized the potential of solar energy in the Gaza Strip. SAM software was used to obtain climate data and to calculate the economic feasibility of solar power plants. The study showed that the (PV) solar cell plants and the parabolic trough system are preferred for the energy market in Gaza, especially parabolic trough system that achieves the levelized cost of electricity (LCOE). But due to the lack of suitable spaces to achieve this system, the PV system, which has flexibility in size and ease of use on the roofs of buildings and facilities, was preferred. The study found that building a 555 MW (PV) system will cost about $800 million and the expected price of electricity will range between ($0,07 - $0,11) per kilowatt-hour, which is four times lower than the current price ($0,29 - $0,46) per kilowatt hour [14].

Nassara and Alsadi in their study, an examination of the present energy landscape within the Gaza Strip was undertaken. Within their work, these scholars not only analyzed the existing energy conditions but also put forth four distinct potential pathways to navigate through the existing challenges. A comprehensive evaluation encompassing economic and environmental aspects was meticulously performed with the objective of ascertaining the scenario that garners superior financial returns. The prospect of constructing independent power facilities or adopting a hybrid model, characterized by an even greater load capacity, emerges as a viable option for the electricity authority. This strategic move can be facilitated through the prudent allocation of funds saved from diminished fuel consumption, thereby simultaneously augmenting environmental conditions [15].

Mohamed Ouda, presented the Gaza Strip's potential for renewable energy, focusing on biogas energy. The data showed the importance of converting waste and sewage water into energy. The solar energy, which is well available in the Gaza Strip, can be used to treat waste and sewage water, which in turn is of great importance to the Gaza Strip's economy and environment [16].

Lubna et all. published a study aimed at solving the problem of shortage of fresh water and energy. A steam cycle power plant uses solar energy in conjunction with concentrating solar thermal power (CSP) technology to generate electricity. The steam is then sent to a desalination facility where it is used to heat saltwater in order to produce freshwater. The researchers also mentioned that this work will achieve economic and environmental benefits [17].

The Islamic University has implemented a project to use the parabolic trough as a source of electricity generation. By bringing the temperature to 200 C°, it was possible to achieve the project's goal of generating 1 KW. To achieve this temperature, It was adopted the length of the parabolic trough solar collector to be 5 m, the width 2,5 m, and the depth 0,75 m. But the project only achieved a temperature of 98 C° for water and 101 C° for oil, due to inaccurate solar energy reflection, a manual sun tracking system, a lack of smooth mirrors, and a coating glass pipe was not available [18].

Al-Najjar et al. studied the best angle of tilt and angle of incidence for the solar water heaters used in homes to obtain higher efficiency. To calculate the solar energy provided by the flat-

panel collector, the researchers used the Transient System Simulation Tool program. And Design-Expert software, which uses a response surface approach to determine the ideal tilt angle. The findings demonstrate that the ideal incidence angle ranges from 10 to 12 degrees. By switching to a typical solar water system from electric water heaters can result in annual energy cost savings of up to $857,87. According to research, solar water heating system's payback period in Gaza will be around 3,4 years [19].

Albarqouni and Hussein in their work, first- and second-order Angstrom-type polynomials were created using long-term data of the monthly mean daily sunlight at several locations close to the Gaza Strip. The radiation estimated by the generated model is contrasted with the radiation actually observed. The calculated values of both models were found to be in good agreement with the observed values from the Bet Dagan and METEOTEST Stations from the comparison of these data, which strengthened the established model and made it simple to apply to the Gaza Strip in Palestine. According to the study, both linear and polynomial models have a mean percentage error of around 6%, while the estimated design model's accuracy is about 94% [20].

Hala and Fady, conducted a study aimed at finding out the main reasons that make families in Gaza depend on solar energy as an alternative source of energy in their homes. By SPSS program, the data collected were analysed through an electronic questionnaire. Only 19,5% of the study sample, according to the authors, had solar panels installed in their houses. The findings of the investigation revealed that factors such as the monthly aggregate energy expenditure, the extent of space feasibly allocated for the installation of solar panels, possession of residential property, and the inclination to distribute costs collaboratively with neighbors exhibited no discernible impact on the determination to adopt solar energy utilization. It was also found that knowledge and awareness of solar energy is the most important factor affecting the decision to use it, in addition to the type of house. Therefore, the study believes that it is necessary to start spreading knowledge about the importance and advantages of using solar energy in Gaza [21].

Omar, in his article, examined the Gazan power shortages and unveiled a straightforward, 5 m^2 off-grid stand-alone PV system that could be easily built and used in residential structures. It is possible to utilize this technique to partially replace Gaza's regular power outages. PV installations on the southern façade and on the roof have had their system

performance compared in these two instances. Because solar energy is so readily available in the Gaza Strip, the results suggest that both of the instances under consideration are realistic. However, the installation on the southern façade has the drawback of reducing PV production by around 27%. Due to the consequent PV shading effect, this decline mostly happens during the summer [22].

Hala et all. also conducted another study on the community's acceptance of the use of solar-powered cooking appliances in the Gaza Strip. The results of the questionnaire, in which nearly 2400 people participated, showed that only 37,7% of the participants support the idea, and 94,55% believe that the use of solar energy for lighting is better. The researchers believe that financing plans and loans are among the main factors in spreading e-cooking. So, it is important to fund some of the experimental projects that the researchers believe will contribute significantly to the extent of society's acceptance of such ideas when they see a real model on the ground [23].

Al-Najjar et al. made a comparison between PV systems and solar thermal collectors in two different climate regions, namely the Gaza Strip and the city of Montreal. Using the TRNSYS program, it was found that in the hot regions the solar collector outperforms PV systems, while in the cold regions both efficiencies become comparable with each other [24].

Abu Dabbousa et al. using PVsyst program, they compared the performance of the PV modules available in Gaza Strip's market, and the amount of production losses of the panels under the same weather conditions and the same load. The Trina Solar module performed the best in low irradiance conditions. In terms of the ohmic wiring loss and temperature effect, the GCL module performed the best. The GCL module generated the greatest benefit as a result of module quality. The Canadian Solar Inc. module saw the least amount of energy loss due to mismatch when compared to the other modules [25].

Abu-Zarifa, measured and designed every component of a PV lighting system for small homes in the Gaza Strip. The outcomes derived from the study indicated that the expense associated with one kilowatt of solar energy for the proposed system is $0,38, which is good compared to the diesel generators currently used in Gaza, which cost 0,75 $/kwh [26].

What was previously mentioned is how the researchers discussed the use of solar energy in the Gaza Strip and benefited from it in different ways and fields. But let's take a look at the recent current technologies that scientists and countries are doing around the world to take advantage of solar energy, especially how to exploit it to generate electricity. Perhaps the most important of these technologies are Concentrated Solar Power (CSP) and Concentrated photovoltaic thermal system (CPV/T).

Concentrated Solar Power (CSP)

CSP system uses the sun’s heat as energy sources, in contrast to PV systems that uses photon energy of the sun. In the context of serving as the thermal heat source responsible for the conversion of water into steam, the majority of electric power facilities rely on various iterations of fossil fuels. Then a large turbine spins the steam, which drives a generator to generate electricity.

There are several technologies that use the heat of the sun to generate electricity, some of them:

- The parabolic trough systems,
- The solar tower systems,
- The Stirling solar dish systems,

Since CSP systems feature in saving spaces and requiring mechanical maintenance, it’s become the most marketed in utilities.

Types of solar collectors

Various solar concentration systems are currently being developed and demonstrated in the solar market and can be split into two categories according to the concentration method: line concentration and point concentration. The parabolic trough collectors and linear Fresnel reflector systems are the most relevant line concentrating technologies. The other kind of concentrating devices focus the incident solar radiation onto a point. The most recognized application for point concentrating technology is Dish Stirling Systems and Central Receiver Systems.

Parabolic trough collector

In Trough systems, a rectangular and parabolic mirror collects the sun's heat energy and focus it. The system consists of a large array of collectors, usually span across the solar field. The system rotates mechanically to track the sun rays from the east to the west.

Figure 1.1. Image of trough system

Mechanically, the mirrors rotate and track the sun east to west, concentrating sunlight on receiver tubes running the length of the mirrors. The receiver tubes are located along each parabolic mirror's focal line.

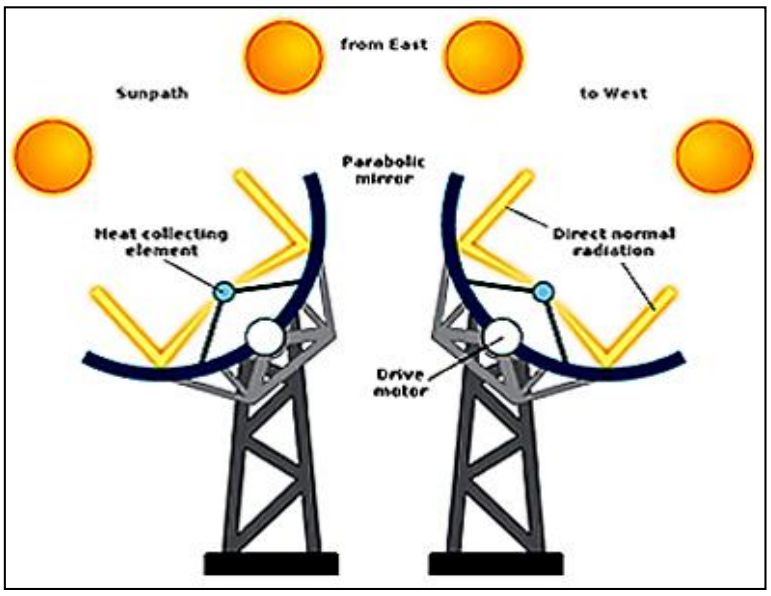

Figure 1.2. A trough system tracks the sun rays from the east to the west

The focused sunlight is received by tubes along the mirrors, these tubes carries a fluid that absorbs the heat getting its temperature reach around 550 degrees [27]. Then, the fluid vapor is used to generate electricity in a conventional steam turbine. The tube is stainless steel characterized by a special sunlight absorbing surface, also mounted on a glass tube to trap he heat and to isolate the tubs by vacuum.

It is easy for Trough systems to emerged easily to electrical grid, since it uses conventional steam turbines that used in fossil fuel systems (hybrid systems). It can compensate the cloudy or bad weathers days because of its storage ability. It has 20% sunlight to electricity conversion efficiency.

Tower system (central receiver)

The heliostats are a reflective mirror with a mechanism and computerized system to make it rotate, its function is to reflect thermal heat from the sun to the central receiver; heliostat is 1300 square feet, and there is 624 of them. What specialize tower systems is its dual axis tracking, where heliostats rotate in two dimensions tracking the sun through the day and year. This ability allows tower systems to produce optimum power in contrast to fixed or one axis systems.

The central receiver four 18 X 39 feet vertical panel arranged in a semi-circle manner and housed in 36 X 36 feet opening. It transfers the reached heat from heliostats to a circulated fluid, usually molten salt. The salt weather stores the energy or transfers it to steam and then to a turbine to generate electricity at the bottom of the tower.

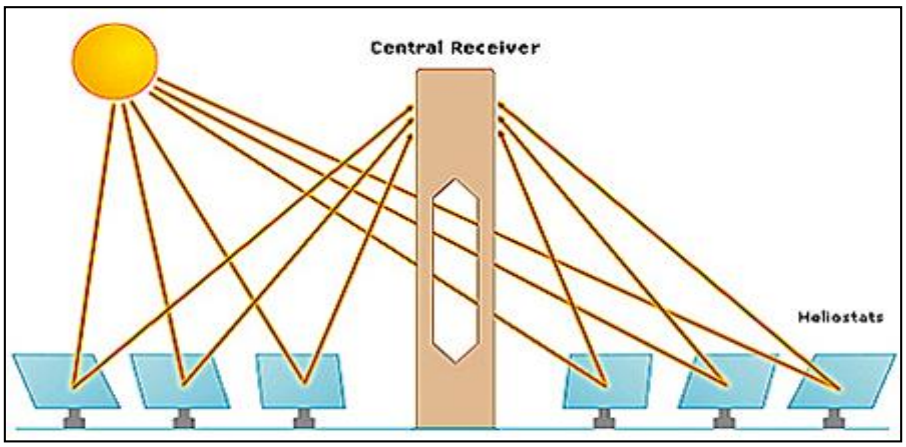

Figure 1.3. Image of tower system

Dish stirling systems

Dish Stirling system components are: parabolic concentrator, solar light receiver and stirling engine. Even though this system uses thermal heat as energy source, it doesn't use water or steam (except for washing concentrators) like the formers. Instead, it uses stirling engine to generate electricity. The solar light receiver heats a working fluid up to approximately 650ºC. this heat causes the piston of the engine to go back and forth 50 or 60 cycles per second generating an AC current.

The system uses Dual axis tracking system to maximize power output. The Infinia Power Dish shown in the Figure 1.4 below is 24% efficient and generate 3.2 kW electricity (per dich). One mega Watt require 334 dishes and 4 acres [27]. This system doesn't need the earth to be flat, and need less areas than the other types.

Figure 1.4. Image of dish stirling system

From Figure 1.5 it can be noticed that parabolic dish collector type has the highest concentration ratio. As a result, it was chosen parabolic dish to use it in our system [28].

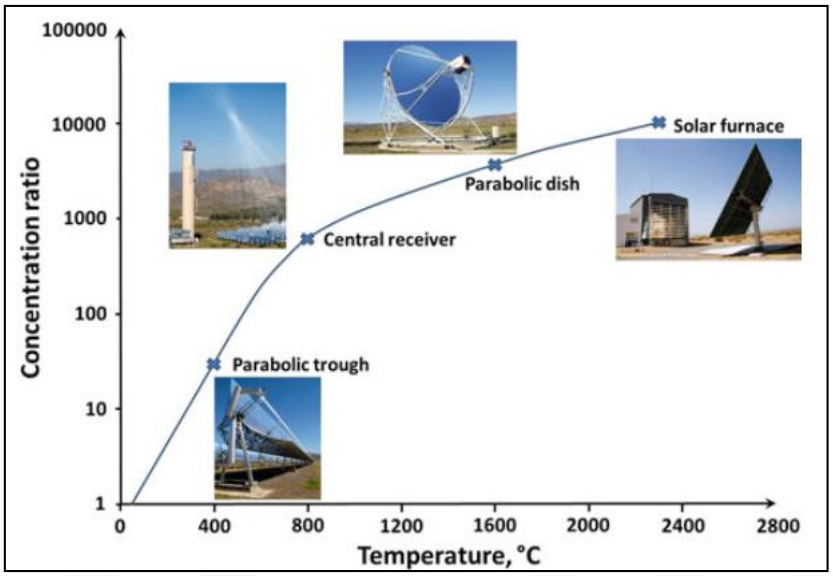

Figure 1.5. Comparison of the concentration ratio of solar collector systems

Fresnel lens

A Fresnel lens is made of plastic that has had a series of concentric rings etched into it. A basic lens component makes up each ring. These lenses are set up in a certain configuration on a flat surface to give out a short focal length. They are made of a light, thin material. Fresnel lenses come in small and large sizes, and because of their outstanding light collecting capacity, they are helpful in a variety of applications. Fresnel lenses are used in magnifiers, image generation, and projection lenses in lighting systems, in addition to solar panels.

The density of solar energy may be increased by using these thin lenses. With a 500:1 concentration ratio, these lenses boost the quantity of sunlight that strikes individual PV cells. It collects the sun's energy and makes it accessible to solar panels. Therefore, a Fresnel lens collector may help you get the most out of a solar power system.

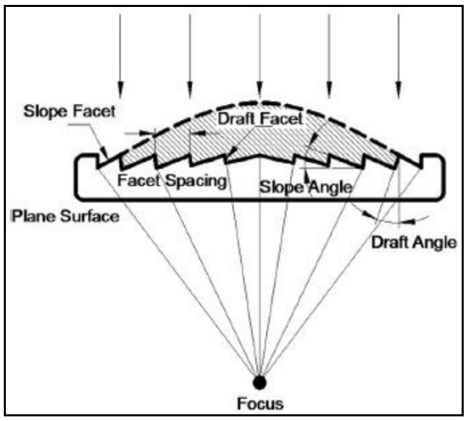

Figure 1.6. Fresnel lens operating theory

Concentrated photovoltaic thermal system (CPV/T)

In recent years, the quest for sustainable and efficient energy solutions has led researchers and engineers to explore novel technologies that can harness the power of solar radiation effectively. Concentrated Photovoltaic Thermal (CPVT) systems have emerged as a promising avenue in this pursuit. By combining the benefits of parabolic dish solar collectors and highly concentrated solar cells, CPVT systems offer the potential to generate both electricity and utilize the surplus heat, making them highly attractive for applications in various sectors. There are four components that make up a concentrated photovoltaic thermal system (CPVT), comprising an absorber, concentrator, solar radiation tracker, and thermal absorber. As the demand for clean energy intensifies, understanding the advancements and challenges in CPVT technology becomes imperative. Within this framework, the current segment undertakes an exhaustive examination of prior investigations pertaining to Compound Parabolic Concentrating Solar Thermal (CPVT) system technologies. The objective is to establish a robust groundwork for our own research and to illuminate the contemporary cutting-edge advancements within this ever-evolving domain. In-depth analyses of both historical and contemporary studies in the realm of CPV-T can be readily accessed in references [29-38], respectively.

Felsberger et al. discussed the benefits of converting a conventional thermal parabolic trough collector to a CPV-T hybrid system employing multi-junction PV cells. The field testing of a hybrid absorber made up of 2*26-10*10 mm^2 Azurspace multi-junction cells is now taking place, and the preliminary findings are encouraging. The researchers report that significant losses in electrical efficiency can be avoided by paying careful attention to cell positioning,

and solar cell efficiency could be easily reaching to 28%. The study demonstrated that the cell could run efficiently at temperatures as high as 86 °C while maintaining 26,5% efficiency and permitting fluid temperatures of about 65 °C [29].

David et al. carried out an experimental study of a parabolic trough concentrating photovoltaic-thermal system in Italy. This system, which moves around two axes and has a concentration ratio of around 130, has an aperture area of 6,857 square meters and a linear receiver that is 2,4 meters long. The PV cells have a 10-millimeter square shape. The researchers reported that the system's overall efficiency was approximately 70% [30].

Yang et al. present a conceptual framework for a photovoltaic thermal (CPVT) system characterized by low-concentration features. This proposed system involves the integration of a quasi-parabolic concentrator alongside planar mirror reflectors. It incorporates a water-cooling mechanism, strategically devised to maintain optimal operating temperatures for the solar panels, while a two-dimensional tracking system adeptly traces the sun's trajectory. Subsequently, a tangible prototype of this system was fabricated and subjected to outdoor experimentation. The outcomes of these trials showcased an electrical efficiency ranging from 16,6% to 20%, coupled with an overarching efficiency of up to 59%. Notably, the system exhibited superior performance during sunny conditions compared to overcast weather scenarios. On average, the comprehensive thermoelectric efficiency of the system reached a commendable 57,3% [31].

Riahi et al. embarked on an inquiry into the realm of concentrated photovoltaic thermal (CPVT) systems, alongside their hybrid counterpart, the concentrated photovoltaic thermal thermoelectric (CPVT-TE) hybrid solar systems. These researchers not only conceptualized and crafted physical prototypes but also conducted a series of outdoor experiments aimed at scrutinizing the systems' performance. Concurrently, they formulated mathematical models to meticulously assess both the electrical and thermal aspects of these systems, further substantiated by empirical data derived from the experiments. The findings demonstrated that the electric power yield of the CPVT-TE system surpassed that of the CPVT system. This superiority was attributed to the incorporation of thermoelectric generators, an integration that culminated in an appreciable 7.46% enhancement in the electrical efficiency of the CPVT-TE configuration. Remarkably, the CPVT-TE system exhibited a satisfactory range of stored water temperatures, thereby rendering it suitable for medium-temperature

applications. Furthermore, the integration of thermoelectric generators facilitated the generation of an additional annual electric energy output of 359 kWh. The authors concluded that the CPVT-TE system is suitable for large-scale application and can provide environmentally friendly and sustainable electricity and hot water while also saving primary energy and reducing CO^2 emissions. They also suggested that improving the physical properties of thermoelectric generators and using flexible materials could be options for future integrated photovoltaic thermoelectric solar systems [32].

Wang et al. studied a compact linear Fresnel reflector (LFR) solar concentrator photovoltaic (CPV) system. One complete type and three hybrid type CLFRs were among the four CLFRs that the researchers created and compared. The modeling findings demonstrated that the complete type produces the maximum concentrated solar radiation, and that was consistent with operational outcomes. Scholars have asserted that the photovoltaic (PV) cell module situated upon the solar Concentrated Photovoltaic (CPV) system attains a photoelectric conversion efficiency of fifteen-point nine percent. Furthermore, for the CLFR-c concentrator, under the condition of a tracking error of zero point two degrees, the system exhibits a typical optical efficiency of zero point eighty-nine [33].

Wang et al. provide an account of a solar Concentrated Photovoltaic (CPV) apparatus and proceed to replicate its functioning through the implementation of a linear Fresnel reflector (LFR) concentrator. The researchers' analysis elucidates a direct correlation between the elevation of the solar panel installation and two pivotal factors: the geometric concentration ratio and the ground utilization ratio. Furthermore, it is observed that the LFR concentrator surpasses the parabolic trough concentrator in terms of solar concentrating uniformity, particularly when operating at identical geometric concentration ratios. Notably, the investigation demonstrates that the CPV system employing the LFR concentrator can achieve a normalized optical efficiency of sixty-two hundredths. Subsequently, the I-V tests conducted yield energy conversion efficiencies of fourteen point seven percent and thirteen point six percent for the solar cell monomer and cell module, respectively [34].

Hussain and Lee undertook a comprehensive examination of a U-shaped solar energy collector model within a Concentrated Photovoltaic-Thermal system, employing both numerical simulations and empirical experimentation. The primary objective of this investigation was to ascertain the upper limits of thermal and electrical power outputs

concerning a specific volumetric flow rate. The integral components of this system encompassed eight triple junction solar cells, eight SOG Fresnel lenses, an adept dual-axis tracking mechanism, and a meticulously designed forced cooling system. By orchestrating variations in the flow rate of the working fluid, all while considering factors such as solar irradiation and ambient temperature, meticulous analyses were conducted. The meticulous alignment between the computational calculations and the real-world measurements of the U-shaped solar energy collector model was striking, with a mere 7% margin of error being observed [35].

Youssef et al. created a 2-D numerical model of a solar thermal concentrator. The triple junction PV cells on the bottom surface of the receiver pipe are the foundation of the suggested CPV/T arrangement. The study show that the electrical efficiency of PV cells will decrease when wind velocity decrease. The average electricity efficiency is improved by 2% as a result of thermal insulation. Moreover, it is noteworthy that the thermal efficiency of the system exhibits a decline as the velocity of the fluid increases beyond a certain threshold, while conversely, it demonstrates an elevation when the fluid velocity is maintained at lower levels exceeding the critical water velocity rate established within the confines of the receiver channel width [36].

Singh and Reddy in their article, presented a method for predicting the focal flux heat distribution of a CPV reflective system utilizing the inverse heat transfer approach. A CPV 3,6 * 3,6 m^2 square parabola dish collector with a dual axis tracking system was employed by the researchers, and an IR camera to gauge the focused receiver surface's temperature. Results Show that, the highest estimated focal heat flux on the receiver was 37,41 kW/m^2, however the flux sensor actually detected a heat flux of 39,15 kW/m^2 with a 4,4% error. The expected heat flow, according to researchers, may be utilized as an input parameter for the thermal analysis of the receiver and, as a result, to forecast the CPV system's power production [37].

Ceylan et al. paper's primary goal is to explore a CPV/T's ability to concurrently convert solar energy into electrical energy and thermal energy, particularly during winter. Energy storage was also done with the help of paraffin wax that acts as a phase change material, and a mixture of water and ethyl alcohol was used as the working fluid. According to the study, the CPV/T's average exergy efficiency was 10% and its overall system efficiency was 88%.

According to the researchers, adding an air collector and PCM to a CPV/T system increased energy efficiency throughout the winter [38].

There are also many studies that talked about different designs of solar collectors and the factors that affect the efficiency of the solar collector, including the following studies.

Hafez et al. in their study, review the parabolic solar dish technologies as well as design elements used in various applications, including material, aperture area and shape of reflector concentrators and receivers, rim angle, concentration ratio, focal length of the parabolic dish, and diameter of the parabolic dish concentrator. It is discovered that the rim angle, receiver diameter, and dish concentration ratio all have a significant impact on the system's performance [39].

Hijazi et al., tried to reduce the cost of parabolic solar dish collector for electricity generation. The researchers improved the dimensions of the ribs and rings that support the reflective surface in order to reduce the weight of the dish. Using Autodesk Inverter, they analyzed the full stress of the dish structure. The study suggests increasing the ribs' angle and the separation between connecting rings, as well as using landscape orientation for the reflected facets [40].

Sahu and colleagues introduce an innovative approach involving the incorporation of heat transfer fluid, concentrated photovoltaic components, or thermoelectric generators onto the receiver unit. Through this strategy, they unveil a novel methodology for the conception and production of an economical solar parabolic dish concentrator, boasting an expansive aperture area of 12.6 square meters. This concentrator design, equipped with dual-axis manual tracking, is distinguished by its dual-purpose functionality, catering to both process heating and concurrent electrical power generation needs. The researchers underscore the cost-effective nature of the manufacturing technique adopted, with the system achieving a remarkable concentration ratio of 466 [41].

Gwani et al. designed and tested a dish solar collector to be used in remote areas for the purpose of cooking or drying. Inexpensive materials were used in addition to a manual sun-tracking system. The experimental results showed that the temperature of the frying oil reaches 180 c and 100 c for water [42].

Ibrahim developed a dish solar collector to heat approximately 40 litres of water to reach 100c for domestic use. Using the Linear actuator to track the sun, the system's thermal efficiency was greater than the planned value of 50%, at 52% to 56% [43].

Hiba et al. explored various parabolic dish receiver configurations to optimize performance. By adjusting receiver height, diameter, and fluid inlet/outlet positions while maintaining constant volume, they used FLUENT and SOLTRACE for temperature and radiation flux analysis. Results highlighted how receiver geometry and inlet/outlet placements impact thermal efficiency. The best-performing setup involved a "low" height cylindrical receiver (H=0.075 m, H=0.048 m) with a bottom tangential inlet and top normal outlet, termed position 2 [44].

Venkatachalam and Cheralathan, present experimental research on the thermal performance of the solar parabolic dish concentrator's conical cavity receiver with various aspect ratios. When anticipated, as the aspect ratio increased, the receiver's surface temperature decreased. However, a decline in thermal performance is seen. And it turns out that lowering receiver surface temperature alone is insufficient to enhance thermal performance; surface area also plays a role [45].

Senthil and Cheralathan, studied the effect of the temperature distribution of the receiver (which contains fins on its inner surface) on heat gain and loss. The mild steel's 0,15 emissivity and 0,85 absorptivity both enhanced heat input to the heat transfer fluid and decreased heat loss from the surface. The researchers noticed an increase in thermal efficiency by 3,8% when using the curved path instead of the water flowing from the bottom to the top of the receiver. In addition to reducing the operating time by 20% [46].

Hafez et al. created a simulation and modelling (by MATLAB) of a parabolic dish Stirling engine in Egypt (similar in climate to the Gaza Strip). They studied all the influencing factors, focusing on the materials, where they used (polymeric film, aluminium anode, and polished stainless), which have reflectivity of 98%, 86.8%, and 50%, respectively. The results showed that the highest output power that can be achieved is 9707 W at 12 noon by using polymeric film, which in turn contributes to the use of a smaller diameter of the solar parabolic dish, which means lower manufacturing cost [47].

This research endeavor aims to address the pressing issue of electricity shortage in the Gaza Strip by developing an innovative solar energy system. The primary objective is to harness solar energy in a novel and efficient manner by integrating a parabolic dish solar collector with a highly concentrated solar cell provided by Azurspace. This integrated system not only aims to generate electricity but also seeks to utilize surplus thermal energy for heating purposes and other household needs. The assessment of the electric power and heat output will be conducted using established equations in the field and advanced modeling techniques through the SAM software.

The proposed system is particularly relevant for independent homes, providing a reliable source of electricity during interruptions. Moreover, its potential suitability for the Gaza Strip conditions, characterized by high population density and limited available space for large-scale projects, is a noteworthy advantage. By requiring minimal installation area and the ability to be mounted on rooftops, the system offers a practical solution to the electricity crisis. This thesis distinguishes itself by exploring the unique combination of a parabolic dish solar collector with a high-concentration solar cell, setting it apart from previous studies that primarily focused on the integration of high-concentration cells with parabolic trough solar collectors or Fresnel lenses. Through this comprehensive investigation, we seek to contribute valuable insights and advancements to the field of Concentrated Photovoltaic Thermal (CPVT) systems.

2. THE ENERGY SITUATION IN THE GAZA STRIP

The Gaza Strip faces significant challenges in meeting its energy and electricity needs. The region experiences a chronic energy deficit, leading to frequent power outages and limited access to reliable electricity for its population. The primary sources of electricity are heavily reliant on external imports and are subject to political and economic uncertainties. Additionally, the limited capacity of existing power infrastructure exacerbates the situation, making it difficult to meet the increasing demand. The energy situation in Gaza has significant implications for daily life, healthcare, education, and economic activities. As a result, there is an urgent need to explore and implement sustainable and alternative energy solutions to alleviate the energy crisis and improve the quality of life for its residents.

2.1. The Impact of Electricity Shortage

Electricity plays a vital role in improving health and achieving the Sustainable Development Goal 7 (SDG7), which emphasizes the importance of establishing an environment that combines health with essential infrastructure, including electricity [48]. Unfortunately, the ongoing electricity crisis in Gaza Strip means that its two million inhabitants have limited access to power supply, with only a few hours of electricity available each day.

This electricity shortage crisis has had a significant impact on the health situation in Gaza. Prolonged power cuts have led to the suspension of dialysis units, the postponement of surgeries, and negative effects on operating rooms and intensive care units due to the suspension of central air conditioning systems [11]. Furthermore, the use of traditional lighting methods such as candles and firewood during power cuts has led to suffocation and even death of many individuals [49].

Electricity shortage also affects the sewage systems in Gaza, with over 70% of households supplied with water through municipal water networks for only a few hours every few days due to insufficient power supply. This means people have to rely on private water sources with low health standards and uncensored. In addition, the wastewater treatment plants have had to shorten their treatment cycles, leading to an increase in pollution levels in the wastewater, which is discharged into the sea, thereby polluting the seawater, fish, and beaches. There is also a constant risk of sewage overflow in the streets [11].

2.1.1. Power outages and health in Gaza: exploring the impact

The electricity crisis in Gaza has resulted in a constant state of emergency and is having a profound impact on the health of the population. In the first four months of 2010 alone, 27 people lost their lives and 37 were injured due to incidents related to the use of generators. These incidents included generator explosions, fires, and carbon monoxide poisoning. Tragically, three of the fatalities were children who died from carbon monoxide poisoning, and another three children were killed in a fire while attempting to refuel a generator [12].

2.1.2. Impact of electricity cuts and shortage on health sector

The health sector in Gaza Strip has been severely affected by the ongoing electricity crisis. Critical surgeries and emergency services have been canceled, leading to a decline in the overall health situation. Sanitation and sterilization of equipment have been cut back, and patients are being discharged early from hospitals due to frequent, intermittent power outages. Essential medical equipment such as neonatal incubators, imaging machines, ventilators, and dialysis machines are breaking down due to the lack of a constant power supply. This has forced hospitals and clinics to rely on backup generators, which are not designed to work for prolonged periods and are often damaged as a result. Moreover, replacement parts for these generators are usually unavailable.

In order to minimize risks to patients, hospitals have faced the necessity of postponing certain elective surgeries due to the unreliable nature of generators. Additionally, they employ Uninterruptible Power Supply (UPS) devices to mitigate the potential harm caused by power outages and fluctuations to delicate medical equipment. However, the efficacy of UPS usage has been hindered by limitations imposed by Israeli authorities on the import of required batteries. Power cuts also have adverse effects on clinic refrigeration, posing a threat to vaccine quality.

The United Nations (UN) coordinates the delivery of fuel to run backup generators to ensure the operation of life-saving equipment and water and sanitation services. However, the situation remains challenging as the use of backup generators is not a sustainable solution to the electricity crisis [12, 50].

Water and sanitation

In Gaza, the operational stability of the sewage treatment facility is contingent upon a continuous power supply spanning a two-week treatment cycle. Power disruptions cause notable sewage treatment setbacks, leading to the release of inadequately treated sewage into the surrounding environment. Limited wastewater treatment capacity necessitates the release of 60-80 million liters of incompletely treated sewage daily into the Mediterranean Sea to prevent residential sewage flooding. Additionally, electricity is pivotal for water pumping, serving both domestic needs and irrigation purposes. Yet, the sporadic operation of pumps results in an insufficiency of domestic water supply, consequently raising concerns concerning hygiene and public health. The provision of synchronized electricity is indispensable to ensure water wells function effectively, yet the current reality is that most households receive a mere 5-7 hours of water supply per day. [12].

Electricity impact on psychosocial & mental health status

In GS more than 148,000 women [1] are exposed to gender-based violence (GBV). Protracted humanitarian crisis in Palestine in general and specifically on GS has been worsening all forms of GBV which include sexual violence, domestic violence and child marriage. Many studies showed that there's a negative impact on women's condition due to the increased crisis of electricity and fuel because it is disrupting their daily life especially household tasks where they are exposed to tension, depression and violence [11].

Electricity cuts are worsening the symptoms of mental health patients and delaying their recovery. E.g., it's so difficult for patients suffering from post-traumatic stress disorder - PTSD- and depression to sleep in a complete dark because it can cause a state of severe anxiety. Another example is patients suffering from obsessive compulsive disorder (OCD), they wash their hands excessively and this access to water can be valid to them by electricity, and the cut off in it will cause extreme relapse to them [51].

2.2. Grid Sources for Power Generation in Gaza

The electricity demand in GS is about 550 MW, which increases up to 622 MW during peak summer and winter months [10]. The three primary sources of power generation in GS are Gaza

Power Plant (GPP), Israeli electricity lines, and Egyptian power lines. GPP has a maximum capacity of 140 MW when all four turbines are operational. However, in summer, only three turbines are used, generating around 62 MW [52]. The plant runs on liquid fuel (diesel), and each turbine consumes between 135 000 to 150 000 liters of diesel per day, with an annual cost of $211 306 350/year when it operates at 110 MW. The second source of electricity, Israeli electricity lines, provides 120 MW to the Palestinian Electricity Authority at an estimated cost of $132 887 051/year. The third source, Egyptian power lines, has a capacity of 23 MW but is currently out of service due to constant malfunctions and requires maintenance [15].

2.3. Alternative Solutions to Overcome the Electricity Shortage

The total available electricity in GS from the three main grid sources is 283 MW. So, the percentage of electricity deficiency is about 50%. Residents tended to find alternative solutions to overcome shortage in electricity. The most striking of these solutions are the PV cells, batteries, and street generators.

Online survey was conducted using google forms. The survey had covered 350 households all over GS. The results of the survey are listed in Table 2.1. More than one third of Gazan population received less than 12 hours electricity power from all electricity sources. The majority of population received additional source of electricity power beside the grid sources. 30,3% of the people can afford to pay for the other sources, 59% of them are paying through borrowing, and 26,3% of the people are not capable to pay.

Table 2.1. Statistics of using electricity sources other than grid sources (according to the questionnaire)

Variable	Category / Frequency	Surveyed people	
		Number	%
Number of hours received per day from all electricity sources (Grid sources, SG, PV solar, Batteries)	24	112	32
	12-20	105	30
	6-12	91	26
	< 6	42	12
Alternative sources of electricity supply used	Street Generators	203	58.1
	Batteries	123	35.2
	PV Cells	14	4
	No other sources (Grid only)	10	2.7
Financial capability to afford the cost of other sources	Capable	106	30.3
	Capable through borrowing	152	43.4
	Not Capable	92	26.3

2.3.1. Street generators (SG)

In order to cope with the electricity crisis in GS, residents turned to commercial generators known as Street Generators (SG) for a solution. Since 2009, SGs have become a popular investment for residents who need electricity in their homes, shops, and institutions. As of September 26, 2020, there were approximately 420 commercial generators operating in GS, which sold electricity to over 50 000 subscribers. Together, these generators produce around 40 MW of electricity. On average, a 200 KW electric generator consumes around 45 liters of diesel per hour, which costs $1,4 per liter. If generators work for eight hours per day, they consume about $504. To run all generators for eight continuous hours per day, they consume around $100800/day. The price of electricity from SGs is sold to consumers for $0,86 - $1,18 per kWh, which is six to eight times higher than the normal price per kWh from the Gaza Electricity Distribution Company. The number of SG beneficiaries is estimated to be around 300 000, or 15% of the population of GS. However, SGs pose many health and environmental risks due to the fumes, gases, and noise they emit, and the smoke they produce contains several toxic components that affect human health, such as sulfur oxide, toxic nitrogen oxides, and carbon monoxide [49].

The researcher gathered electricity data for each individual year from 2017 to 2020, sourcing it from UNITED NATIONS Office for the Coordination of Humanitarian Affairs (OCHA) [53]. Subsequently, these collected data points were amalgamated and visually presented in Figure 2.1 and Figure 2.2.

According to data presented in Figure 2.1, the average number of hours of electricity delivery per citizen per month in the Gaza Strip has experienced a significant decrease from May 2017 to October 2018 [53]. This decline can be attributed to three main factors: instability in the Egyptian power lines in 2017 and their complete disruption from March 2018 onwards, frequent breakdowns in the Israeli power lines, and fuel shortages at the Gaza power plant. However, starting from November 2018, there has been an increase in electricity hours due to the stabilization of Israeli power lines and regular fuel supplies to the power plant. In 2020, there has been an improvement in electricity hours compared to previous years, which can be attributed to the availability of additional fuel for the Gaza Power Plant.

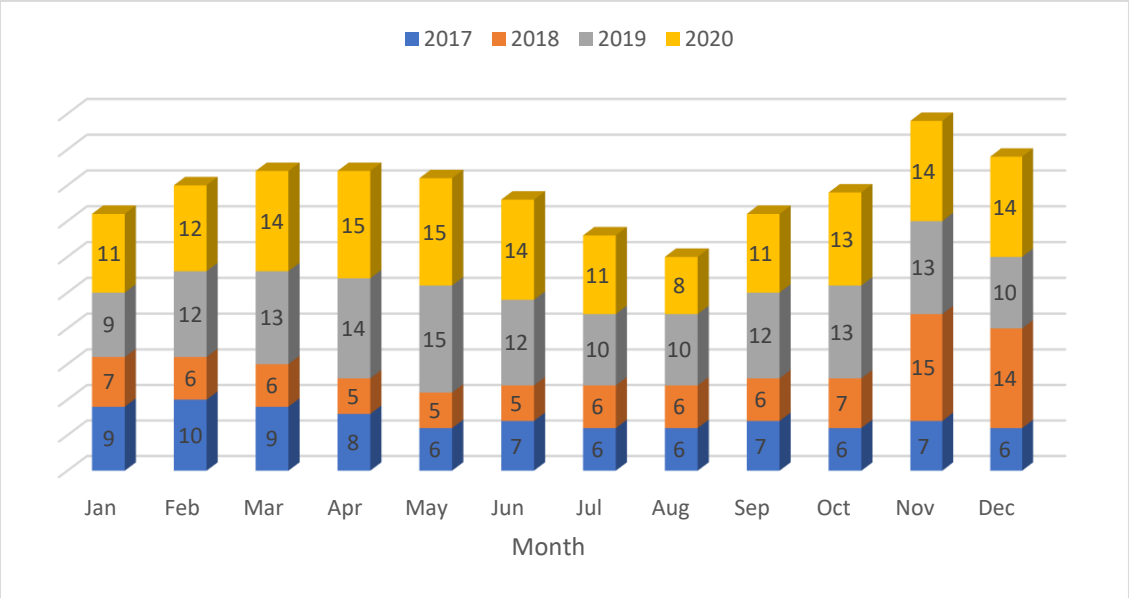

Figure 2.1. Monthly electricity availability (average hours per day)

In Figure 2.2, a comparison is made between the amount of electricity shortage and the amount of electricity available from the three main sources in Gaza Strip, with the average values taken for each season between 2017 and 2020 [53]. On average, there is a shortage of 294 MW of electricity during this period. The largest shortage occurred in spring 2018 when the entry of fuel to the Gaza power plant was prohibited due to political reasons, causing the plant to completely stop in May 2018. Conversely, the smallest gap occurred in spring 2020, even though the available power was not at its highest level. This is because the loads in the summer and winter seasons are higher than those in the spring and autumn seasons.

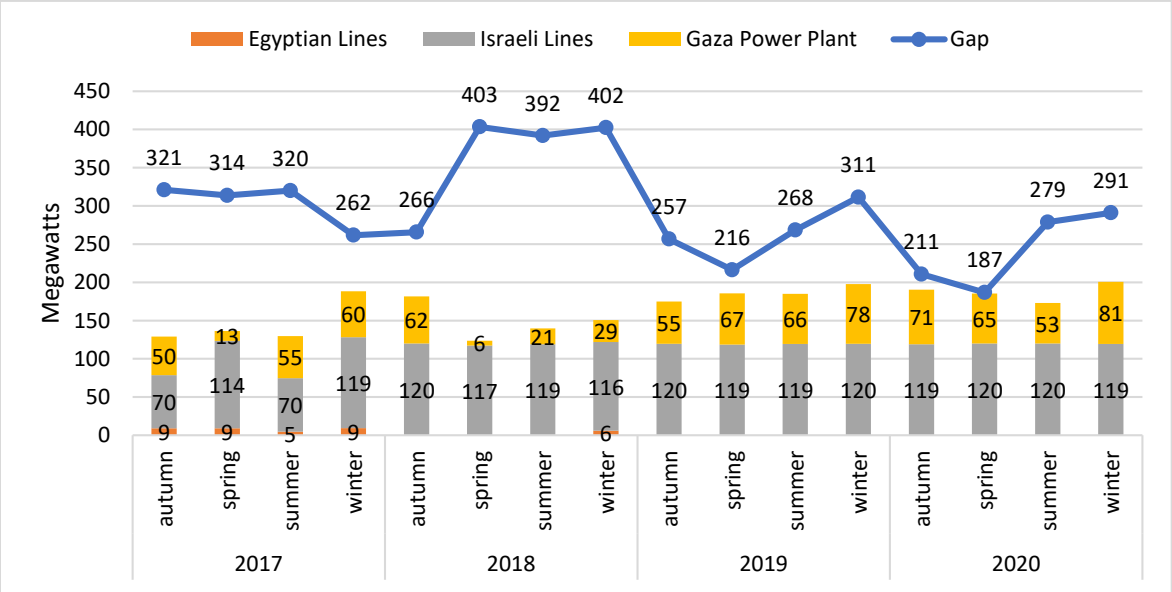

Figure 2.2. Electricity gap in Gaza Strip for 2017-2020

2.4. Potential Renewable Power Technologies in Gaza

The burning of fossil fuels leads to environmental pollution and Climate Change, which is caused by the emission of greenhouse gases such as CO^2. This emission not only threatens the ecological balance of the environment but also depletes the world's reserves of fossil fuels. To address this, renewable and environmentally friendly power sources, like solar energy, wind, biomass, gravity, tides, and geothermal energy are being developed and exploited to preserve resources for future generations. Remarkable advancements have been achieved in enhancing the efficiency and output of renewable energy, alongside notable reductions in operational and maintenance costs. Furthermore, renewable energy is clean, endless, widely available, and does not contribute to environmental pollution.

2.4.1. Wind energy

According to historical data from the European Commission Website, Figure 2.3 illustrates the average wind speed at 10 meters above sea level in GS over five consecutive years from 2012 to 2016 [54]. The data shows that the average wind speed in GS is approximately 2.9 m/s throughout the year and remains relatively constant. This consistency is due to the location of GS, which is a narrow strip next to the sea that is exposed to stable wind patterns year-round [55].

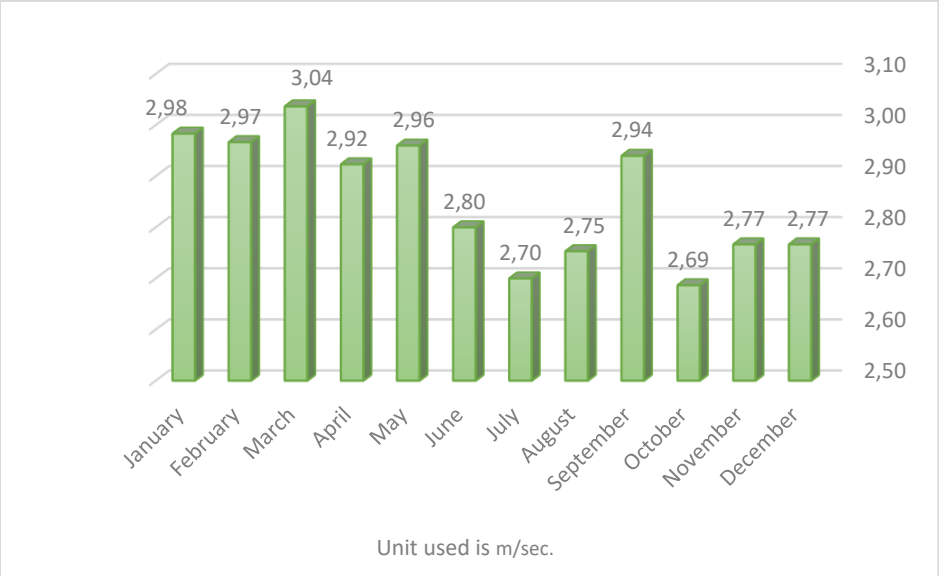

Figure 2.3. Average wind speed in GS

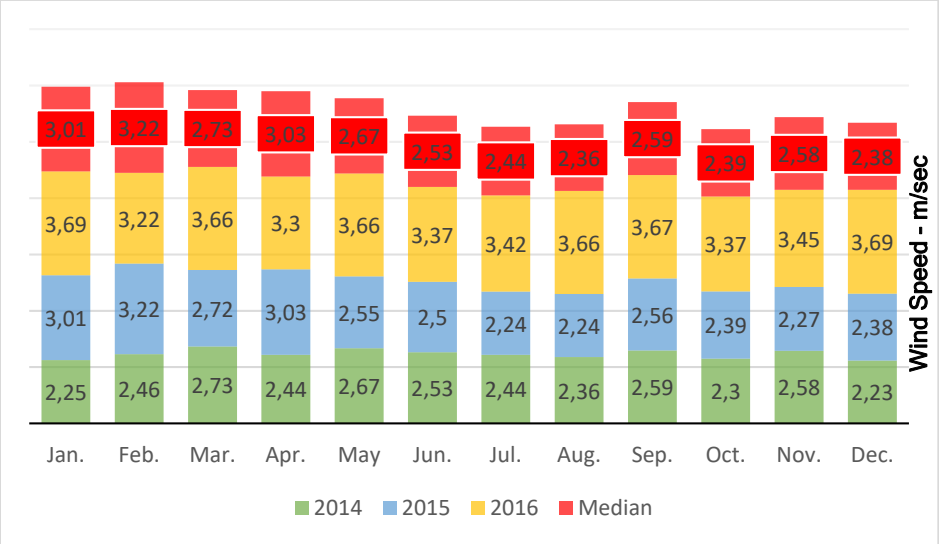

Figure 2.4. Monthly average wind speed over 2014,2015, and 2016 in GS

The graph below Figure 2.5 is called a wind rose diagram. A wind rose is a graphical tool utilized by meteorologists to provide a concise overview of wind speed and direction distribution at a specific location. This graph shows the wind rose diagram for GS. It highlights the wind speeds and directions in Gaza. It is clear that the vast majority of wind directions are in between the west and the south-west. Thus, the south-west direction is approximately the main direction should the wind turbine is a horizontal axis type [56].

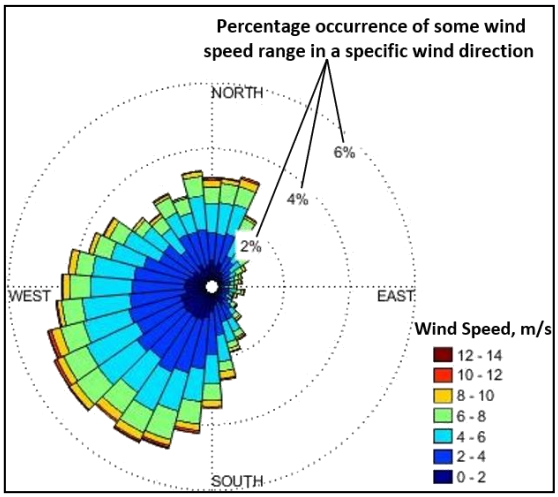

Figure 2.5. Wind Rose Diagram for GS

Wind speed statistical distribution

We used Weibull distribution to analyze the time series data which based on the European Commission Website [54]. The software program used to analyze the data was MATLAB.

Figure 2.6 presents the mean wind speed at different elevations for the Weibull-distributed time series data between 2012 and 2016. Figure 2.7describes the histogram of the average wind speed data over the period 2012-2016 at the elevation of 10 meters [56].

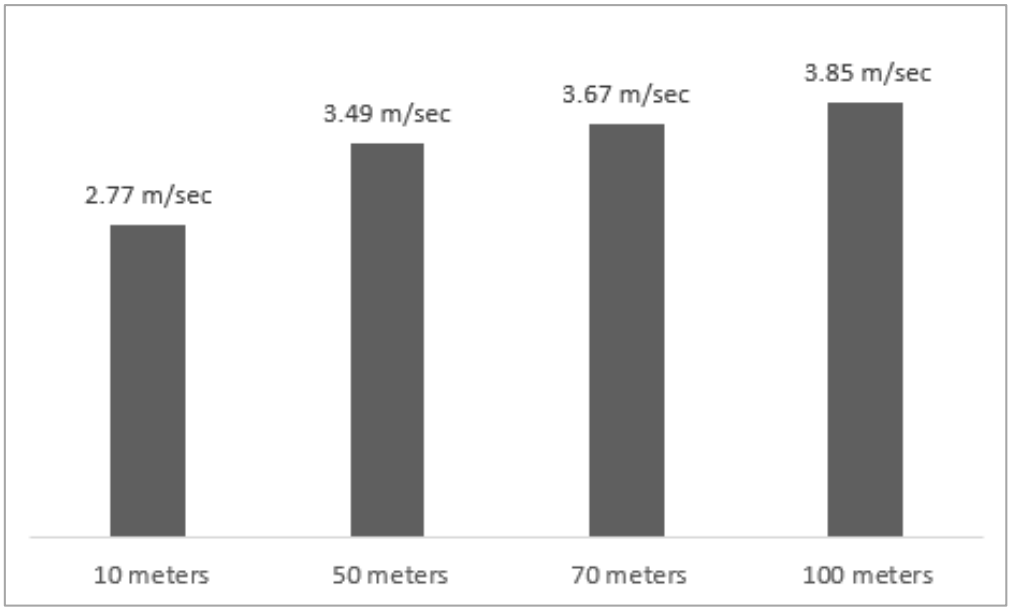

Figure 2.6. Weibull-distributed mean wind speed at different elevations in GS

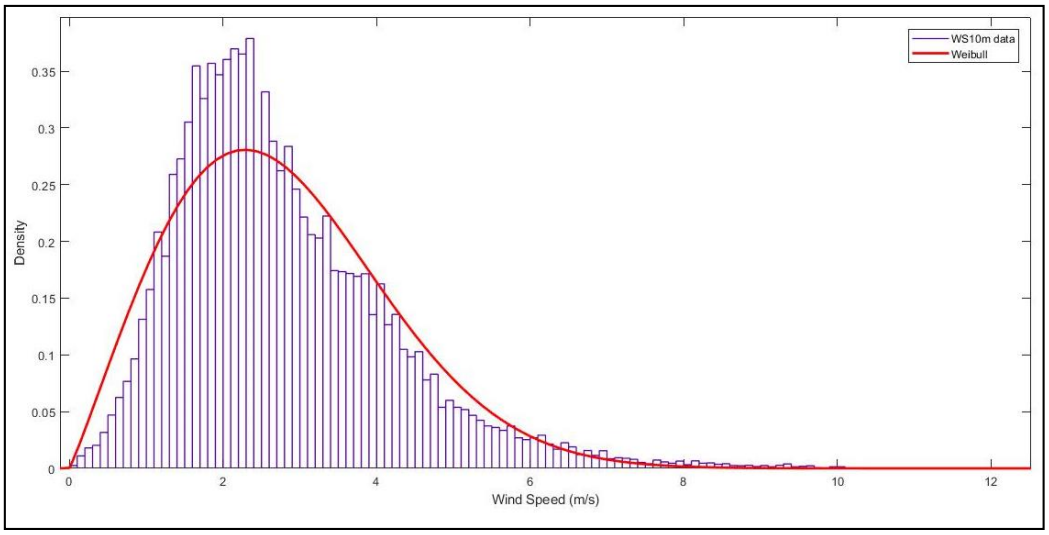

Figure 2.7. Fitted Weibull distribution for the average wind speed over the period 2012-2016 at 10 m elevation

Characteristic curve of wind turbines

A wind turbine generates electricity based on a power chart that represents the relationship between wind speed and the amount of electrical power produced. However, there are limitations to this process. For instance, when wind speeds are below the cut-in speed of the turbine, the blades cannot rotate and no electricity is generated. Moreover, the energy output is directly proportional to the surface of the blades and cubically dependent on wind speed, meaning even a slight change in wind speed has a significant effect on energy output. Typically, the cut-in speed is between 2.7 and 4 m/s. Unfortunately, wind speeds in GS range from 2.77 m/s at 10 m elevation to 3.85 m/s at 100 m elevation, making it infeasible to install wind turbines for electricity generation in GS [57].

To safeguard the integrity of the turbine power train, each wind turbine is equipped with a wind speed limit, known as the rated output speed. This ensures a consistent energy output, referred to as the rated output power. When wind speeds exceed a predetermined threshold beyond this limit, a secondary threshold is triggered, causing the turbine to halt operation to prevent any potential damage. [57].

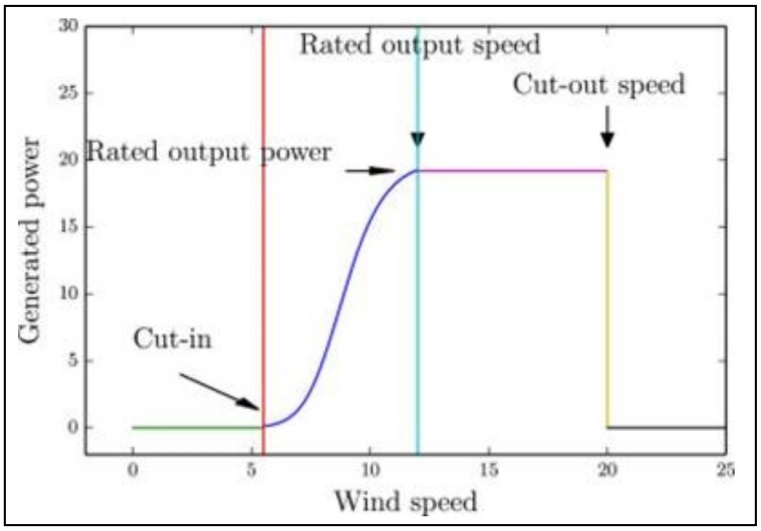

Figure 2.8. Characteristic curve of wind turbines

2.4.2. Wave energy

Extracting energy from sea waves has great potential for renewable energy. This method offers several advantages over other forms of energy generation such as solar or wind energy. Wave energy has a higher energy density compared to these other sources, meaning that more energy can be extracted per unit area [58]. Wave power devices can also generate power up to 90% of the time, which is significantly higher than wind turbines and solar panels [59].

Despite these advantages, there are some challenges facing the use of wave energy. One major challenge is converting slow, random, and high-force oscillatory motion into useful motion. The power levels of waves vary depending on their height and period, which can also make it difficult to position devices optimally. Additionally, harsh weather conditions can make it difficult for wave energy devices to withstand the force of the waves [59].

In the port of Gaza, there is a research wave power station with an output power of almost 10 KW, see Figure 2.9 and Figure 2.10 [60].

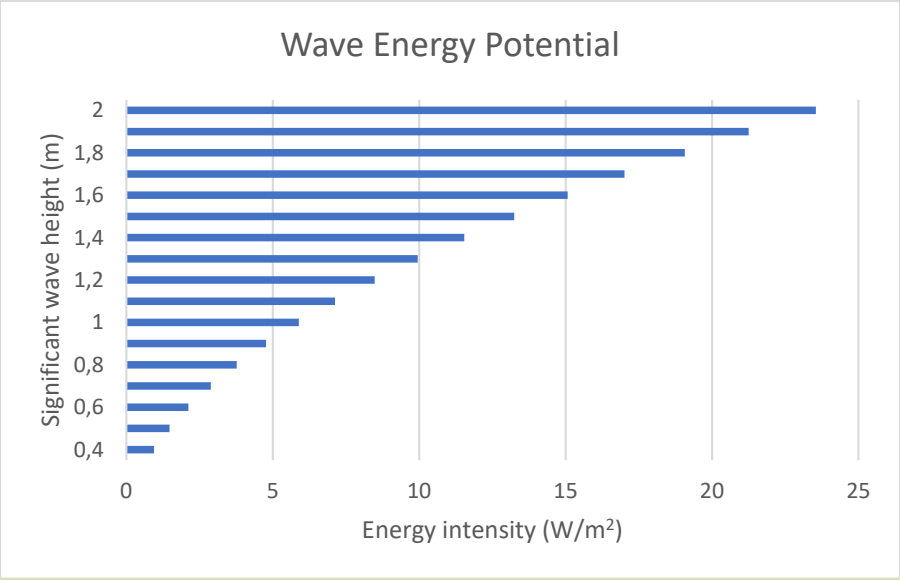

Figure 2.9. Energy intensity per wave hight.

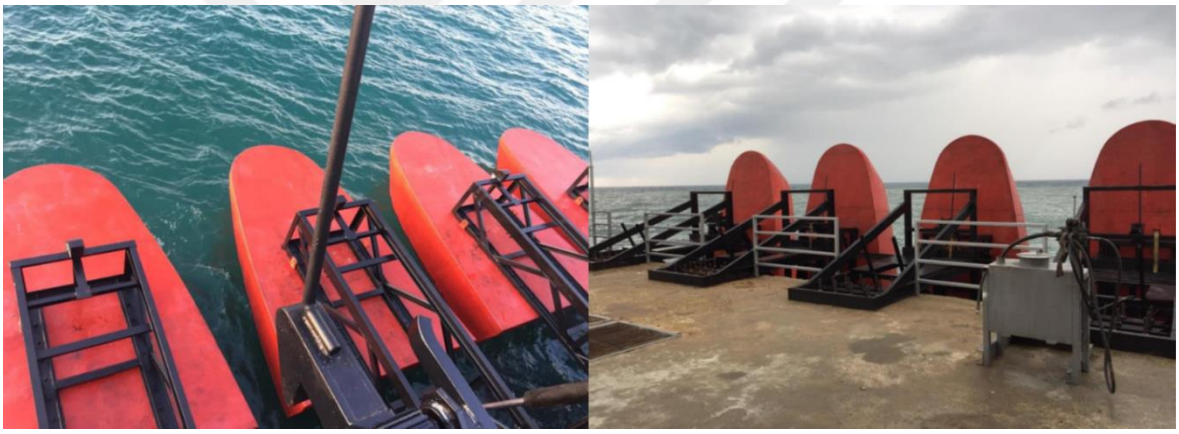

Figure 2.10. Wave to Energy station in operation (left) and in emergency mode (right)

2.4.3. Solid waste to energy

In GS, the average solid waste production is approximately 0.9 kg/day/capita, which results in an estimated 1800 tons/day of waste. The majority of municipal waste is composed of organic matter (50%), plastic (17%), and paper/cardboard (11%). One approach to extracting value from solid waste is through incineration, which can generate electricity. On average, 500 to 600 kWh of electricity per ton of waste incinerated can be produced. Therefore, incinerating the 1,800 tons of waste produced daily in GS could generate approximately 900 MWh of electrical energy. This implies that a power plant with a rated power of approximately 100 MW could be established based solely on incinerating solid waste in GS [61].

2.4.4. Solar energy

Scholarly investigations underscore that Palestine holds considerable solar energy capacity, owed to its noteworthy annual solar radiation average of around 5.4 kilowatt-hours per square meter per day on a horizontal plane, complemented by an annual count of approximately 3000 hours of sunshine. Additionally, the solar radiation incident on a horizontal plane displays fluctuations, spanning from 2,63 kilowatt-hours per square meter per day in December to 8,4 kilowatt-hours per square meter per day in June.

Figure 2.11 reports the data of the monthly average solar radiation in GS. The data in Figure 2.11 are based on the European Commission Website. We can see a clear trend in both months, June and July with an average radiation of around 320 kWh/m^2 per month [54].

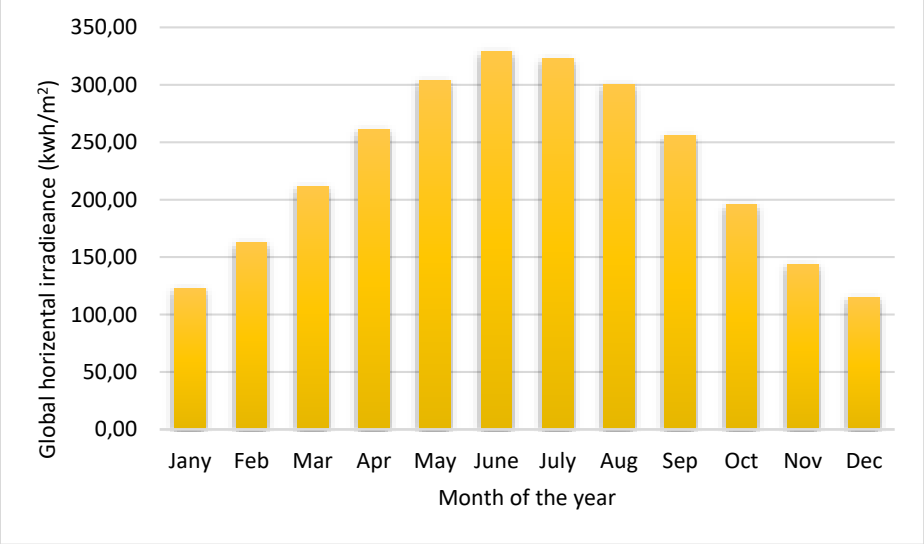

Figure 2.11. Montly average solar radiation in GS

The high solar radiation in Palestine, presents a great opportunity for utilizing solar energy for various applications such as water heating, water pumping, crop drying, water desalination, and electrification of remote areas.

The calculation for estimating the electricity output of a photovoltaic (PV) system worldwide can be expressed by the formula:

$$E = A \times r \times H \times PR \quad (2.1)$$

In this context, the symbol E stands for the energy generated, expressed in kilowatt-hours, while A signifies the overall area of the solar panels measured in square meters. The symbol r is indicative of the system's efficiency, denoted in percentage. The symbol H stands for the annual mean solar radiation received by tilted panels, factoring out any shading effects. Additionally, PR is employed to denote the performance ratio, a value that usually spans between 0.5 and 0.9, with a standard default setting of 0.75 [62].

The performance ratio (PR) value, an important metric in assessing the efficiency of photovoltaic systems, depends on various factors such as the site conditions, technology employed, and system sizing. Detailed analysis reveals specific losses that contribute to the PR value. These losses include inverter losses (4% to 10%), temperature losses (5% to 20%), DC cables losses (1% to 3%), AC cables losses (1% to 3%), losses at weak radiation (3% to 7%), and losses due to dust and snow (2%) [Reference]. Understanding these factors and their associated losses is crucial for optimizing the performance of photovoltaic systems and achieving maximum energy output.

Based on calculations and the average annual radiation of approximately 2723 kWh/m^2 in Gaza, it is determined that a photovoltaic (PV) power plant with an efficiency of 15% and an area of 5 km^2, representing 1.37% of the total area of Gaza Strip (365 km^2), can generate 1531 MWh of electricity using Eq (2.1).

3. FUNDAMENTALS OF SOLAR RADIATION

The human directly exploited the energy of the sun since ancient times in his simple life in heating and obtaining fire and for drying plant and animal foods, then this exploitation developed into developing mechanisms to collect solar energy and make use of it in heating water, heating, drying crops and cooking, and development continued by raising the efficiency of these complexes Solar energy by increasing the effectiveness of absorbing solar radiation in the form of heat on the one hand and increasing thermal insulation, on the other hand, then the exploitation of solar energy developed into the production of electricity, as solar energy was converted into electricity either by photovoltaic conversion (PV) by solar cells or by thermal conversion by concentrated solar power plants (CSP) [63].

Solar energy can be exploited by three methods: photovoltaics, solar heating & cooling (SHC), and concentrating solar power (CSP). In Photovoltaics, the electricity is generated directly from the sun rays by the mean of electronic process; application of Photovoltaics can be small such as calculators and road signs or big like large commercial businesses. In the other two methods (SHC & CSP), the heat provided by the sun is used to heat water in SHC systems, or to operate turbines to generate electricity in CSP systems [63].

3.1. Sun and Earth Relationship

Given that solar radiation from the sun undergoes alterations due to interactions with the Earth's atmosphere (entailing absorption, diffusion, and reflection) and recognizing that the atmosphere has an average thickness of 10 kilometers, the introduction of the concept of Solar Constant (I_o) has become essential. This term pertains to the power density arriving at the Earth's surface, accounting for the effects of atmospheric interactions. The quantification of energy per unit area of a surface orthogonal to the direction of radiation propagation has been achieved through diverse instruments and experimental methods. The outcome for the Solar Constant, Io, is established as 1353 watts per square meter (W/m2), accompanied by an estimated uncertainty of ±1.5%. However, The World Radiation Center has opted for a value of 1367 W/m^2 with a margin of uncertainty of 1%. Presently, the most recent and updated value for I_o is affirmed as 1367 W/m^2 [63].

3.2. Solar Time

Local solar noon time (LST) is the time when the sun crosses the local meridian, and it usually not coincide with 12:00 o'clock. Hence, apparent solar time (AST) is the one that must be used in solar energy calculation to express the time of the day. Two corrections must be made to convert LST to AST: Equation of time (ET) and longitude correction [64].

3.2.1. Equation of time

The values of the ET as a function of the day of the year (N) can be derived roughly from the following equations [64]:

$$\mathrm{ET} = 9{,}87\sin(2\mathrm{B}) - 7{,}53\cos(\mathrm{B}) - 1{,}5\sin(\mathrm{B}) \tag{3.1}$$

$$B = (N - 81) * \frac{360}{364} \tag{3.2}$$

In this context, the symbol N represents the day number that corresponds to a specific date. This value is delineated as the count of days that have transpired in a given year until the specified date, commencing from 1 on 1 January and culminating at 365 on 31 December.

3.2.2. Longitude correction

The reference time of the clock is established in relation to a designated meridian situated near the midpoint of the time zone, or from the prime meridian located at Greenwich, holding a longitude value of 0. To synchronize with the local solar time, an adjustment factor of 4 * (Standard longitude [SL] - Local longitude [LL]) needs to be applied to the standard clock time. This correction is necessitated by the sun's traversal of 1 degree of longitude taking approximately 4 minutes. This correction factor remains constant for a given longitude. To apply this correction, a particular convention must be adhered to: when the location is situated to the east of the designated meridian, the correction is added to the clock time, while it is subtracted if the location lies to the west. When quantifying the Arabian Standard Time (AST), the general equation to be employed is [65]:

$$\mathrm{AST} = \mathrm{LST} + \mathrm{ET} \pm 4(\mathrm{SL} - \mathrm{LL}) - \mathrm{DS} \tag{3.3}$$

If the position is east of Greenwich, the Eq (3) sign is minus (-), and the sign is plus (+) if it is west. Daylight-saving time (DS) must be subtracted from the LST if it is used, Where DS value is either 0- or 60-min. DS term depends on whether or not daylight-saving time (usually between the end of March and the end of October) is in effect. Typically, this term from this equation is ignored and considered only if the calculation is within the DS duration.

In our case, the values of SL and LL can be obtained by:

Standard longitude (SL) for Palestine = 35,227163 East

Local longitude (LL) for Gaza = 34,4667 East

Therefore, the longitude correction is = - 4 (35,227163 – 34,4667) = - 3,041852 min. Thus, Eq. (3.3) can be written as:

$$\mathrm{AST} = \mathrm{LST(HOUR)} + \mathrm{ET(MIN)} - 3{,}041852\mathrm{(MIN)} \qquad (3.4)$$

3.3. Solar Angles

Every 24 hours, the earth completes one rotation about its axis, and every (approximately) 365,25 days completes one revolution around the sun, in an elliptical manner, as shown in Figure 3.1. However, since the earth's orbit eccentricity (e) is very small (0,01673) the orbit is almost circular. At January 3, the distance between the sun and earth is the shortest, and the point where this happened is called perihelion, in the other hand, aphelion is the point where the distance is the longest, which happen at July 4 [65].

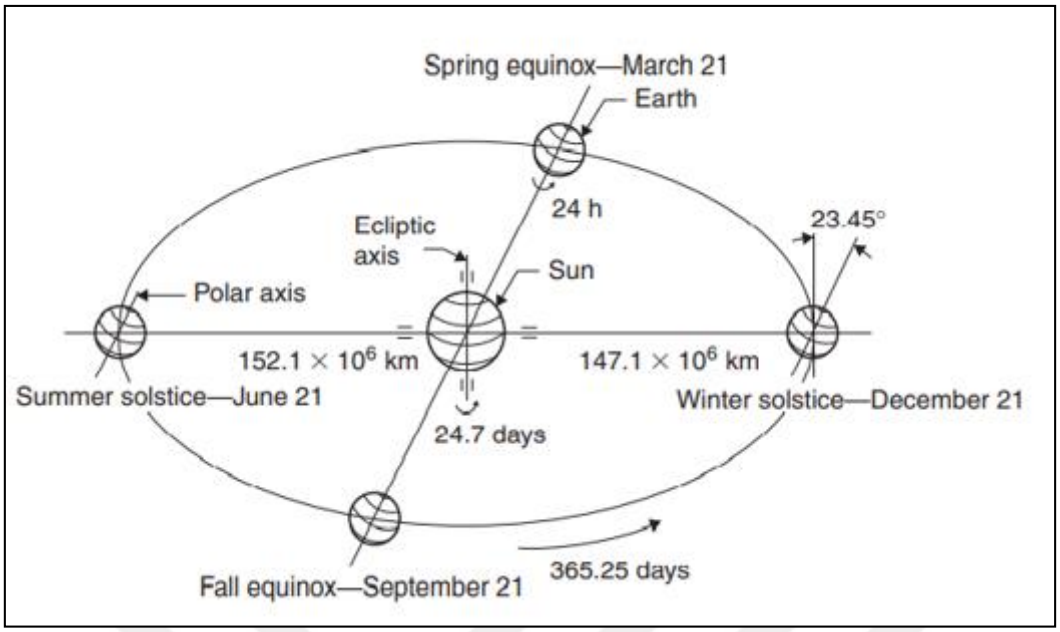

Figure 3.1. Annual motion of the earth about the sun

Accurate anticipation of the sun's location at a specific time of day and year is imperative. The sun's position with respect to the observer is characterized by two fundamental attributes: Solar Altitude (α) and Solar Azimuth (z). Prior to determining Altitude and Azimuth, it is essential to establish two additional parameters: Solar Declination (δ) and Hour Angle (ω).

3.3.1. Declination angle

The angular separation between the path of sunlight rays originating from the sun and their projection onto the equatorial plane is referred to as the Declination Angle, as visually depicted in Figure 3.2. This angle takes on a positive value in the northern hemisphere during summer and a negative value in the southern hemisphere. The fluctuation of the solar declination over the course of a year is demonstrated in Figure 3.3. A reasonable approximation for the declination angle (δ) can be computed using the Eq. (3.5) [65]:

$$\delta = 23{,}45 \sin[\frac{360}{365}(284 + \mathrm{N})] \quad (3.5)$$

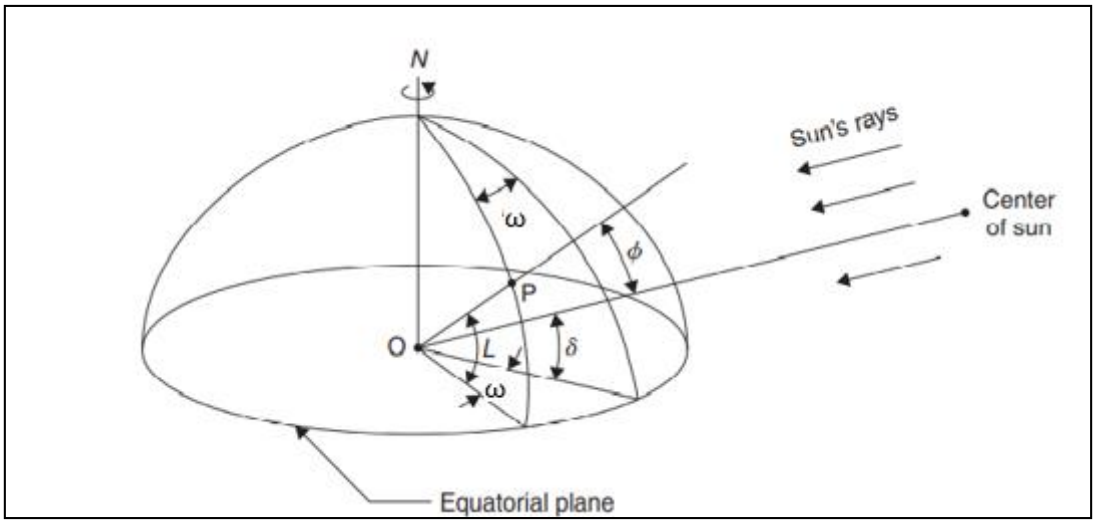

Figure 3.2. Description of latitude, solar declination, and hour angle

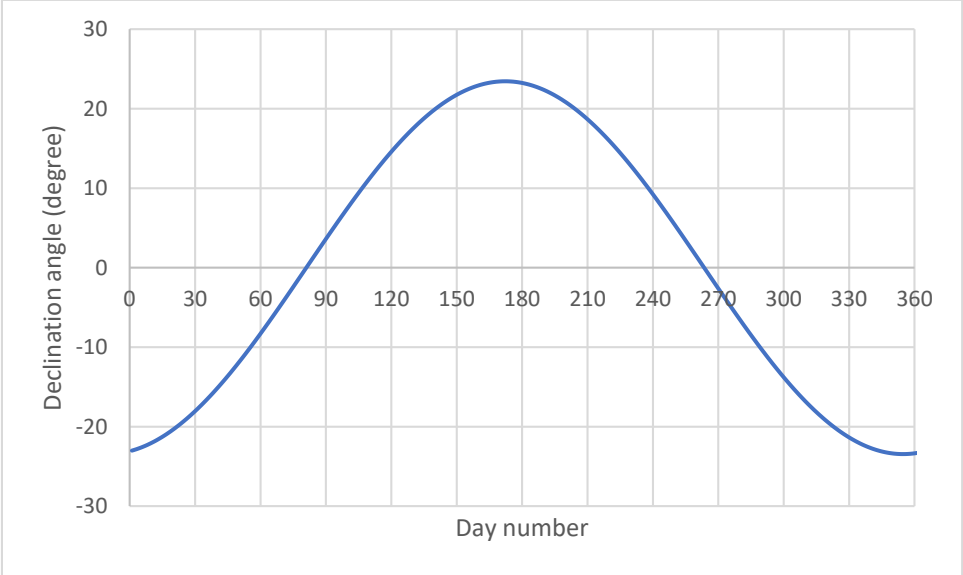

Figure 3.3. Declination angle of the sun

3.3.2. Hour angle

The angle at which the Earth rotates to align the meridian of a specific location directly beneath the sun is referred to as the Hour Angle (ω), as depicted in Figure 3.2. This hour angle corresponds to the angular separation between the projection of point O on the plane of the observer and the projection of the Earth-Sun line. Notably, the hour angle assumes a value of zero at local noon (when Arabian Standard Time, AST, equals 12, resulting in ω = 0). Furthermore, each 15 degrees of longitude corresponds to a one-hour difference. The calculation of the hour angle in degrees is facilitated by the Eq. (3.6) [65]:

$$\omega = \pm 0{,}25\ (\text{Quantity of minutes from the local solar noon.}) \quad (3.6)$$

In this context, the positive symbol denotes the afternoon hours, while the negative symbol signifies the morning hours.

Or the hour angle can be calculated approximately by the Eq. (3.7) [65]:

$$\omega = 15 * (\text{AST} - 12) \quad (3.7)$$

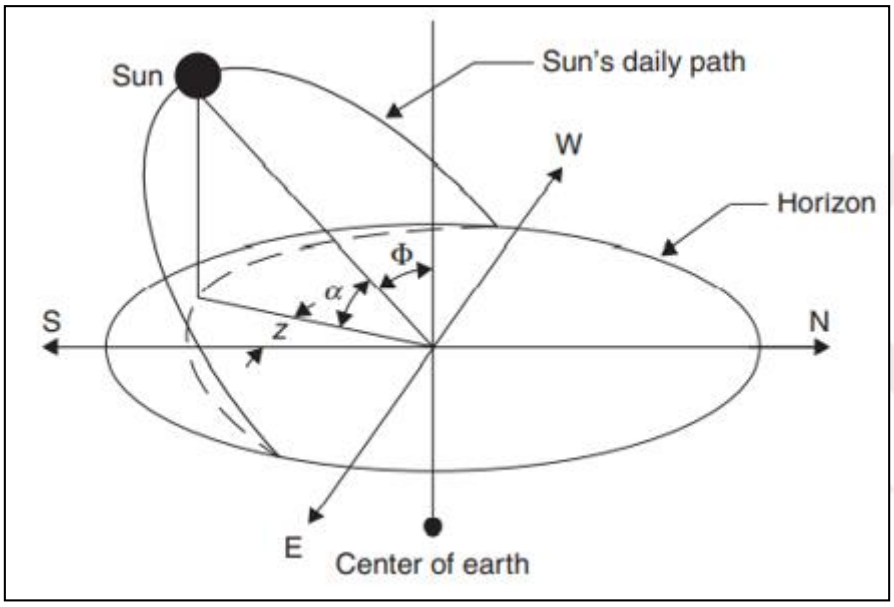

Figure 3.4. The sun's apparent regular journey across the sky from sunrise to sunset

3.3.3. Solar altitude angle

The angle formed between the sun's rays and the horizontal plane is known as the solar altitude angle (α), illustrated in Figure 3.4. The solar altitude angle is closely tied to the solar zenith angle (ϕ), which represents the angle between the sun's rays and the vertical axis.

$$\phi + \alpha = \frac{\pi}{2} = 90° \quad (3.8)$$

The mathematical representation for the solar altitude angle is as follows [66]:

$$\sin(\alpha) = \cos(\phi) = \sin(\text{L})\sin(\delta) + \cos(\text{L})\cos(\delta)\cos(\omega) \quad (3.9)$$

Where L signifies the local latitude, which defines the angle between a line extending from the Earth's center to the specific location and the equatorial plane. Positive values are attributed to locations situated north of the equator, whereas negative values correspond to those located southward. In the case of Gaza, the local latitude (L) is determined as 31.5 degrees North.

3.3.4. Solar azimuth angle

The solar azimuth angle (z) is the angle between the projection of the sun rays on the horizontal plane and, the true south for Northern Hemisphere, or the true north for the Southern Hemisphere [66].

$$\sin(z) = \frac{\cos(\delta)\sin(\omega)}{\cos(\alpha)} \tag{3.10}$$

3.3.5. Incidence angle

The solar incidence angle (θ) signifies the angle between the sun's rays and the axis that is perpendicular to the surface being struck by the sun's rays. Notably, for the horizontal plane, the solar incidence angle is equivalent to the zenith angle (ϕ), as depicted in Figure 3.5. This incidence angle is computed using the formula [65]:

$$\begin{aligned}\cos(\theta) = {} & \sin(L)\sin(\delta)\cos(\beta) - \cos(L)\sin(\delta)\sin(\beta)\cos(z_s) \\ & + \cos(L)\cos(\delta)\cos(\omega)\cos(\beta) \\ & + \sin(L)\cos(\delta)\cos(\omega)\sin(\beta)\cos(z_s) \\ & + \cos(\delta)\sin(\omega)\sin(\beta)\sin(z_s)\end{aligned} \tag{3.11}$$

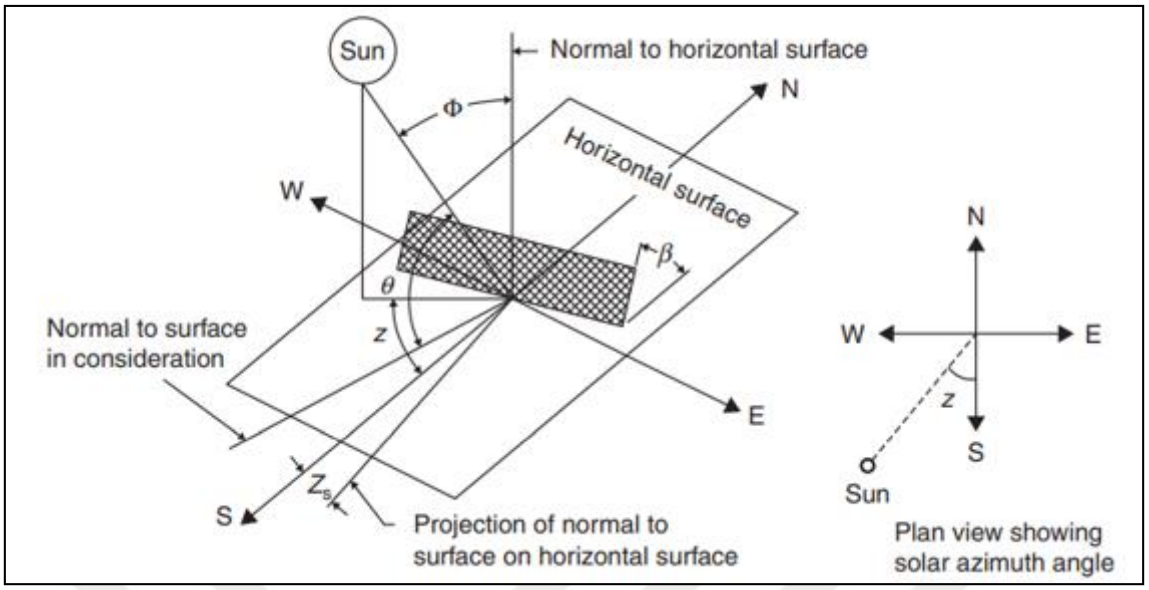

Figure 3.5. Diagram of solar angles

In this context, β represents the surface tilt angle measured from the horizontal plane, while Z_s stands for the surface azimuth angle. The surface azimuth angle is defined as the angle between the normal to the surface and the true south direction, with a positive designation assigned to angles westward from the south direction.

The incidence angle for full tracking

The angle of incidence (Θ) becomes zero when utilizing a two-axis tracking mechanism. In this scenario, the surface is consistently adjusted to directly face the sun at all times.

3.4. Sunrise with Sunset Times and Day Length

The solar altitude equals zero when the sun rises and set. the solar noon is at the middle of the sunrise and sunset hours. For that, the day length is twice the sunset hour. The length of the day in hours is [66]:

$$Day\ length = \frac{2}{15} cos^{-1}[-\tan(L)\tan(\delta)] \tag{3.12}$$

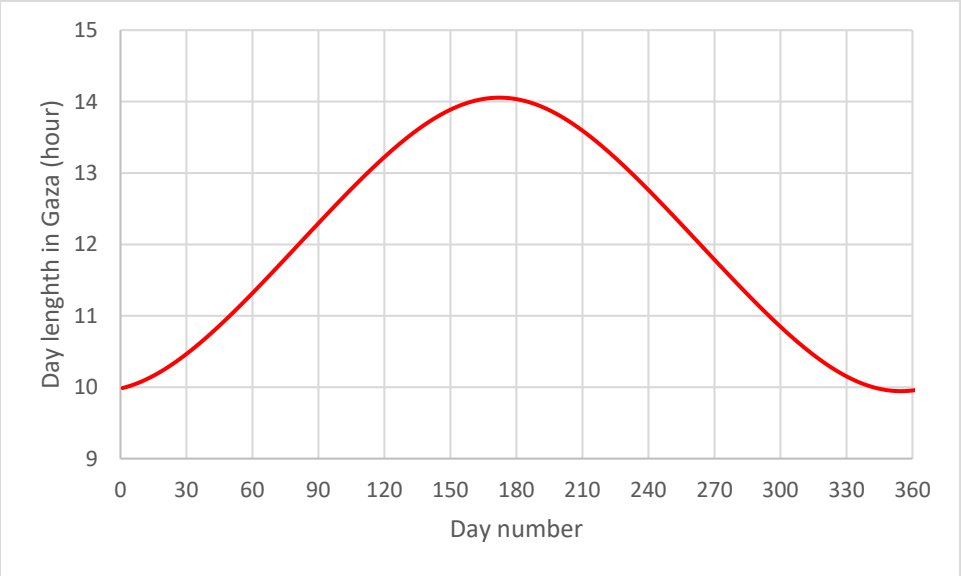

Figure 3.6. Day length in Gaza city

3.5. Extraterrestrial Solar Radiation

The solar radiation intensity at the outer edge of the Earth's atmosphere is approximately 1400 watts per square meter (W/m²) at the outer edge of earth on January 3 (the sun is closest), and about 1330 W/m^2 on July 4 (the sun is farthest).

The extraterrestrial radiation, denoted as Ion, fluctuates within the confines of these boundaries, as depicted in Figure 3.7., encompassing a range of 3.3%. The extraterrestrial radiation (I_{on}) can be calculated by Eq. (3.13) [66]:

$$I_{on} = I_0 \left[1 + 0{,}033 \cos\left(\frac{360 * N}{365}\right)\right] \tag{3.13}$$

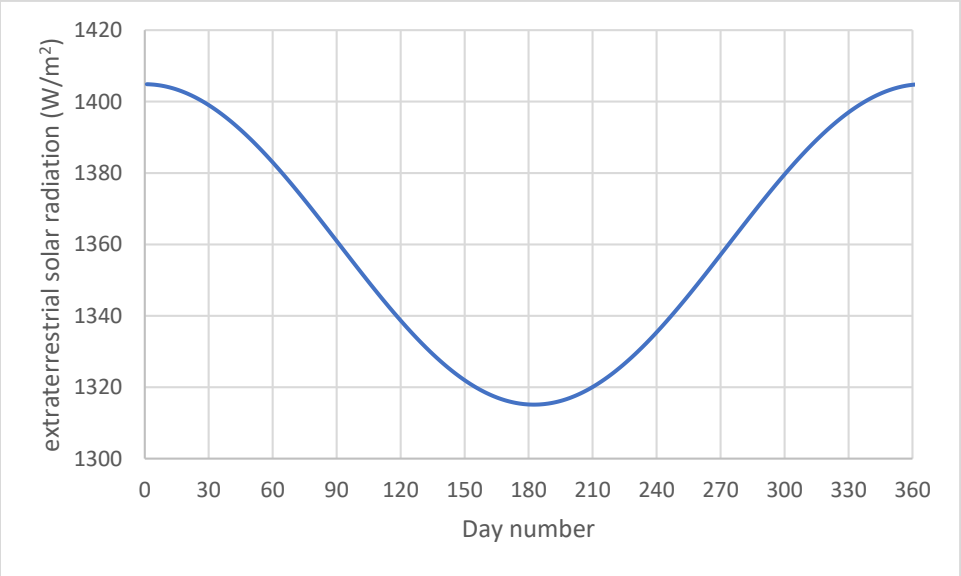

Figure 3.7. Daily variation of extraterrestrial solar radiation

3.6. Solar Radiation at Earth

A portion of solar radiation traverses the atmosphere, with some being reflected, some absorbed by air and water, and others scattered. A fraction of this radiation ultimately reaches the Earth's surface, referred to as beam radiation. Furthermore, there exists scattered radiation from the sky, recognized as sky diffuse radiation.

Atmospheric extinction of solar radiation

The Atmospheric Extinction of Solar Radiation pertains to the extent of solar radiation absorbed, scattered, and reflected by the atmosphere prior to its arrival at the Earth's surface. As the extraterrestrial solar radiation experiences attenuation upon entry into the planet's atmosphere, the aggregate solar radiation received at the Earth's surface can be expressed as [65]:

$$I_{TN} = I_{on} * \exp\left[-\frac{P_L}{P_0} * \frac{B}{\sin(\alpha)}\right] \tag{3.14}$$

Where, $\frac{P_L}{P_0}$ is the pressure ratio at location concerned relative to the standard atmospheric pressure, B is the atmospheric extinction coefficient, given as:

$$B = 0{,}175 * [1 - 0{,}2 * \cos(0{,}93 * N)] - 0{,}0045 * [1 - \cos(1{,}86 * N)] \quad (3.15)$$

$$\frac{P_L}{P_0} = \exp(-0{,}0001184 * H_{alt}) \quad (3.16)$$

The total solar beam radiation at the earth's surface I_B for fix plane is represented as:

$$I_B = I_{TN} * Cos\,(\phi) \quad (3.17)$$

As was mentioned before the angle of incidence is equal to zero (Θ = 0) for a two-axis tracking system, but even if the angle of incidence is zero, the Beam Radiation on the Collector will not necessarily be equal to The Atmospheric Extinction of Solar Radiation.

The Atmospheric Extinction of Solar Radiation refers to the amount of solar radiation that is absorbed, scattered, and reflected by the atmosphere before it reaches the Earth's surface. It is affected by factors such as the composition and density of the atmosphere, as well as weather conditions such as clouds, haze, and pollution.

Conversely, the Beam Radiation on the Collector specifically pertains to the direct component of solar radiation that directly impacts the collector's surface. Interestingly, even in scenarios where the angle of incidence is zero, the quantity of beam radiation reaching the collector surface remains contingent on atmospheric factors, including cloud cover and atmospheric extinction.

If the angle of incidence is zero and the collector is perfectly aligned with the sun, then the Beam Radiation on the Collector would be equal to the Atmospheric Extinction of Solar Radiation. This is because all of the direct solar radiation is being collected by the surface of the collector, without any loss due to oblique angles of incidence.

The composition and density of the atmosphere, as well as weather conditions, can affect the amount of solar radiation that reaches a collector. So, the primary factors that affect the transmission of solar radiation through the atmosphere are:

Air Mass: The amount of atmosphere the solar radiation must pass through to reach the collector. The air mass is affected by the angle of the sun in the sky and the altitude of the collector location.

Aerosols: Small particles in the atmosphere that scatter and absorb solar radiation. Aerosols can be natural (such as dust and sea salt) or anthropogenic (such as pollution).

Water Vapor: Water vapor in the atmosphere can absorb and scatter solar radiation.

Cloud Cover: Clouds can reflect, scatter, and absorb solar radiation, reducing the amount of radiation that reaches the collector.

Ozone: Ozone in the upper atmosphere absorbs solar radiation, protecting the Earth from harmful ultraviolet radiation. However, ozone in the lower atmosphere can contribute to the absorption and scattering of solar radiation.

To estimate the effect of these factors on the amount of solar radiation that reaches a collector, various models and tools can be used. One widely used tool is the (NREL) Solar Radiation and Climate Experiment (SOLRAX) model, which uses satellite data and ground-based measurements to estimate the amount of solar radiation that reaches a specific location. Other models include the SMARTS and MODTRAN (MODerate resolution atmospheric TRANsmission) models.

It's important to note that these models are not perfect and may have limitations or uncertainties. Therefore, it's always recommended to validate model results with ground-based measurements whenever possible.

In this study, the above-mentioned equations were utilized to calculate The Atmospheric Extinction of Solar Radiation. However, due to the challenges associated with estimating the factors influencing the transmission of solar radiation through the atmosphere, the data provided by the (NREL) for Beam Radiation on the Collector in Gaza Stripe will be relied upon.

For instructions on utilizing the equations in calculations, please consult Appendix A.

4. NOVEL SYSTEM DESIGN

Noval system design with parabolic dish and high concentration solar cell for electricity generation and thermal utilization

The main idea of this research is to use solar energy to generate electricity for a small house and take advantage of thermal energy to heat water for daily use or heating. High concentration photovoltaic cells from Azurspace will be used, with an estimated cell efficiency of about 32%. And because the sun's rays will gather and focus on the cell by the collector, this will raise the cell's temperature, so there must be a cooling system. The water used to cool the CPV cell will be used to heat the house or for daily use as shown in Figure 4.1 (this figure was built by the researcher.

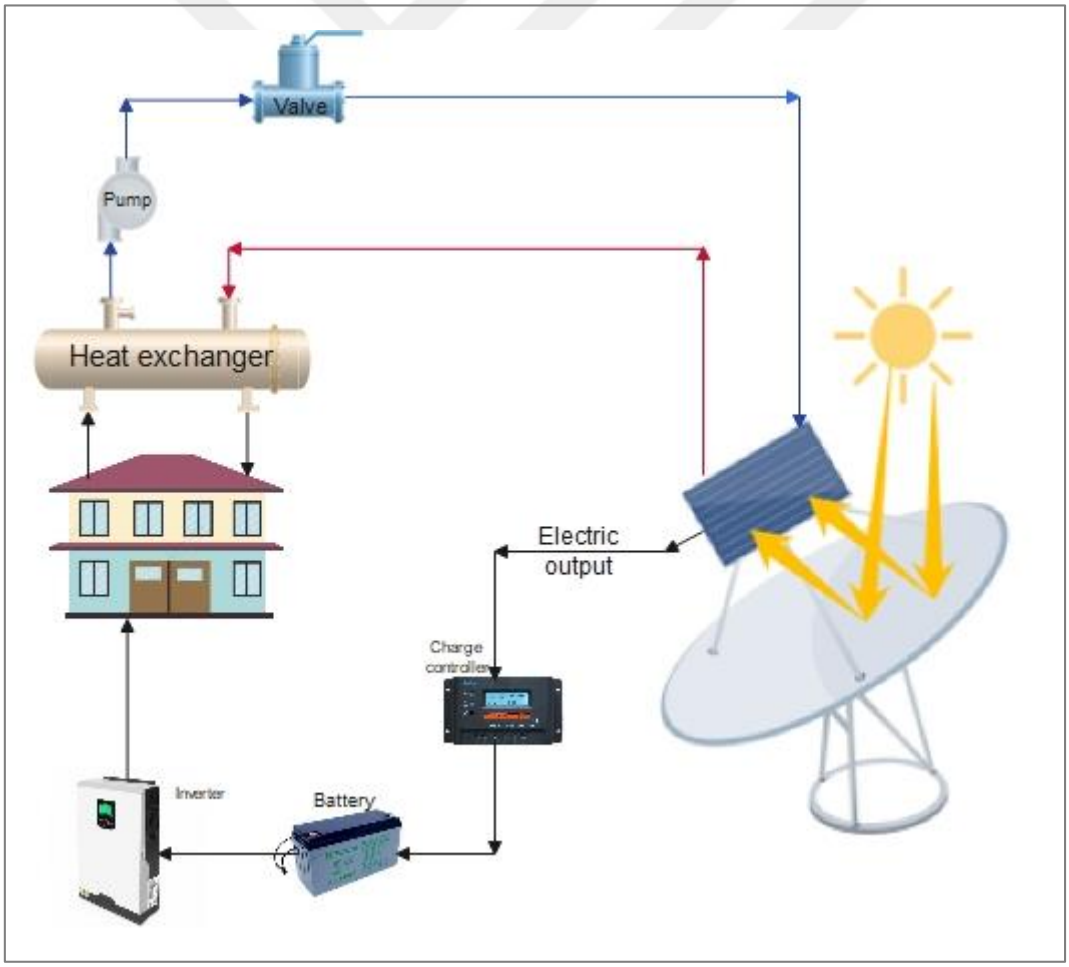

Figure 4.1. Concentrating photovoltaic thermal system for small house

The primary emphasis of this investigation will be directed towards the high concentration solar cell and the parabolic solar collector, with exclusion of the remaining system components, including but not limited to the inverter, valves, pump, heat exchanger, and related elements. In Sections 0 and 0 of the manuscript, a comprehensive analysis and in-depth exploration of the high concentration solar cell and the parabolic solar collector are presented, providing a thorough understanding of their respective mechanisms, characteristics, and operational principles. These sections delve into the intricate details, elucidating the underlying concepts and highlighting the key features of each technology.

4.1. High Concentration Solar Cells

High concentration solar cells (HCSCs) are advanced photovoltaic devices designed to achieve higher efficiency by utilizing concentrated sunlight. Unlike conventional solar cells, which convert sunlight directly into electricity, HCSCs employ optical systems, such as lenses or mirrors, to concentrate sunlight onto a smaller area of the solar cell.

Advantages of high concentration solar cells

- Increased Efficiency: By focusing sunlight onto a smaller cell area, HCSCs can achieve higher energy conversion efficiency compared to conventional solar cells. The concentration of sunlight allows for more photons to be absorbed by the active material, resulting in improved electrical output.
- Reduced Material Usage: Concentrating sunlight onto a smaller area allows for the use of fewer semiconductor materials, reducing the overall cost of the solar cell.
- Lower System Cost: The use of concentrator optics can enable the reduction of expensive semiconductor material, making HCSC systems more cost-effective, especially for large-scale installations.
- Space Efficiency: HCSCs require less land area compared to conventional solar panels to generate the same amount of electricity, making them suitable for installations with limited space.
- Multifunctionality: The concentrated solar energy collected by HCSCs can be used not only for electricity generation but also for various thermal applications, such as heating water or space heating.

Some of the prominent companies in the field of high concentration solar cells

1. AzurSpace Solar Power GmbH.
2. Solar Junction (Acquired by Siva Power).
3. Suncore Photovoltaic Technology Co., Ltd.

4.2. The Advanced Dense Array Module (ADAM)

In this study the Advanced Dense Array Module (ADAM) will used. It developed by AZUR SPACE is specifically designed for application in High Concentration Photovoltaic (HCPV) receivers that employ reflective optics, such as parabolic mirrors. The module consists of a two-dimensional array of high-efficiency solar cells integrated onto a cooling element. Bypass diodes are incorporated to ensure electrical protection of the solar cells against reverse voltage. The solar cells and diodes within the ADAM module are interconnected, with the sole provision for electrical connection to the external circuitry and the cooling system to be made by the system integrator. To achieve the desired thermal management, the module requires an active liquid cooling system. Furthermore, it is crucial to provide adequate protection to the ADAM module against environmental factors such as water, humidity, dust, pollution, and other potential influences. More details about the ADAM module can be found in Table 4.1 and Table 4.2 and in Figure 4.2 [67].

Table 4.1. Design and mechanical data of ADAM module

Base Material for Solar Cells	GaInP/GaAs/Ge on Ge substrate
Base Material for Cooling	Copper and AlN Ceramic
Anti-Reflective Coating for Solar Cells	TiOx/Al2Ox
Module Dimensions	17,8 cm x 12,7 cm
Active Area of the Module	11,77 cm x 12,1 cm = 142,417 cm^2
Cooler Thickness Excluding Attachments	0,9 cm
Cooler Thickness with fittings	2,9 cm
Total Module Thickness	3,4 cm
Electrical plus contact	Suitable for clamp process
Electrical minus contact	Suitable for clamp process

Table 4.2. Typical electrical data for ADAM module (Measurement condition: 1.5 AMd – 1000 W/m² (ASTM G 173-03), T = 25° C)

Sun concentration	I_{SC} [A]	V_{OC} [V]	I_{MPP} [A]	V_{MPP} [V]	P_{MPP} [KW_{MPP}]	FF [%]	η [%]
x 700	53	76	50	64	3,20	79,5	32

The recommended cooling unit for the ADAM module is equipped with two inlet and two outlet fittings located on the rear side of the wafer. The suggested flow rate for the wafer is within the range of 14 to 18 liters per minute. The pressure drop at a flow rate of 15 liters per minute is approximately 0.3 bar. It is essential to ensure that the maximum water inlet temperature does not exceed 60°C, and the system's peak pressure should not exceed 3 bar. To prevent damage, it is crucial to avoid any failure of the cooling unit or interruption of the cooling flow, as such occurrences can lead to immediate damage. The thermal power output at a concentration of 700 suns is estimated to be around 6 kW [67].

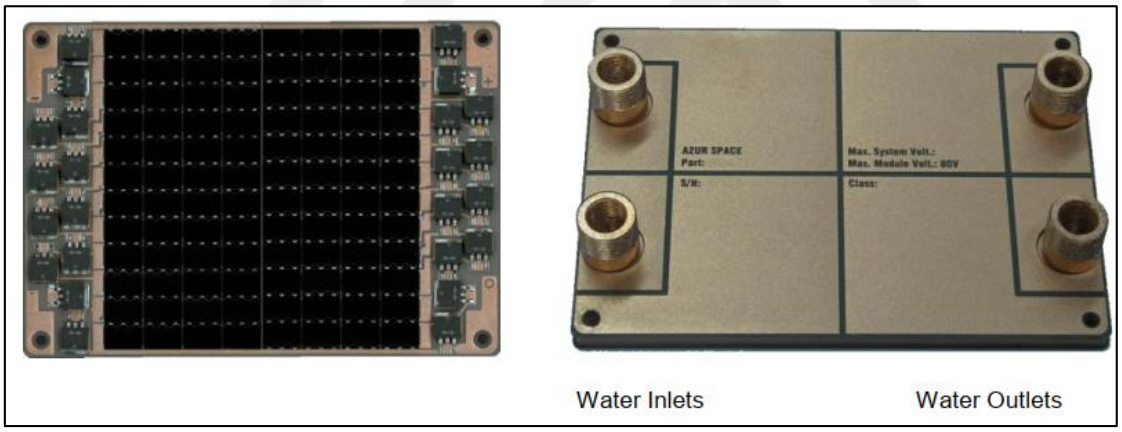

Figure 4.2. The front side and rear side of the ADAM module

5. DESIGNING AN EFFICIENT PARABOLIC DISH SOLAR COLLECTOR

The parabolic dish solar collector is a form of solar energy technology that employs a curved reflective surface resembling a parabolic dish to concentrate sunlight onto a central focal point. Its purpose is to gather and concentrate a significant quantity of solar radiation onto a designated receiver situated precisely at this focal point. Typically positioned at the dish's center, the receiver contains a working fluid, such as water or oil, which is heated by the intensified solar energy. This resultant thermal energy can serve diverse applications, encompassing electricity generation, water heating, space heating, and industrial processes.

The parabolic shape of the dish allows it to concentrate sunlight from a wide range of angles, optimizing its performance throughout the day as the sun moves across the sky. This concentration of sunlight significantly increases the intensity of the solar radiation reaching the receiver, resulting in higher temperatures and greater energy conversion efficiency compared to non-concentrating solar collectors.

One of the key advantages of parabolic dish solar collectors is their high thermal efficiency. The concentrated solar energy allows for efficient heat transfer to the working fluid, resulting in higher temperatures and improved energy conversion. Additionally, the compact size of the parabolic dish collector makes it suitable for decentralized applications, such as individual homes or small-scale installations.

Parabolic dish solar collectors have been employed in various settings, including residential, commercial, and industrial applications. They have demonstrated excellent performance in sunny regions with high direct normal irradiance. However, the high cost of manufacturing and complex tracking systems required to follow the sun's movement are some of the challenges associated with this technology.

Overall, parabolic dish solar collectors offer a promising approach for harnessing solar energy efficiently and can contribute to renewable energy generation and sustainability. Ongoing research and development efforts continue to improve the design, materials, and efficiency of these collectors, making them an exciting area of study in the field of solar energy.

5.1. The Factors Affecting on The Design of Parabolic Dish Solar Collector

Numerous factors exert influence on the design of a parabolic dish, encompassing the choice of reflector concentrator material, the diameter of the parabolic dish concentrator, the dimensions of the concentrator's aperture area, the focal length of the parabolic dish, the diameter of the focal point, the dimensions of the receiver's aperture area, the concentration ratio, and the rim angle. These considerations extend to encompass parameters related to solar radiation and the thermal properties of the receiver.

5.1.1. The aperture area of collector

The aperture area of the dish concentrator (Acon) is defined as the cumulative surface area of the solar concentrator exposed to incident solar energy. This parameter can be quantified using Eq. (5.1) [68]:

$$A_{con} = \frac{8\pi f^2}{3} * \left(\left(1 + \frac{{D_{con}}^2}{16 f^2} \right)^{\frac{3}{2}} - 1 \right) \tag{5.1}$$

5.1.2. Focal length of the parabolic dish

The focal length (f) referring to the distance from the dish collector to the focal point can be computed using Eq. (5.2) [47]:

$$\frac{f}{D_{con}} = \frac{1}{4 \tan\left(\frac{\psi}{2}\right)} \tag{5.2}$$

And the depth of dish collector (Y) can be calculated by Eq. (5.3):

$$\boldsymbol{Y = \frac{{D_{con}}^2}{16 f}} \tag{5.3}$$

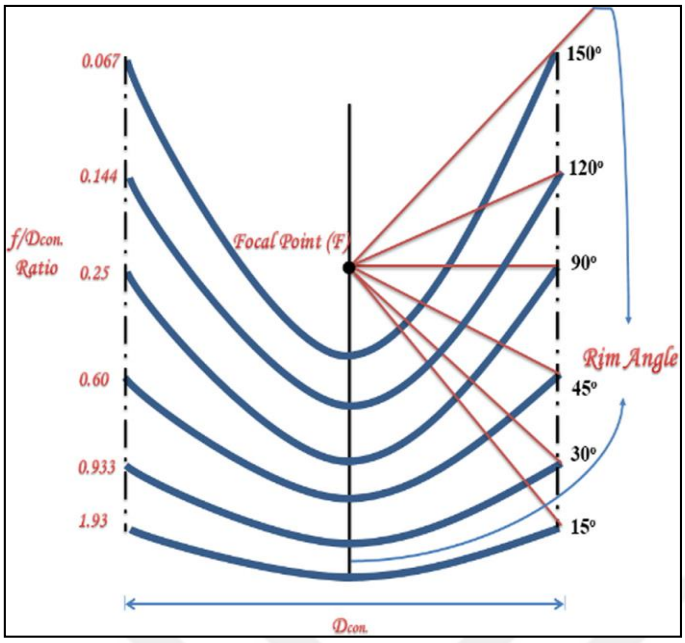

Figure 5.1. Difference between the value (f / Dcon.) of the concentrator at the same diameter and the different rim angles

5.1.3. The aperture area of receiver

The receiver functions as a heat absorber for the fluid, capturing the entirety of the reflected solar radiation originating from the dish concentrator. However, there exist losses in heat transfer due to both radiation and convection, with these losses escalating as the aperture area of the receiver (Ar) expands.

$$A_r = \frac{\pi d^2}{4} \tag{5.4}$$

Here, d represents the diameter of the focal point of the parabolic dish, and its measurement is facilitated by Eq. (5.5). The dimensions of the receiver are directly affected by this parameter, as demonstrated by Eq. (5.4).

$$d = \frac{f * \acute{\emptyset}}{cos\psi(1 + cos\psi)} \tag{5.5}$$

In this context, Ǿ signifies the acceptance angle pertaining to the parabolic dish. This angle represents the most challenging condition where the collector captures all reflected solar radiation from the concentrator during the initial tracking stages, see Figure 5.2 [47].

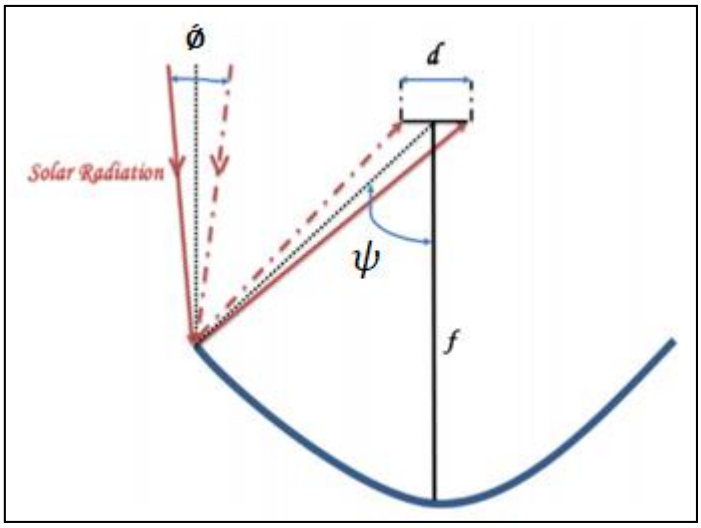

Figure 5.2. The geometry of the parabolic concentrator with the acceptance angle and the receiver diameter, focal length, and rim angle

5.1.4. Area concentration ratio

The concentration ratio (C) denotes the proportion between the aperture area of the concentrator and that of the receiver. It is crucial to design a solar dish with a concentration ratio surpassing 10. This can be evaluated using Eq. (5.6).

$$\boldsymbol{C = \frac{A_{con}}{A_r}} \tag{5.6}$$

The temperature reached is directly proportional to the concentration ratio. Parabolic dish collectors have higher concentration ratio than the other types.

5.1.5. Rim angle

The rim angle plays a pivotal role in governing the solar radiation intake and the output of the parabolic dish. Stine introduced the rim angle as the angle gauged at the truncated focus from the axis to the rim of the solar parabolic structure. Its measurement is attainable through Eq. (5.7).

$$tan\psi = \frac{1}{\left(\frac{D_{con}}{8Y}\right) - \left(\frac{2Y}{D_{con}}\right)} \tag{5.7}$$

5.1.6. Solar radiation at the collector

The higher solar radiation, the less area needed.

5.1.7. Reflector materials

The solar radiation to the receiver is greatly affected by the reflectivity of the material.

6. THEORETICAL THERMAL ANALYSIS OF CPV/T SYSTEM

In this section, we will do the thermal analysis the is necessary to be taken into account during the design of the Dish collector in order to ensure that enough solar energy is collected on the cell so that the cell work without any problems.

Like the examined dish reflector, focused collectors with high concentrative ratios use only direct solar beam radiation (I_B) and the available solar energy is measured as the product of the unshaded collector aperture area (A_a) and the beam radiation [65]:

$$Q_s = I_B * A_a \tag{6.1}$$

The proportion of energy absorbed by the receiver relative to the energy incident at the collector's aperture gives rise to the optical efficiency. This metric hinges upon the optical characteristics of the materials involved, the collector's geometry, and any imperfections stemming from the collector's fabrication. The estimation of optical efficiency can be achieved utilizing the subsequent expression [65]:

$$\eta_o = Ʀ * Б * ¥ [\cos(Ɵ) * (1 - A_f \tan(Ɵ))] \tag{6.2}$$

Where,

Ʀ = reflectance of the mirror.

Б = absorptance of the receiver.

A_f = geometric factor (shaded area/total aperture area).

Ɵ= angle of incidence.

¥= intercept factor.

The intercept factor denotes the ratio of radiation reaching the receiver's aperture in comparison to the radiation that gets reflected off the mirror. Its determination is once again contingent upon the geometric mirror's quality, alongside factors such as the shape, size, and

positioning of the receiver aperture, as well as the precision of tracking. When solely the central regions of the solar image, characterized by higher radiant flux density, impinge on the receiver aperture, a reduced intercept factor curtails the energy transmission to the receiver. Conversely, it can amplify the mean radiant flux density when only the central portions of the solar image, replete with higher radiant flux density, strike the receiver aperture.

In our case we have 2-axis tracking system, so Ɵ = 0 as mentioned before, and we assume ¥ = 0.85. Then Optical efficiency will become:

$$\eta_o = Ʀ * Б * 0.85 \quad (6.3)$$

It is possible to measure the rate of absorbed energy from the receiver (Qr) using the optical efficiency of the collector (η_o):

$$Q_r = \eta_o * Q_s \quad (6.4)$$

AZUR ADAM-3C30M cell (receiver) made of GaInP-GaInAs-Ge and active area of 121x117 mm^2 has typical electrical efficiency of 32% under concentration ratio of 700x (x=1000 w/m^2). Energy that will be converted into electricity directly via CPV is calculated by:

$$CPV\ (0ut) = Q_r * \eta_{PV} \quad (6.5)$$

The net rate of solar energy delivered by the receiver to the water it can be determined from an energy balance to be:

$Q_u = Q_r - Q_{loss} – CPV\ (out)$

$Q_{loss} = Q_{conduction} + Q_{radiation} + Q_{convection}$

$$Q_u = Q_r - \{Q_{cond} * Q_r + A_r[\sigma * \varepsilon * (T_r{}^4 - T_a{}^4) + h_{air}(T_r - T_a)]\} - CPV(out) \quad (6.6)$$

The coefficient of heat convection between the receiver and the ambient can be defined by the by the subsequent equation:

$$h_{air} = 2{,}8 + 3 * V_{air} \tag{6.7}$$

Because we do not know the details of the inner layers of the cell, its components, and the materials it is made of, it was difficult for us to calculate the heat loss by conduction between the outer surface of the cell and the cooling fluid. Therefore, it was assumed that the heat loss by conduction between the outer surface of the cell and water (Q_{cond}) is 10%. It was assumed that the cell's absorbance and emission are equal to 85%.

Also, the beneficial heat output, derived from the energy equilibrium within the fluid volume It can be calculated by Eq. (6.7), and this Q_u will be used for heating the small house or for daily use:

$$Q_u = \dot{m} * cp * (T_o - T_i) \tag{6.8}$$

We will assume the initial temperature of receiver (T_r), the initial ambient temperature (T_a) and the initial inlet water temperature (T_i) will be 25c.

The thermal efficiency of the system can be obtained by Eq. (6.9) [65]:

$$\eta = \frac{Q_u}{I_B A_a} \tag{6.9}$$

7. RESULTS AND DISCUSSION

The project is centered on the concept of integrating a high concentration solar cell with a parabolic dish solar collector. The primary objective of this integration is to harness a substantial amount of solar energy while minimizing the requirement for large surface areas. For this purpose, we will utilize the Advanced Dense Array Module (ADAM)-3C30M, a highly concentrated triple junction solar cell provided by Azurspace, renowned for its exceptional efficiency of up to 32%. The cell will be strategically positioned at the focal point of the parabolic dish solar collector, enabling the direct concentration of all reflected solar rays onto the cell. Consequently, a portion of the captured energy will be transformed into electrical power, while the remainder will be converted into heat. To prevent any adverse effects on the cell, a cooling system will be implemented, and the resulting thermal energy will be effectively utilized for residential purposes.

This section presents the theoretical results derived from the equations discussed in the preceding sections, which will be compared with the simulated outcomes obtained through the utilization of the SAM software. It is worth highlighting that, throughout this presentation, our focus will predominantly revolve around the solar collector and the solar cell. By delving into their individual results, we aim to provide valuable insights into their performance and offer an extensive evaluation of their capabilities, while other components of the system, such as the battery, inverter, charging regulator, heat exchanger, valves, pump, and related elements, will not be addressed in this context. However, it is crucial to acknowledge that the successful operation of the entire system necessitates the seamless coordination and harmonious interaction of all its components.

Considering the inherent limitations of the cell's size and capacity, it becomes imperative to ascertain the appropriate area and dimensions of the solar collector that are in line with its specifications. This crucial step will enable us to determine the feasibility and compatibility of the solar collector with the given cell. Subsequently, we will emphasize the quantified amount of electrical and thermal energy generated by the integrated system. The outcome of this assessment will be instrumental in establishing the system's viability as a self-sufficient and environmentally friendly energy source. Ultimately, the findings will contribute to the knowledge and understanding of utilizing highly concentrated PV cells integrated with

parabolic dish solar collectors as an effective means of electricity generation, paving the way for future advancements in this field.

Evaluating the performance of solar collectors and cells in theory and simulation

The thesis explores two scenarios: The first scenario presents results for a solar collector area of approximately 10 m^2, while the second scenario focuses on an area of about 18 m^2. These sections highlight the respective outcomes and performance of the system under these different collector sizes.

Despite our diligent efforts and numerous communications with Azurspace, certain values were challenging to obtain. Consequently, Table 7.1. presents the assumed values employed during the design phase in both scenarios. This table provides an overview of the specific parameters and their corresponding assumptions utilized in our study. These assumed values serve as essential inputs for the system's design and enable us to conduct a comprehensive analysis and evaluation of its performance.

Table 7.1. Assumed values employed in design phase for both scenarios

Receiver emissivity	0,85	-
Receiver absorptance	0,85	-
Initial receiver temperature (Tr)	298	k
Initial Ambient temperature (Ta)	298	k
Initial inlet water temperature (Ti)	298	k
Average wind speed in Gaza	1,4	m/s
Stefan–Boltzmann constant	5,67E-08	-
Coefficient of heat convection (h_{air})	7	-
Fluid mass flow rate	0,25	kg/s
Cp of fluid	4206,25	j/kg.k
Intercept factor (¥)	0,85	-
Collector reflectivity	0,9	-

Furthermore, it has been hypothesized that the efficiency of the solar cell will exhibit a reduction of 1,6% for every incremental deviation of the beam solar radiation intensity from the reference value, as elucidated in Table 7.2.

Table 7.2. Effect of beam solar radiation intensity deviation on solar cell efficiency

Beam solar radiation (w/m^2)	Cell efficiency %
Scenario 1 (reference value 1000 w/m^2 at 700x)	
200	19,2
400	22,4
550	24,8
630	26,08
1000	32
Scenario 2 (reference value 550 w/m^2 at 1272x)	
200	26,4
400	29,6
550	32
630	30,72
1000	24,8

Based on the information provided in Section 0, the data for Beam Radiation in Gaza Strip will be relied upon in this study, which is provided by the (NREL). NREL has provided the necessary data in the form of Excel files for the years 2017, 2018, and 2019. These files were diligently obtained and compiled for analysis. Subsequently, the average beam solar radiation for the specified duration of three years was calculated, serving as the basis for this study. The calculated average values have been adopted as crucial inputs in assessing the performance and behaviour of the system under investigation.

The first scenario

This section presents the outcomes of the researcher's first proposed scenario. The objective was to calculate the solar collector's area as 700 times the area of the solar cell, disregarding the solar radiation levels in the Gaza region. The fixed area of the solar cell is 142 cm^2, as recommended by the manufacturer (AzurSpace) for achieving maximum efficiency at a concentration of 700x. Applying Eq. (5.4), the required area for the solar collector amounts to approximately 10 m^2.

Table 7.3. The parameters of parabolic dish solar collector in the first scenario

Parameter	Value
Total area	10 m^2
Focal length (f)	2,1 m
Diameter (D_{con})	3,5 m
Depth (Y)	36 cm
Rim angle	45,2°
f/D	0,6

Table 7.3 illustrates the dimensions of the solar collector that meet the desired area of 10 m². Furthermore, Figure 7.1 exhibits the electrical energy output of the system on January 21st, comparing the modeling results obtained from the SAM software with the theoretical outcomes. The error between the two results is merely 5,4%. Similarly, Figure 7.2 demonstrates the system's electrical energy production on July 21st, with a discrepancy rate of 6,8% between the theoretical values and the typical results provided by the SAM software. These results indicate that the annual average error percentage remains within 9%, as depicted in Figure 7.3.

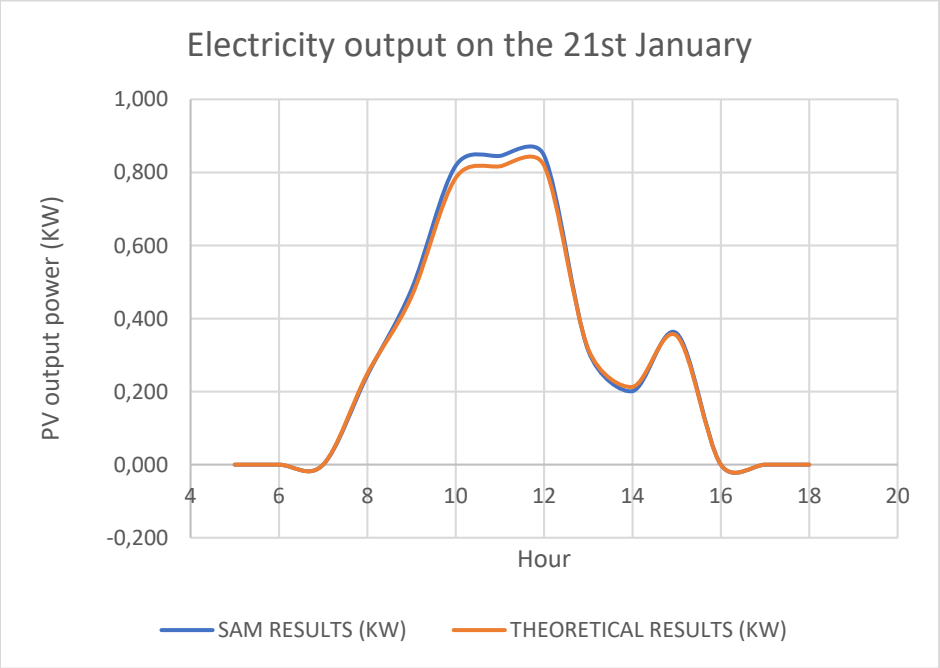

Figure 7.1. Electrical energy output of the system on January 21st in the first scenario

Table 7.4. Error between SAM software and theoretical calculations on January 21st in the first scenario

1/21/2023	SAM Results (kw)	Theoretical Results (kw)	Error
8:00:00 AM	0,245	0,249	1,74
9:00:00 AM	0,480	0,460	4,21
10:00:00 AM	0,818	0,785	4,23
11:00:00 AM	0,845	0,817	3,48
12:00:00 PM	0,846	0,819	3,33
1:00:00 PM	0,312	0,316	1,30
2:00:00 PM	0,201	0,213	5,40
3:00:00 PM	0,360	0,353	1,88

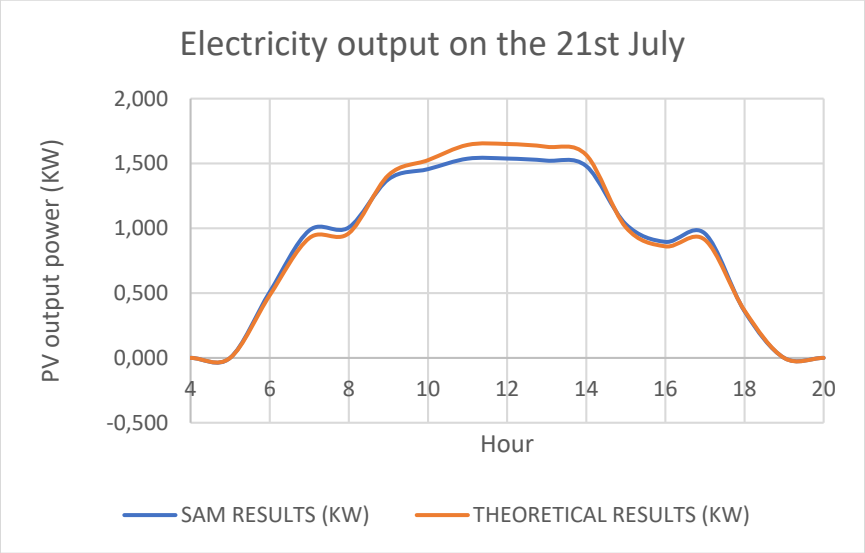

Figure 7.2. Electrical energy output of the system on July 21st in the first scenario

Table 7.5. Error between SAM software and theoretical calculations on July 21st in the first scenario

7/21/2023	SAM Results (kw)	Theoretical Results (kw)	Error
6:00:00 AM	0,507	0,483	5,114
7:00:00 AM	0,983	0,924	6,367
8:00:00 AM	1,006	0,962	4,643
9:00:00 AM	1,377	1,409	2,258
10:00:00 AM	1,456	1,525	4,563
11:00:00 AM	1,537	1,643	6,463

Table 7.5. (contd.) Error between SAM software and theoretical calculations on July 21st in the first scenario

12:00:00 PM	1,538	1,650	6,809
1:00:00 PM	1,522	1,629	6,565
2:00:00 PM	1,480	1,566	5,483
3:00:00 PM	1,031	1,008	2,332
4:00:00 PM	0,895	0,860	4,002
5:00:00 PM	0,959	0,911	5,303
6:00:00 PM	0,360	0,365	1,606

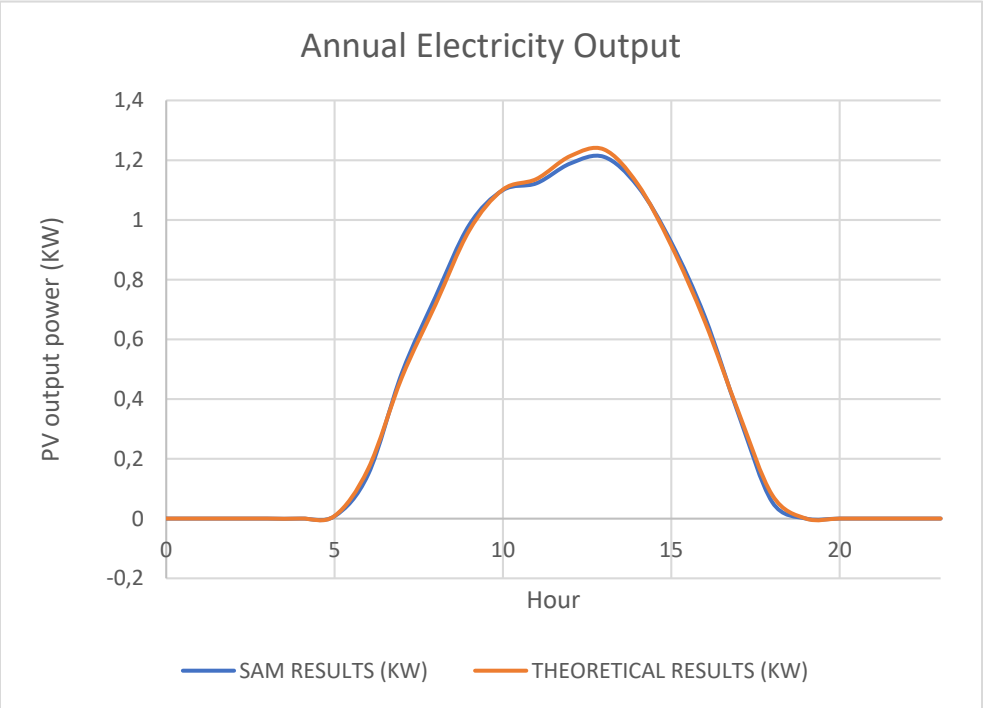

Figure 7.3. Annual electrical energy output of the system in the first scenario

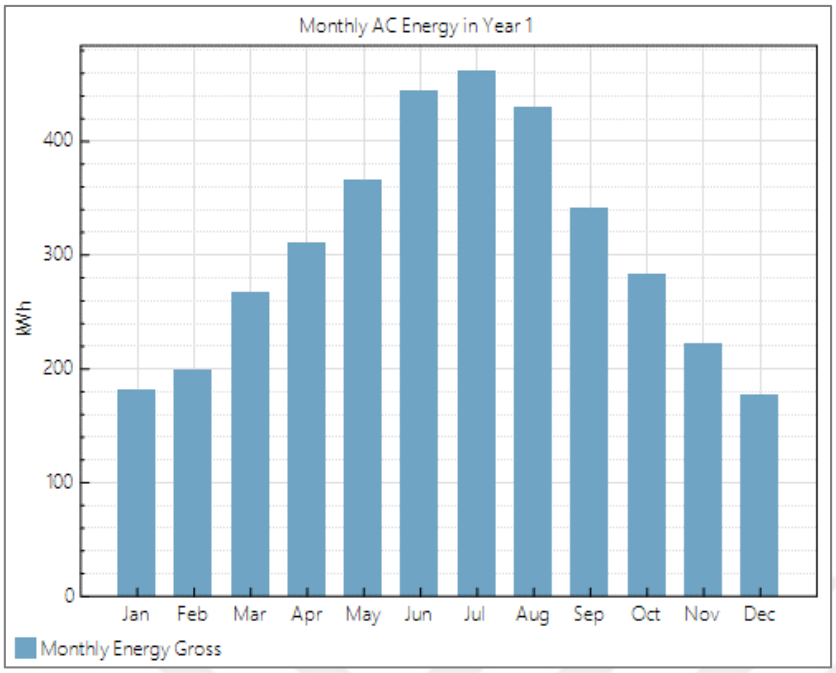

Figure 7.4. The average monthly energy produced by the system in the first scenario

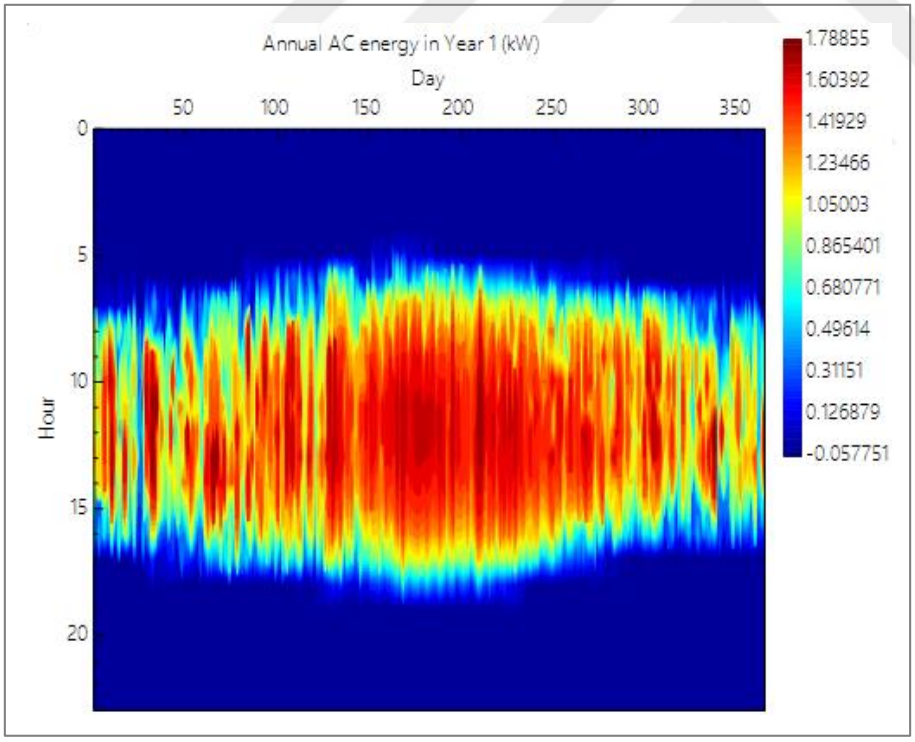

Figure 7.5. The hourly energy produced by the system in the first scenario

Additionally, Figure 7.6 displays the cell temperature throughout the day, reaching its peak of approximately 76°C on July 30th. Figure 7.7 provides insights into the cell's efficiency. Notably, Figure 7.1 shows a relatively low energy production, with the cell generating a

maximum of 1.8 kilowatts, despite its capacity being 3,2 kilowatts. This limitation stems from the solar radiation collected on the cell, which does not surpass 735 kW/m² throughout the year, as demonstrated in Figure 7.8 due to the small size of the solar collector. Although the manufacturer indicates that the cell achieves its highest efficiency at a solar radiation concentration of 700 kW/m², it is evident that the energy output remains restricted. Consequently, the study will progress to the second scenario, considering the beam solar radiation when calculating the solar collector's area.

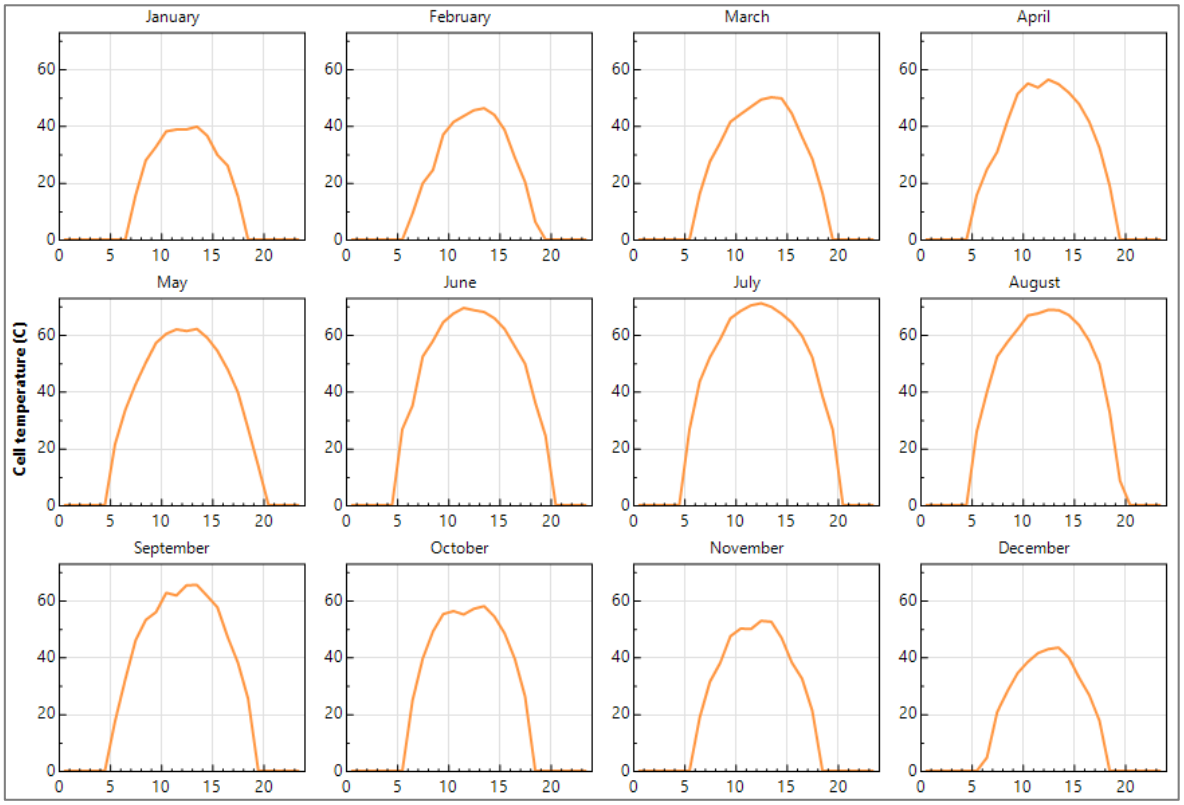

Figure 7.6. Monthly average cell temperature in the first scenario

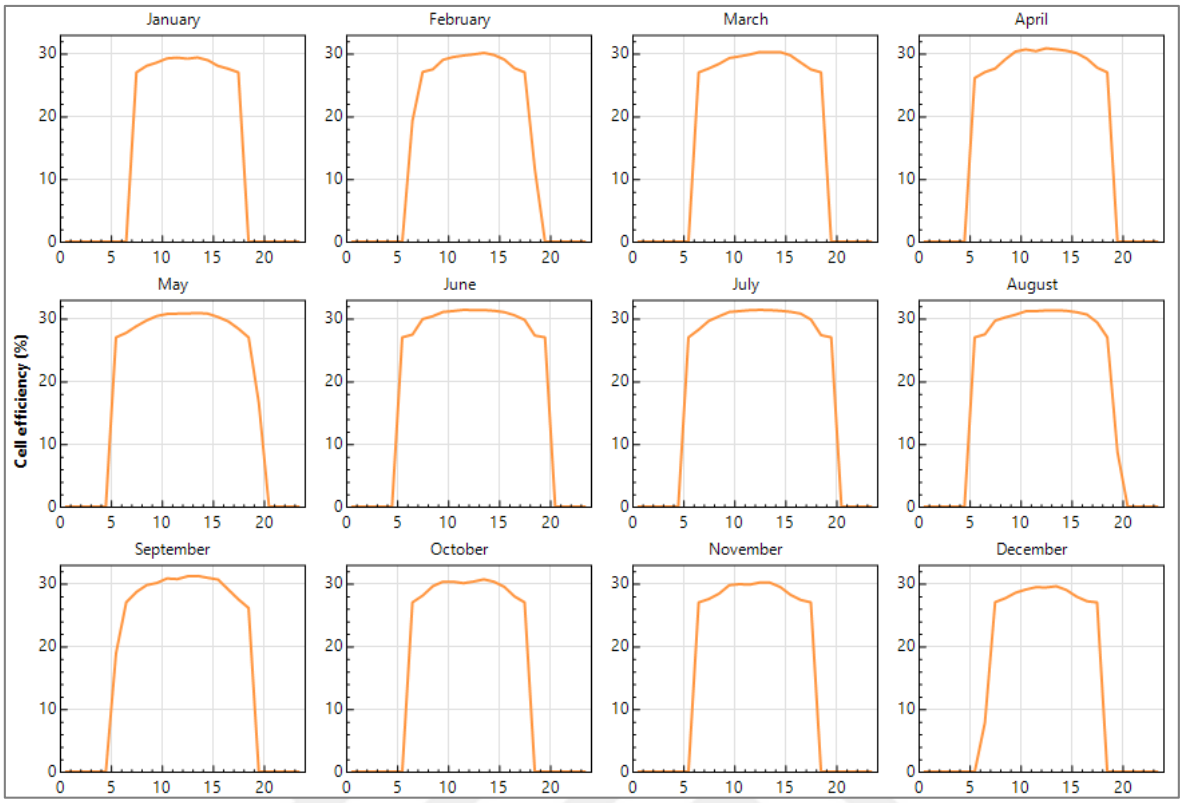

Figure 7.7. Monthly average cell efficiency in the first scenario

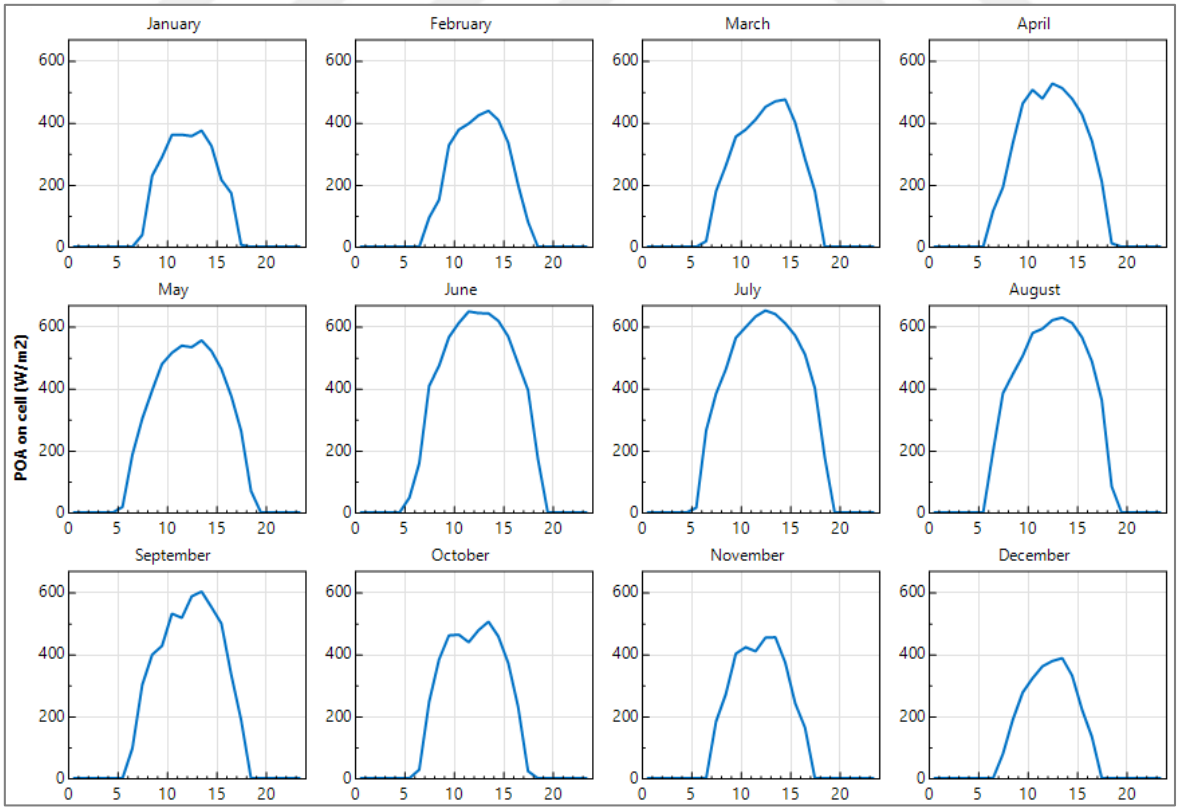

Figure 7.8. Solar radiation intensity collected on the cell in the first scenario

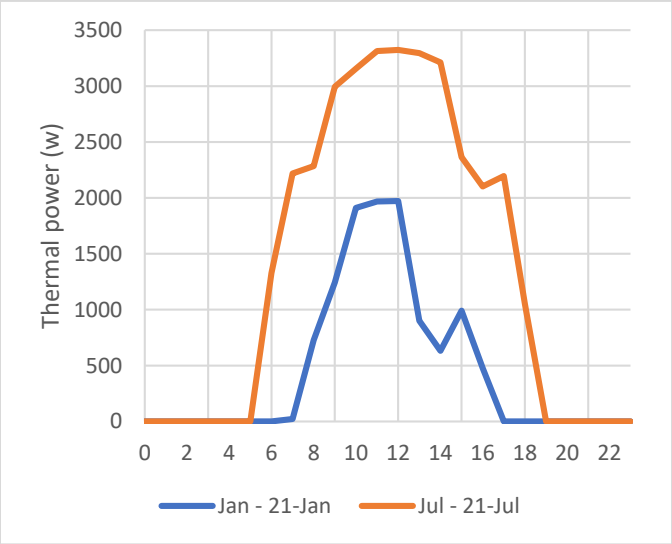

Figure 7.9. Thermal energy output of the system on January 21st and July 21st in the first scenario

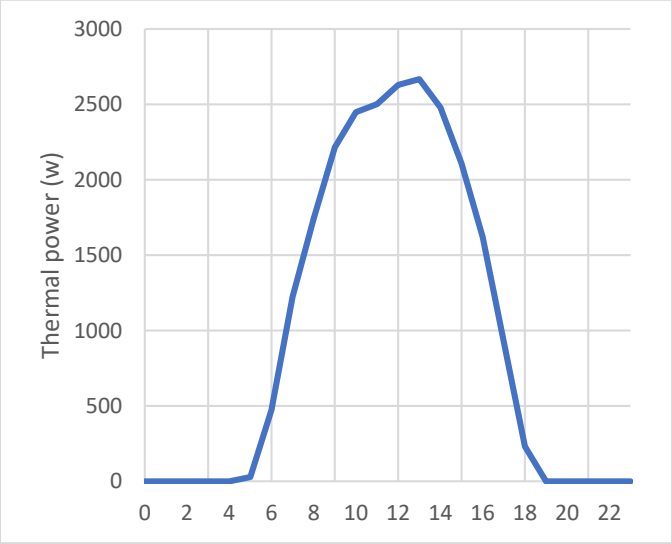

Figure 7.10. Annual thermal energy output of the system in the first scenario

Second scenario

This section delves into the outcomes derived from investigations conducted on a solar collector with an expanded area of approximately 18 square meters. By increasing the collector's size, we aim to assess the impact of additional surface area on the energy generation potential and overall performance of the system. The results presented in this section shed light on the improvements, if any, in terms of energy output and efficiency achieved through the larger collector area.

Based on the premise of maintaining a constant concentration ratio of 700, regardless of the solar radiation intensity in the region, it becomes evident that this approach is flawed. It is not logical to assume that the same solar collector area would be suitable for both icy and desert regions. Hence, in this scenario, the solar radiation intensity specific to the region will be taken into consideration.

For the calculation of the solar collector area, a reference value of 550 W/m2 will be utilized. This value is chosen due to its close proximity to the annual average solar radiation intensity in the Gaza Strip. In order to achieve the desired concentration of 700 kW/m^2 on the solar cell (the optimum operating efficiency of the cell), a concentration factor of 1272 is required. Accordingly, employing Eq. (5.4), the estimated solar collector area needed is approximately 18 m^2. Detailed specifications of the solar collector dimensions are provided in Table 7.6.

Table 7.6. The parameters of parabolic dish solar collector in the second scenario

Parameter	Value
Total area	18 m^2
Focal length (f)	2,8 m
Diameter (D_{con})	4,7 m
Depth (Y)	49 cm
Rim angle	45,4°
f/D	0,6

Figure 7.11 showcases the system's electrical energy generation on January 21st, comparing the results obtained from the SAM software with the theoretical predictions. The disparity between the two sets of results is a mere 5,37%. Similarly, Figure 7.12 illustrates the system's electrical energy production on July 21st, with a discrepancy of 4,088% between the theoretical values and the typical outcomes provided by the SAM software. These findings indicate that the average annual error percentage remains within 6%, as depicted in Figure 7.13.

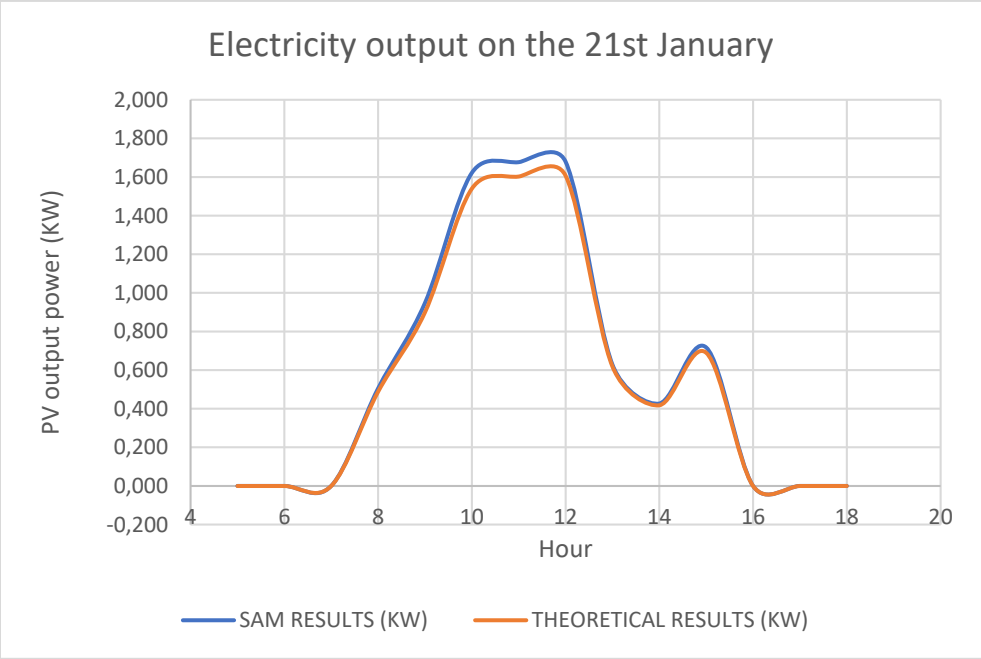

Figure 7.11. Electrical energy output of the system on January 21st in the second scenario

Table 7.7. Error between SAM software and theoretical calculations on January 21st in the second scenario

1/21/2023	SAM results (kw)	THEORETICAL RESULTS (kw)	Error
8:00:00 AM	0,505	0,488	3,42
9:00:00 AM	0,948	0,899	5,37
10:00:00 AM	1,622	1,540	5,30
11:00:00 AM	1,677	1,603	4,63
12:00:00 PM	1,680	1,607	4,50
1:00:00 PM	0,628	0,619	1,50
2:00:00 PM	0,427	0,418	2,04
3:00:00 PM	0,717	0,690	3,95

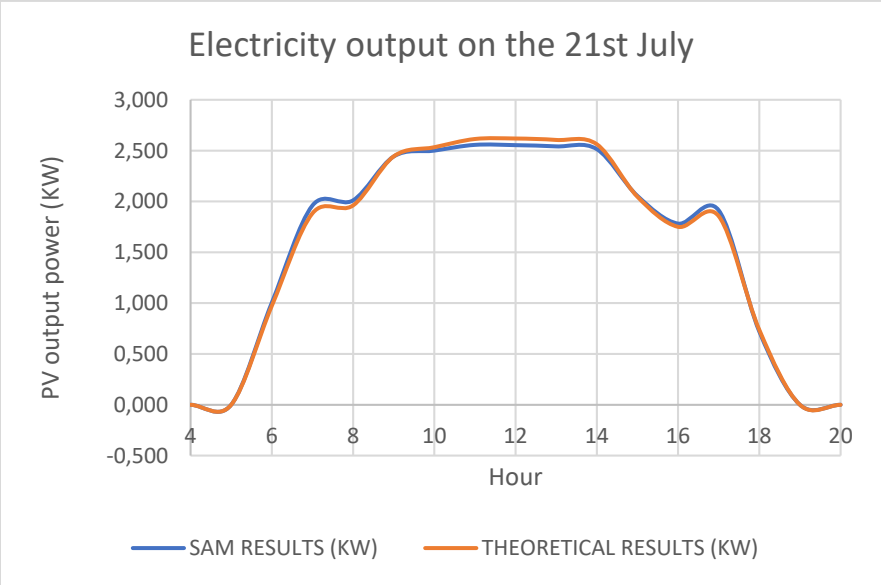

Figure 7.12. Electrical energy output of the system on July 21st in the second scenario

Table 7.8. Error between SAM software and theoretical calculations on July 21st in the second scenario

7/21/2023	SAM Results (kw)	Theoretical Results (kw)	ERROR
6:00:00 AM	1,003	0,973	3,092
7:00:00 AM	1,961	1,884	4,088
8:00:00 AM	2,011	1,961	2,519
9:00:00 AM	2,443	2,444	0,044
10:00:00 AM	2,501	2,534	1,295
11:00:00 AM	2,557	2,615	2,198
12:00:00 PM	2,554	2,619	2,489
1:00:00 PM	2,542	2,605	2,424
2:00:00 PM	2,515	2,562	1,868
3:00:00 PM	2,054	2,046	0,391
4:00:00 PM	1,782	1,751	1,801
5:00:00 PM	1,913	1,856	3,074
6:00:00 PM	0,720	0,736	2,184

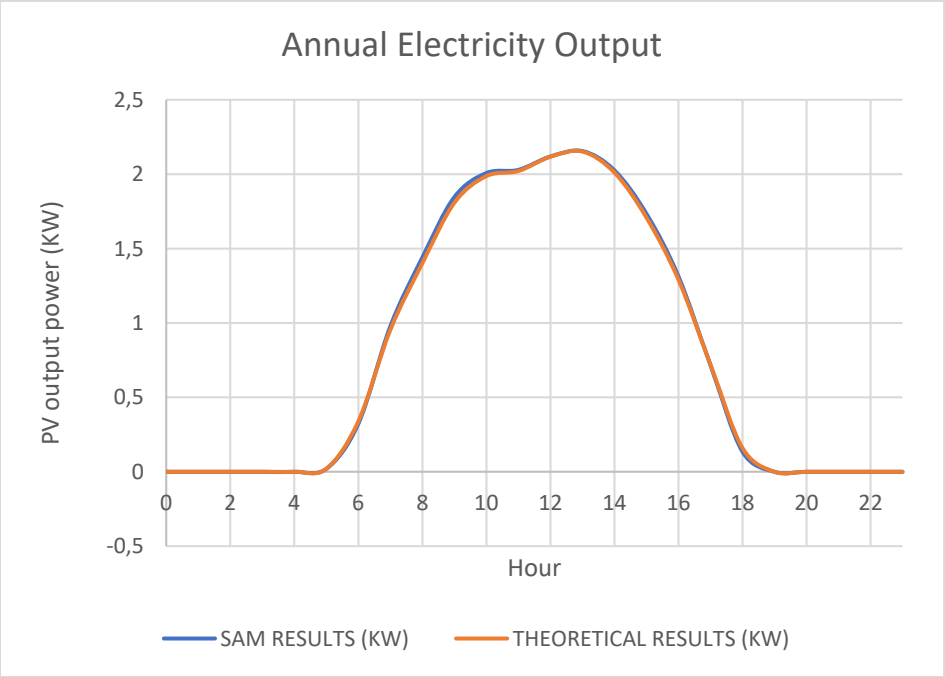

Figure 7.13. Annual electrical energy output of the system in the second scenario

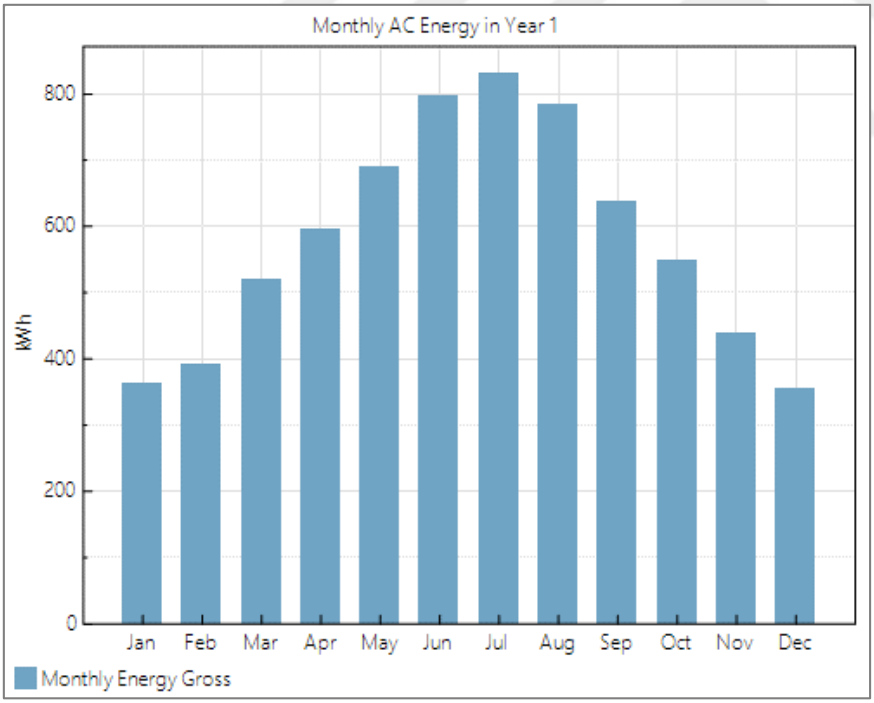

Figure 7.14. The average monthly energy produced by the system in the second scenario

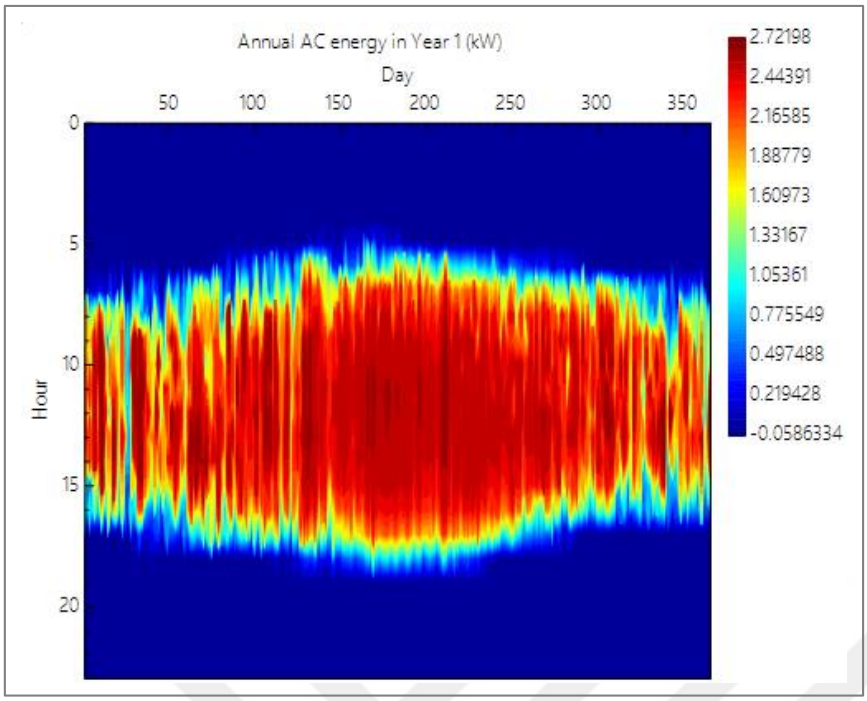

Figure 7.15. The hourly energy produced by the system in the second scenario

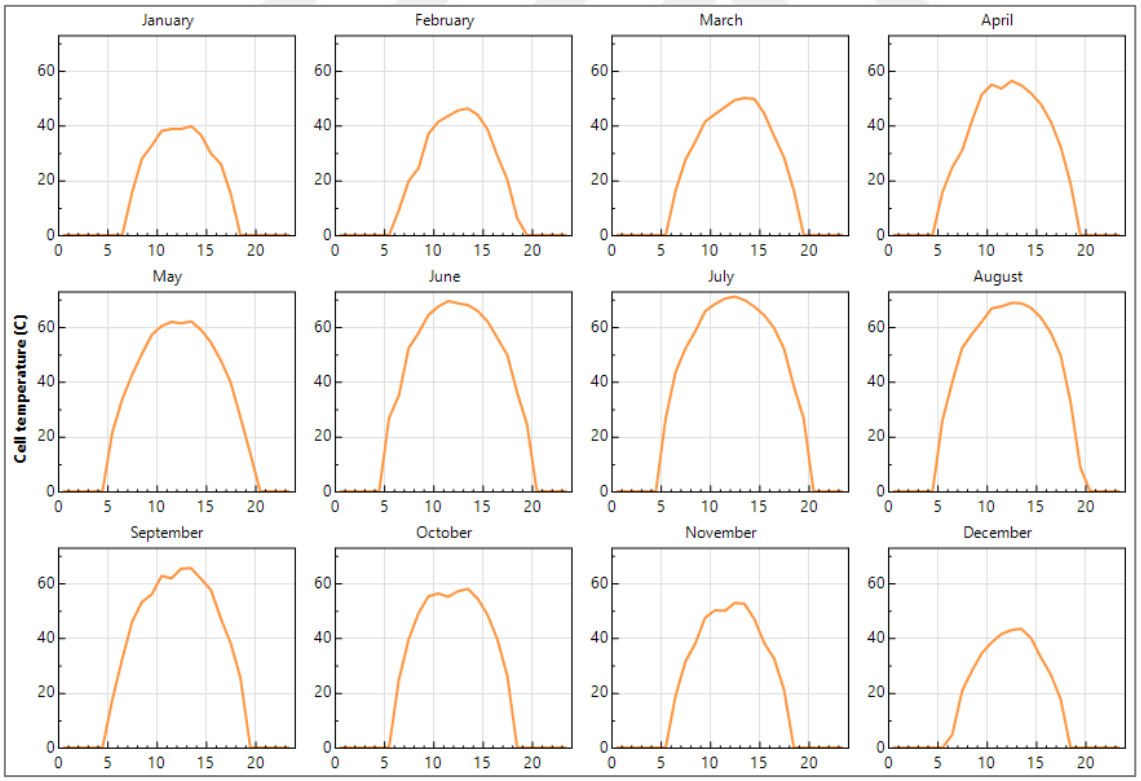

Figure 7.16. Monthly average cell temperature in the second scenario

Furthermore, Figure 7.16 showcases the variation of the cell temperature across the different months of the year, reaching its highest point at approximately 77,2 °C on July 30th at 11:00

AM. To gain a deeper understanding of the system's performance, Figure 7.17 highlights the efficiency of the solar cell. Additionally, Figure 7.18 depicts the average intensity of solar radiation that impinges on the cell throughout the entire year. These figures collectively contribute to a comprehensive analysis of the system's thermal characteristics, cell efficiency, and the overall solar radiation received by the cell.

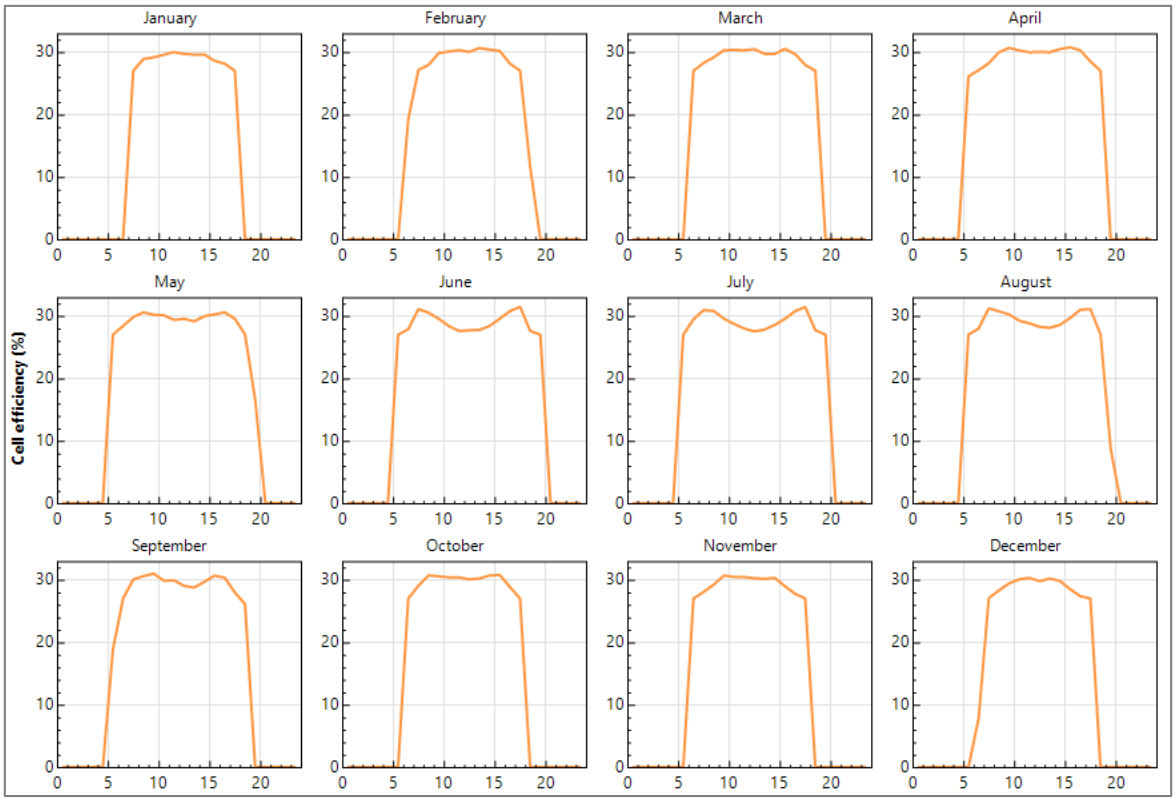

Figure 7.17. Monthly average cell efficiency in the second scenario

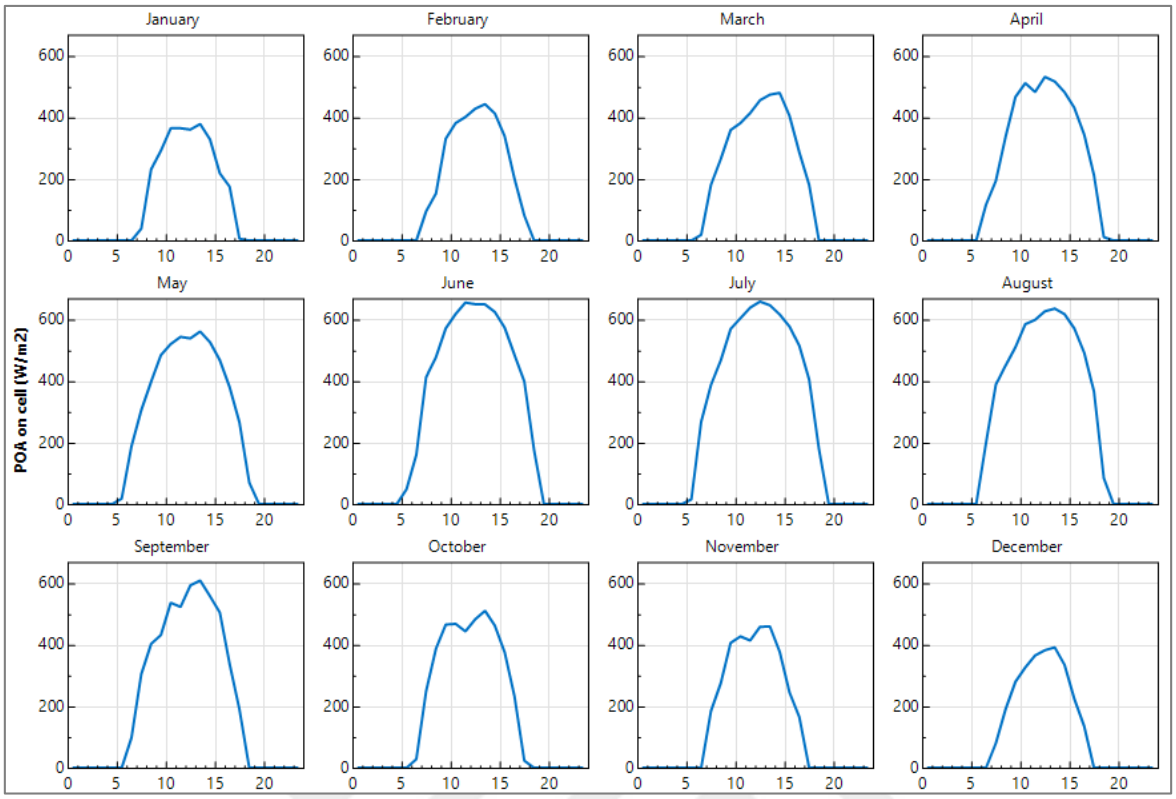

Figure 7.18. Solar radiation intensity collected on the cell in the second scenario

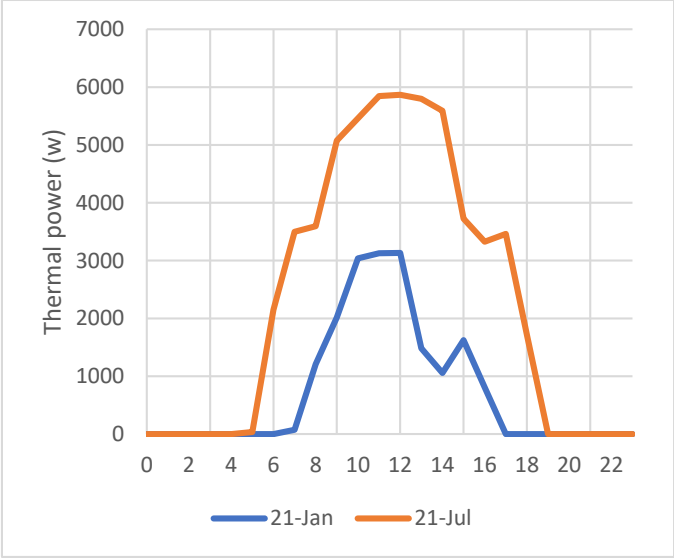

Figure 7.19. Thermal energy output of the system on January 21st and July 21st in the second scenario

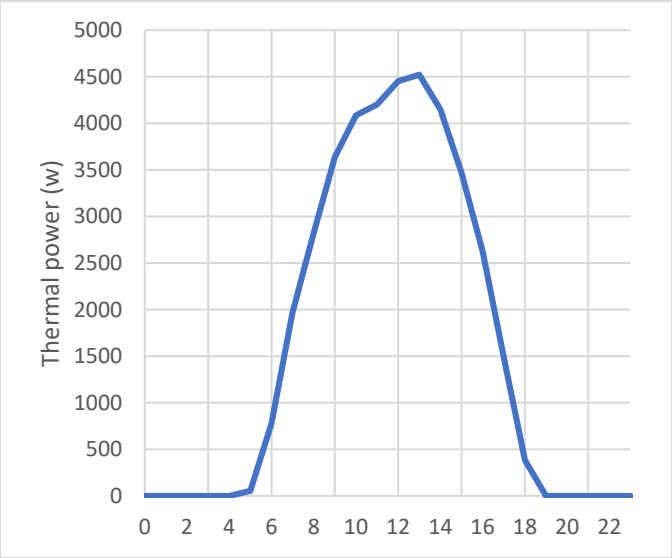

Figure 7.20. Annual thermal energy output of the system in the second scenario

8. CONCLUSIONS AND RECOMMENDATIONS

The Gaza Strip confronts a significant energy shortage, predominantly in the form of electrical energy, which detrimentally affects residents' mental and physical well-being, as well as their daily lives. Existing solutions to this crisis tend to be individualistic, yielding adverse consequences; for instance, candles have led to numerous fires, and standalone generators incur substantial costs. The adoption of renewable energy faces numerous hurdles in the region, encompassing insufficient governmental backing, low community awareness, funding constraints, technological limitations, and inadequate investment in the renewable energy sector. Overcoming the challenge of limited space due to high population density necessitates maximizing the utilization of abundant solar energy and enhancing focus on wave energy production. The multifaceted energy crisis in the Gaza Strip is compounded by factors including the occupying power's blockade, transportation difficulties, distribution challenges, and resource limitations.

This study has embarked on a significant journey to tackle the prevalent electricity scarcity in the Gaza Strip by introducing an innovative solar energy system. The amalgamation of a parabolic dish solar collector with a high-concentration solar cell from Azurspace stands as the focal point of this research, with the primary aim of efficient solar energy utilization encompassing both electricity generation and thermal applications. Through a meticulous process of assessment, utilizing established mathematical equations and advanced modeling within the SAM software, the electric power and thermal output of this integrated system have been thoroughly evaluated. Placed strategically at the collector's focal point, the high-concentration solar cell adeptly converts harnessed solar energy into both electricity and usable heat.

This study's significance is underscored by its exploration of two distinct scenarios, each emphasizing system performance across varying collector dimensions. The validation achieved through the SAM software confirms the system's effectiveness, with notably superior performance observed during summer conditions. Importantly, the second scenario demonstrates a more pronounced advantage over the first, showcasing superior electricity and thermal energy production. Specifically, during the summer season, the first scenario (small size) achieves an electricity output of 1,600 watts and a thermal energy yield of approximately 3,300 watts. In contrast, the second scenario (big size) attains an electricity

output of approximately 2,600 watts and a corresponding thermal energy yield of approximately 5,800 watts.

The proposed system addresses a critical need for independent homes, offering a dependable source of electricity amidst interruptions. Its suitability for the unique conditions of the Gaza Strip, characterized by high population density and restricted available space, enhances its relevance. By minimizing installation area requirements and enabling rooftop placement, this system offers a pragmatic solution to the electricity crisis. This research distinguishes itself by exploring a novel combination of a parabolic dish solar collector with a high-concentration solar cell, setting it apart from previous studies primarily focused on integrating high-concentration cells with other solar collector types.

While this study has shed light on the effects of varying solar collector sizes on the system's efficiency, it is important to acknowledge that numerous other factors also exert significant influence on the results. Parameters such as coolant flow rate, the number of cells utilized, geographic location, collector type, and material properties can all have substantial impacts on outcomes. Small adjustments to these factors could lead to significant changes in the overall system performance. As future research endeavors, the researcher intends to delve deeper into these variables and factors, aiming to comprehensively understand their roles in system efficiency. Furthermore, the potential impact of manufacturing a practical model on the ground cannot be overstated, as this would enable a direct comparison between theoretical, analytical, and real-world results.

Here are the summarized recommendations for this thesis:

1. Governmental Support and Funding: Advocate for increased government support and collaborate with institutions to secure funding for renewable energy projects in the Gaza Strip.
2. Community Awareness and Investment: Develop educational campaigns to raise awareness about renewable energy benefits and encourage investments in the sector.
3. Maximize Solar Energy Utilization: Focus on developing solar energy technologies tailored to confined spaces and high population density.

4. Research and Practical Implementation: Continue research on optimizing solar collector sizes and investigating system parameters while emphasizing practical model implementation.
5. Academic and Practical Contribution: Contribute to the academic community through research publication and collaborate with practitioners to implement solutions effectively.

In essence, this study's findings hold considerable promise for ameliorating electricity shortages through an innovative fusion of solar technologies. Its adaptability to space constraints and ability to provide consistent energy supply position it as a compelling solution for the prevailing challenges in the Gaza Strip. By contributing novel insights to the domain of Concentrated Photovoltaic Thermal (CPVT) systems, this research extends the boundaries of solar energy exploration, with the potential to usher transformative changes both within academia and practical applications.

REFERENCES

1. Internet: The Palestinian Central Bureau of Statistics. (2022). *PCBS, 11*. Web: https://www.pcbs.gov.ps/site/lang__ar/803/default.aspx, Last Date of access: 22.03.2023.

2. Hamed, T., Flamm, H., and Azraq, M. (2012). Renewable energy in the Palestinian Territories: Opportunities and challenges. *Renewable and Sustainable Energy Reviews*, 16(1), 1082-1088.

3. Yaseen, B. (2009). *Renewable energy applications in Palestine. Palestinian energy and environment research center (pec)–energy authority, technical department, Palestine*. In 2nd International Conference for the Palestinian Environment, Palestine.

4. Internet: Sandano, R. (2016). *A Techno-economical Appraisal of a PV Domestic Plant on a Irish Dwelling.* Technological University Dublin. Web: https://arrow.tudublin.ie/cgi/viewcontent.cgi?article=1125&context=engscheleart2, Last Date of access: 22.03.2023.

5. Bernal-Agustín, J., Dufo-López, R., and Rivas-Ascaso, D. M. (2006). Design of isolated hybrid systems minimizing costs and pollutant emissions. *Renewable Energy*, 31(14), 2227-2244.

6. Ismail, M., Moghavvemi, M., and Mahlia, T. (2013). Analysis and evaluation of various aspects of solar radiation in the Palestinian territories. *Energy Conversion and Management*, 73, 57-68.

7. Mekhilef, S., Saidur, R., and Kamalisarvestani, M. (2012). Effect of dust, humidity and air velocity on efficiency of photovoltaic cells. *Renewable and Sustainable Energy Reviews*, 16(5), 2920-2925.

8. Çağlar, A., Yamalı, C., Baker, D., and Kaftanoğlu, B. (2013). Measurement of solar radiation in Ankara, Turkey. *Journal of Thermal Science and Technology*, 33(2), 135-142.

9. Sancho Ávila, J., Riesco Martín, J., Jiménez Alonso, C., Sánchez de Cos, M., Montero Cadalso, J., and López Bartolomé, M. (2012). *Atlas de radiación solar en españa utilizando datos del SAF de clima de EUMETSAT* (1. Edition). Spain: Agencia Estatal de Meteorologia, 162.

10. Gaza Electricity Distribution Company report. (2019). The annual report of the power distribution station in Gaza. *GEDC Report*, Gaza, 130.

11. United Nations Office for the Coordination of Humanitarian Affairs. (2015). The humanitarian impact of gaza's electricity and fuel crisis. *OCHA Report*, Gaza, 8.

12. United Nations Office for the Coordination of Humanitarian Affairs. (2010). Gaza's electricity crisis: the impact of electricity cuts on the humanitarian situation. *OCHA Report*, Gaza, 4.

13. Abualkhair, A. (2007). Electricity sector in the Palestinian territories: Which priorities for development and peace? *Energy Policy*, 35(4), 2209-2230.

14. Nassar, Y. F., and Alsadi, S. Y. (2019). Assessment of solar energy potential in Gaza Strip-Palestine. *Sustainable Energy Technologies and Assessments*, 31, 318-328.

15. Nassar, Y., and Alsadi, S. (2016). Economical and environmental feasibility of the renewable energy as a sustainable solution for the electricity crisis in the Gaza Strip. *International Journal of Engineering Research and Development,* 12(3), 35-44.

16. Internet: Ouda, M. J. E. R. (2003). Prospects of Renewable Energy in Gaza Strip. *Energy Research Development Center*. Web: http://site.iugaza.edu.ps/mouda/files/2010/02/NET2001_con_paper.pdf, Last Date of access: 22.03.2023.

17. Hamdan, L. K., Zarei, M., and Chianelli, R. R., Gardner, E. (2008). Sustainable water and energy in Gaza Strip. *Renewable Energy*, 33(6), 1137-1146.

18. Mogheir, Y., Tayef, M. A., Gabayen, S., and Foul, A. A. (2013). Concentrating Solar Power Using Parabolic Trough, (Pilot Project in Islamic University of Gaza). *Energy Procedia*, 42, 754-760.

19. Elnaggar, M., El-Khozondar, H. J., Bashir, M. J. K., and Salah, W. A. (2023). Enhancing solar water heater system for utmost useful energy gain and reduction in greenhouse gas emissions in Gaza. *International Journal of Environmental Science and Technology*, 20(4), 3749-3764.

20. Hussein, M., and Albarqouni, S. (2010). Developing empirical models for estimating global solar radiation in Gaza Strip, Palestine. *The Islamic University Journal (Series of Natural Studies and Engineering),* 18(2), 73-83.

21. El-Khozondar, H. J., and El-batta, F. (2022). Solar energy implementation at the household level: Gaza Strip case study. *Energy, Sustainability and Society*, 12(1), 1-19.

22. Asfour, O. S. (2012). Integration of a stand-alone photovoltaic solar system into Gaza Strip residential buildings. In *World Congress on Sustainable Technologies*, 71-74.

23. El-Khozenadar, H. J., Khatib, T., Attaee, B., and El-Khozondar, R. J. (2022). Assessment of solar e-cookers social acceptance in Gaza Strip. *Scientific Reports*, *12*(1), 17226.

24. Elnaggar, M., Edwan, E., Alnahhal, M., Farag, S., Samih, S., and Chaouki, J. (2019). Investigation of energy harvesting using solar water heating and photovoltaic systems for Gaza and Montreal QC climates. *Palestinian International Conference on Electrical and Computer Engineering (PICECE)*, 1-7.

25. Dabbousa, T. A., Al-Reqeb, I., Al-Mutayeb, Y., Alattar, J., and Zainuri, M. A. A. M. (2021). Performance Comparison of Different Manufacturers Solar PV Modules Used in Gaza Strip. *International Conference on Electric Power Engineering–Palestine (ICEPE-P)*, 1-5.

26. Abu-Zarifa, A. (2014). System Design of Photovoltaic-Solar Home Lighting for Household in Gaza Strip. In *3 rd International Conference on Geological and Environmental Sciences. IACSIT Press, Singapore*, 14, 73.

27. Internet: Comprehensive Solar. (2021). *SCC*, 9. Web: http://solarcellcentral.com/csp Last Date of access: 05.08.2021.

28. Serrano, R., and Isabel, M. (2017). Optimisation of solar receivers. *Concentrating Solar Thermal Technologies: Analysis and Optimisation by CFD Modelling*, 39-72.

29. Felsberger, R., Buchroithner, A., Gerl, B., and Wegleiter, H. (2020). Conversion and testing of a solar thermal parabolic trough collector for CPV-T application. *Energies*, 13(22), 6142.

30. Del Col, D., Bortolato, M., Padovan, A., and Quaggia, M. (2014). Experimental and numerical study of a parabolic trough linear CPVT system. *Energy Procedia*, 57, 255-264.

31. Yang, F., Wang, H., Zhang, X., Tian, W., Hua, Y., and Dong, T. (2018). Design and experimental study of a cost-effective low concentrating photovoltaic/thermal system. *Solar Energy*, 160, 289-296.

32. Riahi, A., Ali, A. B. H., Fadhel, A., Guizani, A., and Balghouthi, M. (2020). Performance investigation of a concentrating photovoltaic thermal hybrid solar system combined with thermoelectric generators. *Energy Conversion and Management*, 205, 112377.

33. Wang, G., Shen, F., Wang, F., and Chen, Z. (2020). Design and experimental study of a solar CPV system using CLFR concentrator. *Sustainable Energy Technologies and Assessments*, 40, 100751.

34. Wang, G., Wang, F., Shen, F., Jiang, T., Chen, Z., and Hu, P. (2020). Experimental and optical performances of a solar CPV device using a linear Fresnel reflector concentrator. *Renewable Energy*, 146, 2351-2361.

35. Hussain, M. I., and Lee, G. H. (2015). Experimental and numerical studies of a U-shaped solar energy collector to track the maximum CPV/T system output by varying the flow rate. *Renewable Energy*, 76, 735-742.

36. Youssef, W. B., Maatallah, T., Ménézo, C., and Nasrallah, S. B. (2018). Modeling and optimization of a solar system based on concentrating photovoltaic/thermal collector. *Solar Energy*, 170, 301-313.

37. Singh, N. P., and Reddy, K. S. (2020). Inverse heat transfer technique for estimation of focal flux distribution for a concentrating photovoltaic (CPV) square solar parabola dish collector. *Renewable Energy*, 145, 2783-2795.

38. Ceylan, I., Gürel, A. E., Ergün, A., Ali, I. H. G., Ağbulut, Ü., and Yıldız, G. (2021). A detailed analysis of CPV/T solar air heater system with thermal energy storage: A novel winter season application. *Journal of Building Engineering*, 42, 103097.

39. Hafez, A. Z., Soliman, A., El-Metwally, K. A., and Ismail, I. M. (2017). Design analysis factors and specifications of solar dish technologies for different systems and applications. *Renewable and Sustainable Energy Reviews*, 67, 1019-1036.

40. Hijazi, H., Mokhiamar, O., and Elsamni, O. (2016). Mechanical design of a low cost parabolic solar dish concentrator. *Alexandria Engineering Journal*, 55(1), 1-11.

41. Sahu, S. K., K, A. S., and Natarajan, S. K. (2021). Design and development of a low-cost solar parabolic dish concentrator system with manual dual-axis tracking. *International Journal of Energy Research*, 45(4), 6446-6456.

42. Gwania, M., Abubakar, G. A., Abbas, M., Allah, M. N., and Danyaroe, J. (2015). Design, fabrication and experimental study of solar parabolic dish concentrator for remote area application. *International Journal of Sciences: Basic and Applied Research*, 23(1), 230-241.

43. Mohammed, I. L. (2012). Design and development of a parabolic dish solar water heater. *International Journal of Engineering Research and Applications*, 2(1), 822-830.

44. Cherif, H., Ghomrassi, A., Sghaier, J., Mhiri, H., and Bournot, P. (2019). A receiver geometrical details effect on a solar parabolic dish collector performance. *Energy Reports*, 5, 882-897.

45. Venkatachalam, T., and Cheralathan, M. (2019). Effect of aspect ratio on thermal performance of cavity receiver for solar parabolic dish concentrator: An experimental study. *Renewable Energy*, *139*, 573-581.

46. Senthil, R., and Cheralathan, M. (2017). Effect of non-uniform temperature distribution on surface absorption receiver in parabolic dish solar concentrator. *Thermal Science*, 21(5), 2011-2019.

47. Hafez, A. Z., Soliman, A., El-Metwally, K. A., and Ismail, I. M. (2016). Solar parabolic dish Stirling engine system design, simulation, and thermal analysis. *Energy Conversion and Management*, 126, 60-75.

48. Chen, Y. J., Chindarkar, N., and Xiao, Y. (2019). Effect of reliable electricity on health facilities, health information, and child and maternal health services utilization: evidence from rural Gujarat, India. *Journal of Health, Population and Nutrition*, *38*, 1-16.

49. Internet: Possible solutions between commercial generators and smart counters. (2018). *A.-M. C. f. H. Rights*. Web: http://mezan.org/post/27064, Last Date of access: 05.08.2021.

50. United Nations Office for the Coordination of Humanitarian Affairs. (2018). Immediate risk' of mass hospital closures and infrastructure collapse for 2 million in Gaza. *OCHA Report*, Gaza, 5.

51. World Health Organization. (2017). WHO report for 2017. *WHO Report*, United Nations, 80-110.

52. Younis, S. (2021, 25 December). *Muhammad Al-Shanti spoke about the status of the power plant in the Gaza Strip.* Gaza Power Plant, Gaza.

53. United Nations Office for the Coordination of Humanitarian Affairs. (2017-2020). Electricity in Gaza Strip. *OCHA Report*. Gaza. 10-17.

54. Internet: European Commission Website. (2016). *ECW*. Web: https://commission.europa.eu/index_en Last Date of access: 17.10.2022.

55. Abu-Zarifa, A. (2014). Design of a stand-alone power wind turbine optimized for low wind speed in Gaza. *International Journal of Energy Engineering*, 4(5), 89-93.

56. Elnaggar, M., Edwan, E., and Ritter, M. (2017). Wind energy potential of Gaza using small wind turbines: A feasibility study. *Energies*, 10(8), 1229.

57. Manwell, J. F., McGowan, J. G., and Rogers, A. L. (2010). *Wind energy explained: theory, design and application*. (2. Edition). Hoboken: John Wiley & Sons, 705.

58. Clément, A., McCullen, P., Falcão, A., Fiorentino, A., Gardner, F., Hammarlund, K., Thorpe, T. (2002). Wave energy in Europe: current status and perspectives. *Renewable and Sustainable Energy Reviews*, 6(5), 405-431.

59. Drew, B., Plummer, A., and Sahinkaya, M. (2009). A review of wave energy converter technology. *Journal of Power and Energy*, 223(8), 887-902.

60. Younis, S. (2020, 12 July). *Taleb Alrayyes spoke about wave energy situation in Gaza Strip.* Aknan-Tech company, Gaza.

61. Thöni, V., Matar. S. (2019). Solid waste management in the occupied Palestinian territory west bank including east Jerusalem & Gaza strip. *CESVI Report*. Gaza. 102.

62. Messenger, R., and Ventre, J. (2010). *Photovoltaic Systems Engineering*. (3. Edition). Abingdon: Taylor & Francis Group.

63. Mohanty, P., Muneer, T., Gago, E. J., Kotak, Y. (2015). *Solar radiation fundamentals and PV system components.* (3. Edition). Cham: Springer International Publishing, 7-47.

64. Zhang, X., Li, Y., Lu, S., Hamann, H. F., Hodge, B. M., and Lehman, B. (2018). A solar time-based analog ensemble method for regional solar power forecasting. *Transactions on Sustainable Energy*, 10(1), 268-279.

65. Kalogirou, S. A. (2013). *Solar energy engineering: Processes and systems*. (3. Edition). California :Academic Press, 815.

66. Chandra, L., and Dixit, A. (2018). *Concentrated solar thermal energy system.* (1. Edition). Singapore: Springer Nature Singapore, 264.

67. Internet: AZUR SPACE COMPANY. (2012). Web: https://www.azurspace.com/index.php/en/products/products-space/space-solar-cells, Last Date of access: 28.04.2023.

68. Gunther, M., and Shahbazfar, R. (2011). Solar dish technology. *Advanced CSP Teaching Materials*, 1, 1-63.

APPENDICES

APPENDIX-1. Solar Calculations (for Particular Day of June 21th)

Calculations performed for Gaza City using the provided equations in section 0 Given the following values:

- I_0 (extraterrestrial radiation) = 1367 W/m²
- H_{alt} (altitude above sea level) = 10 m
- Latitude = 31,522561
- Longitude = 34,453593
- At local standard time (LST) = 12:00

1. Determine the day of the year (N) corresponding to June 21st:

Since it is June 21st, N = 172.

2. Calculate the Equation of Time (ET) using Eq. (3.1):

ET = 9,87 * sin(2B) – 7,53 * cos(B) – 1,5 * sin(B)

Calculate B using Equation (3.2):

B = (N - 81) * 360 / 364

Substituting B = (172 - 81) * 360 / 364:

B = 90

Plugging B into the equation:

ET = 9,87 * sin (2 * 90) – 7,53 * cos (90) – 1,5 * sin(90)

ET = -1,5 min

3. Calculate the Longitude Correction (LC):

LC = -3,041852 min (for Gaza City)

APPENDIX-1. (Continue) Solar Calculations (for Particular Day of June 21th)

4. Calculate the Apparent Solar Time (AST) using Eq. (3.3):

AST = LST (hour) + ET (hour) + LC (hour)

Since it is 12:00 local time, LST = 12.

Plugging in the values:

AST = 12 + (-1,5/60) + (-3,041852/60)

AST = 11,9243

5. Calculate the Solar Declination (δ) using Eq. (3.5):

$\delta = 23.45 * \sin[(360/365) * (284 + N)]$

Plugging in N = 172:

$\delta = 23{,}45^{\circ}$

6. Calculate the Hour Angle (ω) using Eq. (3.6):

$\omega = 15 * (AST - 12)$

Plugging in AST = 11,9243:

$\omega = -1{,}1354$

7. Calculate the Solar Altitude Angle (α) using Eq. (3.9):

$\sin(\alpha) = \cos(L) * \sin(\delta) + \sin(L) * \cos(\delta) * \cos(\omega)$

Plugging in L = 31,522561, δ = 23,45 and ω = -1,1354:

$\alpha = 81{,}865^{\circ}$

8. Calculate the Solar Azimuth Angle (z) using Eq. (3.10):

$\sin(z) = (\cos(\delta) * \sin(\omega)) / \cos(\alpha)$

Plugging in δ = 23,45 and ω = -1,1354:

$z = -7{,}381^{\circ}$

APPENDIX-1. (Continue) Solar Calculations (for Particular Day of June 21th)

9. Calculate the Day length using Eq. (3.12):

Day length = (2/15) * cos^ (-1) (-tan(L) * tan(δ))

Plugging in L = 31,522561 and δ = 23,45:

Day length = 14,06 hour

10. Calculate the Extraterrestrial solar radiation using Eq. (3.13):

$I_{on} = I_0 * [1 + 0{,}033 * \cos((360 * N) / 365)]$

Plugging in $I_0 = 1367$ and $N = 172$:

$I_{on} = 1316\ W/m^2$

11. Calculate the Pressure Ratio (P_L/P_0) using Eq. (3.16):

$P_L/P_0 = \exp(-0{,}0001184 * H_{alt})$

Plugging in $H_{alt} = 10$:

$P_L/P_0 = 0{,}999$

12. Calculate the Atmospheric Extinction Coefficient (B) using Eq. (3.15):

$B = 0{,}175 * (1 - 0{,}2 * \cos(0{,}93 * N)) - 0{,}0045 * (1 - \cos(1{,}86 * N))$

Plugging in N = 172:

B = 0,21

13. Calculate the Atmospheric Extinction of Solar Radiation (I_{TN}) using Eq. (3.14):

$I_{TN} = I_{on} * \exp[-(P_L/P_0) * B / \sin(\alpha)]$

Plugging in the given values:

$I_{on} = 1316\ W/m^2$

$P_L/P_0 = 0{,}999$

B = 0,21

$\alpha = 81{,}865^\circ$

APPENDIX-1. (Continue) Solar Calculations (for Particular Day of June 21th)

I_{TN} = 1316 * exp [-(0,999) * (0,21) / sin (81,865)]]

I_{TN} = 1068 W/m²

Table 1.1. Solar position and atmospheric extinction data for Gaza City on June 21st

JUNE 21th					
Local standard time	Apparent Solar Time (AST)	Hour angle (h)	Solar altitude angle (α)	Solar azimuth angle (z)	Atmospheric Extinction of Solar Radiation (I_{TN})
8	7,92	-61,14	35,84	-82,37	924,69
9	8,92	-46,14	48,59	-89,41	999,03
10	9,92	-31,14	61,33	-81,45	1039,82
11	10,92	-16,14	73,59	-64,51	1060,92
12	11,92	-1,14	81,86	-7,38	1068,02
13	12,92	13,86	75,31	60,09	1062,82
14	13,92	28,86	63,24	79,66	1044,08
15	14,92	43,86	50,52	89,41	1006,88
16	15,92	58,86	37,76	83,37	939,10
17	16,92	73,86	25,18	76,85	809,66
18	17,92	88,86	12,92	70,23	522,27

APPENDIX-2. Solar position for Gaza Strip

Figures 2.1 and 2.2 display the solar altitude angle and solar azimuth angle at 15-minute intervals. These angles are essential for accurate sun tracking using a 2-axis system, maximizing solar panel efficiency. By continuously adjusting the panel's orientation based on these angles, optimal absorption of solar radiation is achieved, reducing energy losses and improving output. This dynamic tracking capability ensures prolonged exposure to sunlight, leading to increased energy production and enhanced system performance in applications such as solar power plants and concentrators.

The results related to the solar calculations for the Gaza Strip were extracted and presented as follows, as shown in the pictures and tables below.

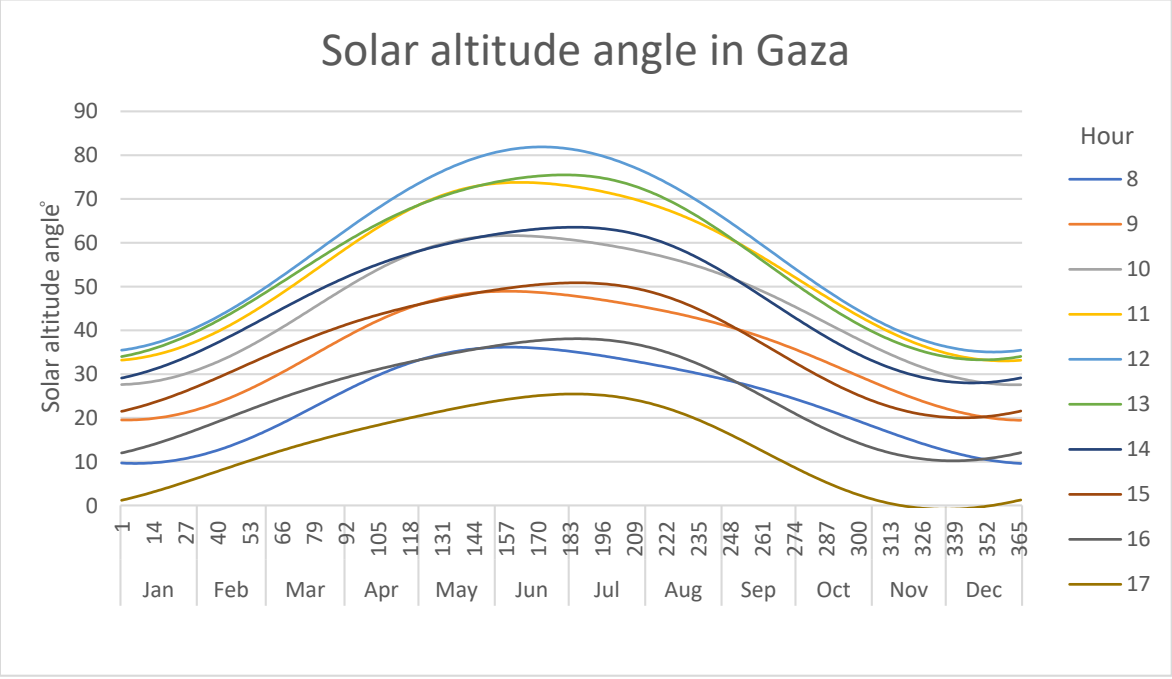

Figure 2. 1. Solar altitude angle (α) in Gaza city every day from 8 AM to 5 PM

APPENDIX-2. (Continue) Solar position for Gaza Strip

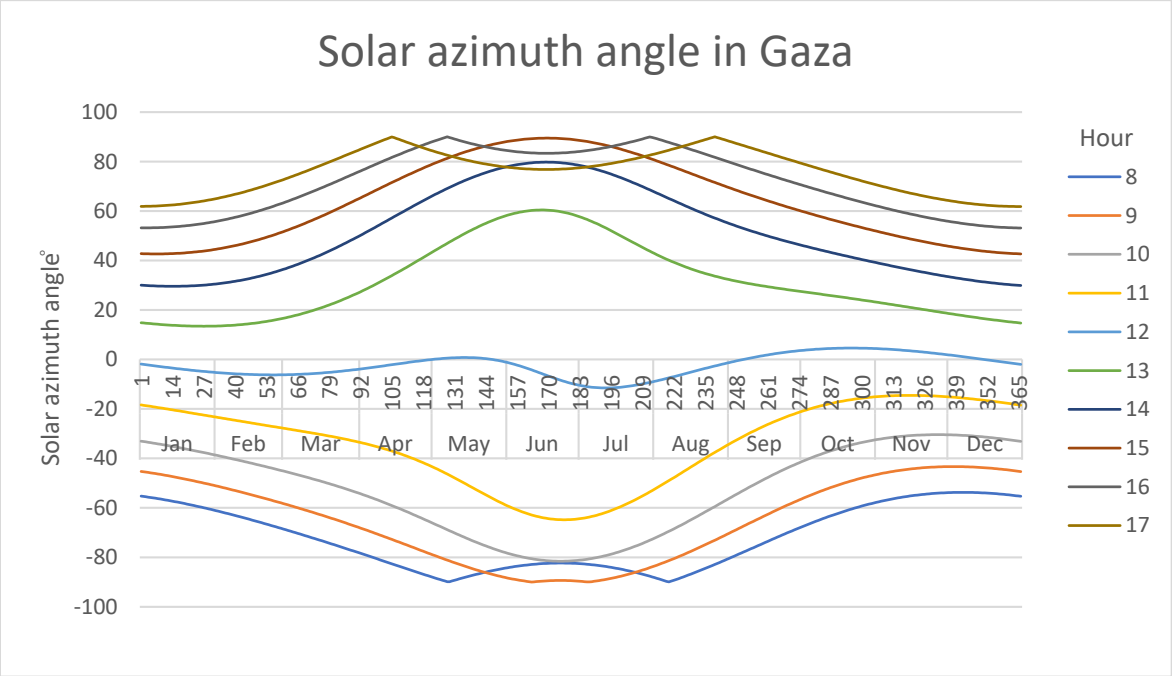

Figure 2. 2. Solar azimuth angle (z) in Gaza city every day from 8 AM to 5 PM

APPENDIX-3. Atmospheric Extinction of Solar Radiation for Gaza Strip

Table 3.1. Hourly average of Atmospheric Extinction of Solar Radiation for each month in Gaza city

Months	Solar radiations during day hours (w/m^2)									
Time of the day	8	9	10	11	12	13	14	15	16	17
Jan	110	324	505	627	679	657	563	404	199	12
Feb	182	414	608	740	801	784	692	532	318	84
Mar	329	568	760	889	944	920	820	652	429	176
Apr	477	705	884	999	1041	1007	899	727	503	250
May	548	762	928	1032	1068	1031	926	760	546	304
Jun	545	754	917	1021	1060	1030	933	776	572	340
Jul	507	721	890	1002	1046	1021	928	774	571	338
Aug	460	683	859	973	1018	989	888	724	510	267
Sep	403	627	801	909	944	901	785	606	378	133
Oct	316	532	696	794	817	764	639	452	223	19
Nov	206	412	572	668	691	641	520	341	126	0
Dec	122	325	491	598	635	598	492	326	123	0

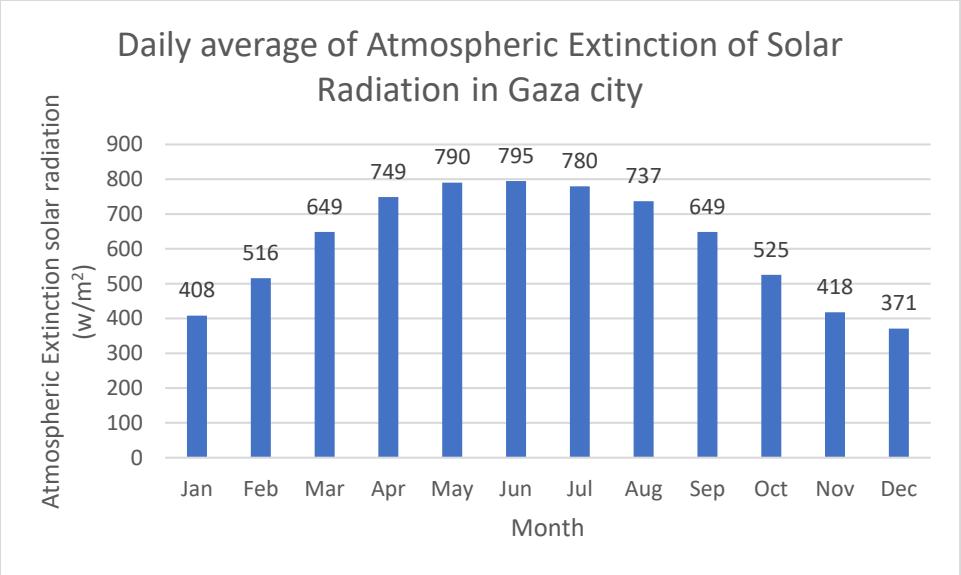

Figure 3.1. Daily average of atmospheric extinction solar radiation in Gaza city during 9 hours (from 8 to 17)

Gazili olmak ayrıcalıktır